

High-precision and low-depth eigenstate property estimation: theory and resource estimation

Jinzhao Sun,^{1, 2,*} Pei Zeng,^{3, †} Tom Gur,^{2, ‡} and M. S. Kim^{1, §}

¹Blackett Laboratory, Imperial College London, London SW7 2AZ, United Kingdom

²Computer Laboratory, University of Cambridge, Cambridge CB3 0FD, United Kingdom

³Pritzker School of Molecular Engineering, The University of Chicago, Illinois 60637, USA

(Dated: June 7, 2024)

Estimating the eigenstate properties of quantum many-body systems is a long-standing, challenging problem for both classical and quantum computing. For the task of eigenstate preparation, **quantum signal processing (QSP)** has established near-optimal query complexity $\mathcal{O}(\Delta^{-1} \log(\varepsilon^{-1}))$ by querying the block encoding of the Hamiltonian H where Δ is the energy gap and ε is the target precision. However, QSP is challenging for both near-term noisy quantum computers and early fault-tolerant quantum computers (FTQC), which are limited by the number of logical qubits and circuit depth. To date, early FTQC algorithms have focused on querying the perfect time evolution e^{-iHt} . It remains uncertain whether early FTQC algorithms can maintain good asymptotic scaling at the gate level. Moreover, when considering qubit connectivity, the circuit depth of existing FTQC algorithms may scale suboptimally with system size. Here, we present a full-stack design of a random sampling algorithm for estimating the eigenenergy and the observable expectations on the eigenstates, which can achieve high precision and good system size scaling. The gate complexity has a logarithmic dependence on the inverse precision $\mathcal{O}(\log^{1+o(1)}(1/\varepsilon))$ for generic Hamiltonians, which cannot be achieved by methods using Trottersiation to realise e^{-iHt} like in QETU. For n -qubit lattice Hamiltonians, our method achieves near-optimal system size dependence with the gate complexity $\mathcal{O}(n^{1+o(1)})$. When restricting the qubit connectivity to a linear nearest-neighbour architecture, The method shows advantages in circuit depth, with $\mathcal{O}(n^{o(1)})$ for lattice models and $\mathcal{O}(n^{2+o(1)})$ for electronic structure problems. We compare the resource requirements (CNOT gates, T gates and qubit numbers) by state-of-the-art methods, including phase estimation, QSP, and QETU, in tasks of lattice models and molecular problems. We provide a toolbox for analysing resource requirements for these advanced methods when compiled at the gate level.

I. INTRODUCTION

Estimating the properties of the ground state and excited states of quantum many-body systems is a long-standing problem of fundamental interest, which has applications in condensed matter physics, quantum chemistry and material science [1–4]. However, this is a challenging task for both classical computing and quantum computing. Indeed, estimating the ground state energy of a two-local Hamiltonian is a QMA-complete problem [5] (see numerical evidence in [6]). Nevertheless, quantum computing is a promising paradigm for addressing this problem under certain assumptions, which include a non-vanishing energy gap Δ and a non-vanishing overlap of the initial state and the target state. There has been considerable progress in the development of quantum computing algorithms (see [4] for a review), which include quantum phase estimation (QPE) [7–13], spectral filter algorithms (e.g., spectral filter by a linear combination of unitaries (LCU) [14–16], random sampling [17–28], quantum signal processing (QSP) [29, 30], quantum singular value transformation (QSVT) [12, 31]),

dissipation-based algorithms [32–34], variational algorithms [35–37], and others [38–44]. For the task of eigenstate preparation, spectral filter-based methods provide a rigorous and deterministic solution with clear assumptions of the initial overlap and energy gap, which will be the major focus of this work.

In spectral filter methods, QSP has achieved near-optimal query complexity $\mathcal{O}(\Delta^{-1} \log(\varepsilon^{-1}))$ for target precision ε , which is a widely accepted as one of the state-of-the-art algorithms [29]. While it is favourable in the long term, QSP hinges on querying the block encoding of the Hamiltonian H , which is challenging for near-term noisy intermediate-scale quantum (NISQ) or early fault-tolerant quantum computing (FTQC) applications. In the early FTQC regime [19, 45], where the number of logical qubits is limited, minimising controlled operations and achieving low circuit depth are essential goals. Considering physical devices, qubit connectivity must be taken into account, as depth and controlled operations are often interrelated. Compiling a nonlocal controlled gate into nearest-neighbour gates [46] can significantly increase both the required qubit count and the overall circuit depth. Therefore, it is desirable to design quantum algorithms tailored for NISQ and early FTQC, which satisfy the constraints of fewer qubit numbers and low circuit depth.

Considering the feature of early FTQC [19], there has been considerable progress on quantum algorithms for

* jinzhao.sun.phys@gmail.com

† peizeng@uchicago.edu

‡ tom.gur@cl.cam.ac.uk

§ m.kim@imperial.ac.uk

ground-state property estimation [13, 19–27]. In 2021, Lin and Tong proposed a spectral filter algorithm based on random sampling [19], which achieved the Heisenberg limit for ground-state energy estimation. Using similar techniques, Zeng *et al.* [20] and Zhang *et al.* [22] showed that the time complexity can achieve logarithmic in precision $\log(1/\varepsilon)$ for the ground state property estimation problem [47]. On the other hand, following the spirit of QSP, Dong *et al.* proposed the quantum eigenvalue transformation of unitaries (QETU) algorithm [48] to prepare the ground state. QETU achieves near-optimal asymptotic scaling but avoids querying the block-encoding of the Hamiltonian by querying time evolution, making it appealing to early fault-tolerant quantum computers. The above algorithms assume the usage of only one ancillary qubit and achieve good asymptotic sample and time complexity, which are competitive for the application of noisy intermediate-scale quantum and early FTQC. However, these algorithms assume perfect and efficient queries to the time evolution operator e^{-iHt} . It remains unclear whether the good properties of the above early FTQC algorithms can be preserved if we further expand e^{-iHt} into elementary gates. For example, if e^{-iHt} is implemented using Trotterisation methods, this will eliminate the advantage of logarithmic scaling in precision. On the other hand, if we introduce advanced block-encoding-based methods to realise e^{-iHt} , it needs many ancillary qubits and nonlocal controlled gates, which violates the spirit of early FTQC. Moreover, the system-size dependence of the algorithms is rarely discussed in existing works, as it highly depends on the detailed circuit-level implementation of e^{-iHt} as well as the qubit connectivity of the device. This raises the question **when considering the gate complexity and qubit connectivity, whether we can design high-precision and low-depth algorithms for NISQ and early FTQC applications.**

In this work, we provide an efficient quantum algorithm from end to end for the task of eigenstate property estimation by taking advantage of the recent advances in spectral filters and Hamiltonian simulations. We consider realising a non-unitary spectral filter through real-time evolution, accompanied by a high-precision Hamiltonian simulation scheme. To do so, we build up a framework based on random composite LCU formulae for analysing the gate complexity for the task of eigenstate property estimation. It contains several hierarchies. We consider realising the non-unitary operator by random sampling real-time evolution e^{-iHt} with different time lengths t [20–27]. To preserve high precision when implementing time evolution, we choose to compensate the Trotter error [49] by using a composite LCU formula, as opposed to only implementing the Trotter formulae in conventional Trotter methods. The first contribution of this paper is that the gate complexity for each circuit (at a single run) is shown to be $\mathcal{O}(\text{poly log}(\varepsilon^{-1}))$, outperforming the QPE-based method and matching the result by QSP. We note that QETU can achieve high-precision

ground state preparation with one ancillary qubit. However, QETU hinges on a coherent implementation of e^{-iHt} , which rules out any random sampling method, and thus, it is not straightforward to achieve logarithmic dependence on inverse precision. Furthermore, we can achieve near-optimal system size scaling for lattice Hamiltonians by exploiting the commutation relations. In this work, we mainly discuss the use of $2k$ th-order Trotter formula and then compensate the Trotter error. For n -qubit lattice Hamiltonians, the total gate count is shown to be $\mathcal{O}(n^{1+\frac{2}{4k+1}}\varepsilon^{-\frac{1}{4k+1}})$ where $2k$ is the order of the Trotter formula used in this work. Our result shows better system size dependence compared with QSP, and a better precision scaling compared with QETU, as can be found in [Table I](#).

In addition to addressing gate complexity for generic Hamiltonians, the second contribution of our work is the advantages in circuit depth for various physical problems. These include lattice models and second-quantised plane-wave electronic structures with n spin orbitals and $L = \mathcal{O}(n^2)$ terms in the Hamiltonian. Notably, the 2D Fermi-Hubbard model falls within the problem class. In theory, for problems that conserve certain symmetries, we demonstrate the ability to achieve high-precision and low-depth eigenstate property estimation without the need for ancillary qubits. To accomplish this, we design new Trotter and Trotter-error compensation circuits that maintain the system's symmetries. Thanks to this ancilla-free feature, when restricting the qubit connectivity, the random sampling method shows advantages in circuit depth over existing best practices. When restricted to nearest-neighbour architecture, for lattice models, the circuit depth scales as $d = \mathcal{O}(n^{\frac{2}{4k+1}})$, while the circuit depth for QETU combined with Trotter scales as $d_{\text{QETU}} = \mathcal{O}(n^{1+\frac{1}{2k}})$. For second-quantised plane-wave electronic structures, the circuit depth is $d = \mathcal{O}(n^{2+\frac{2}{4k+1}})$, while naive implementation of the QETU-Trotter method requires $d_{\text{QETU}} = \Omega(n^{3+\frac{1}{2k}})$.

To address the application in the NISQ and FTQC eras, we present the actual gate count and number of qubits required for solving practical problems accordingly. In the existing resource estimation works [50–54], the energy estimation or eigenstate preparation for practical problems, such as second-quantised quantum chemistry problems with $L = \mathcal{O}(n^4)$ terms [55–57] and condensed-phase electrons [58, 59], is predominantly based on phase estimation. A typical strategy is to encode the eigenspectra of the Hamiltonian in a unitary for phase estimation by the evolution e^{-iHt} , which is synthesised by Trotterisation [58, 59], or a qubitised quantum walk [55, 56] with eigenspectrum proportionally to $e^{\pm i \arccos(H/\lambda)}$, where λ is a parameter related to the norm of the Hamiltonian. However, due to the cost of phase estimation, the circuit depth will inevitably be polynomial in the precision, which is not optimal for eigenstate energy and property estimation.

The third contribution is to present resource estima-

tions with the method developed in this work, which has better asymptotic scaling in precision and system size in theory, and also has a smaller circuit compilation overhead in practice. In the NISQ applications, the major bottleneck is the number of two-qubit gates for the noisy quantum computer. The major overhead for the error-corrected quantum computer is the T gate count [56], which requires more gates to perform error correction than Clifford gates. Therefore, we study the resource requirement in terms of CNOT and T gates for ground-state property estimation for representative physical models in condensed matter and chemistry. We provide a systematic comparison with the existing advanced methods, which include QPE combined with Trotter formulae or qubitised quantum walk (as have been used in [52, 55, 56]), QSP [29] and QETU. The CNOT gate cost for a 20-site Heisenberg model is about 3×10^5 while the T gate cost is about 6×10^6 . A notable contribution of this work is that for different query models, we provide a useful toolbox for researchers to analyse the individual costs for elementary units (like block encoding and controlled real-time evolution), and thus enable comparison across different eigenstate preparation methods with various initial conditions. We hope that our framework (decomposing the task into the elementary operations) and the toolbox for analysing the cost for each elementary operation can be useful as a building block for resource estimations for other quantum algorithms based on querying the block encoding of H or the time evolution.

The rest of this paper is organised as follows. In Sec. II, we outline the algorithm and overview the main results in this work. In Sec. III, we show the construction of a spectral filter with the random-sampling composite LCU formula. We show the methods for eigenenergy estimation and eigenstate property estimation, and provide the circuit depth and gate complexity for the two tasks. In Sec. IV, we present the resource cost in terms of the ancillary qubits, CNOT gates and non-Clifford gates (T gates and single-qubit Pauli rotation gates) for various physical systems, including the lattice models and quantum chemistry problems.

II. FRAMEWORK AND MAIN RESULTS

In this section, we introduce the framework of eigenenergy and eigenstate property estimation with the random-sampling composite linear-combination-of-unitary (LCU) formulae. Let us consider an n -qubit gapped quantum system with the Hamiltonian H . The eigenstate $|u_j\rangle$ and the corresponding eigenenergy E_j of the Hamiltonian satisfy, $H|u_j\rangle = E_j|u_j\rangle$, for $j \leq 2^n$. The tasks concerned in this work are (1) to estimate the eigenenergy E_j , and (2) to estimate an eigenstate property, characterised by an observable expectation on the target eigenstate $\langle u_j | O | u_j \rangle$. The problems with the assumptions and the notations used in this work are stated

below.

Problem 1 (Eigenstate property estimation). *Consider a gapped n -qubit Hamiltonian with a Pauli decomposition $H = \sum_{l=1}^L \alpha_l P_l := \lambda \sum_{l=1}^L \tilde{\alpha}_l P_l$ where P_l is a Pauli operator, $\lambda := \sum_l |\alpha_l|$, and $\tilde{\alpha} := \alpha_l/\lambda$. The task is to estimate the expectation value of an observable O on the j th eigenstate of H , $|u_j\rangle$. We assume that we have an estimate of E_j , \hat{E}_j with a small estimation error $\kappa := |\hat{E}_j - E_j|$. We assume that we have a good initial state $|\psi_0\rangle$ which has a nonvanishing overlap with the target eigenstate, $\eta := |\langle \psi_0 | u_j \rangle|^2 = \Omega(1/\text{poly}(n))$. We assume a nonvanishing energy gap $\Delta := \min(E_{j+1} - E_j, E_j - E_{j-1})$.*

Suppose the observable has a Pauli decomposition as $O = \sum_{l=1}^{L_O} o_l P_l$ with Pauli operators P_l and positive coefficients o_l , and $\|O\|_1 := \sum_{l=1}^{L_O} |o_l|$. The aim is to find an estimator \hat{v} , such that it is close to $\langle u_j | O | u_j \rangle$ with at least probability $1 - \vartheta$, i.e., $\Pr(|\hat{v} - \langle u_j | O | u_j \rangle| \leq \varepsilon) \geq 1 - \vartheta$.

Note that in Problem 1, we follow the convention in [20], which has a slight difference in the definition of the initial overlap η compared to Refs. [29, 48].

Problem 2 (Eigenenergy estimation). *Under the same definitions and assumptions introduced in Problem 1, the aim is to find an eigenenergy estimator \hat{E}_j , such that it is κ -close to E_j with at least probability $1 - \vartheta$, i.e., $\Pr(|\hat{E}_j - E_j| \leq \kappa) > 1 - \vartheta$.*

The design of the eigenstate property estimation algorithm is sketched in Algorithm 1 and illustrated in Fig. 1. To access the physical properties of eigenstates, a natural idea is to apply a spectral filter to the initial state that projects out the contributions from the other unwanted eigenstates, as illustrated in Fig. 1(b1). While the spectral filter g is non-unitary by construction, we can effectively realise it using LCU techniques, either by coherent [14, 15] or random-sampling implementation [17, 20–24, 26]. The decomposition of g into real-time evolution $U(t_i) = e^{-iHt_i}$ with time length t_i is shown in Fig. 1(a1). We further realise each $U(t_i)$ by another random LCU formula. Within each time segment, the LCU formula involves both the Trotter formula S and the Trotter-error-compensation term V , as shown in Fig. 1(a2). Overall, it forms a composite LCU formula illustrated in Fig. 1(a3), which involves the summation and product of individual LCU components. The hierarchy of different LCU components is illustrated in Fig. 2. The error propagation will be analysed in Sec. III and Appendix in order to prove the main theorems. The quantum circuit realisation is shown in Fig. 1(c), including both one-ancilla and ancilla-free schemes. A more detailed Hamiltonian-dependent circuit compilation method will be discussed in Sec. III D. Below, we elaborate on the composite LCU formula for eigenstate property estimation.

The spectral filter g is a non-unitary operator defined on the n -qubit system, which is usually a function of the target Hamiltonian H . Choices for spectral filters include

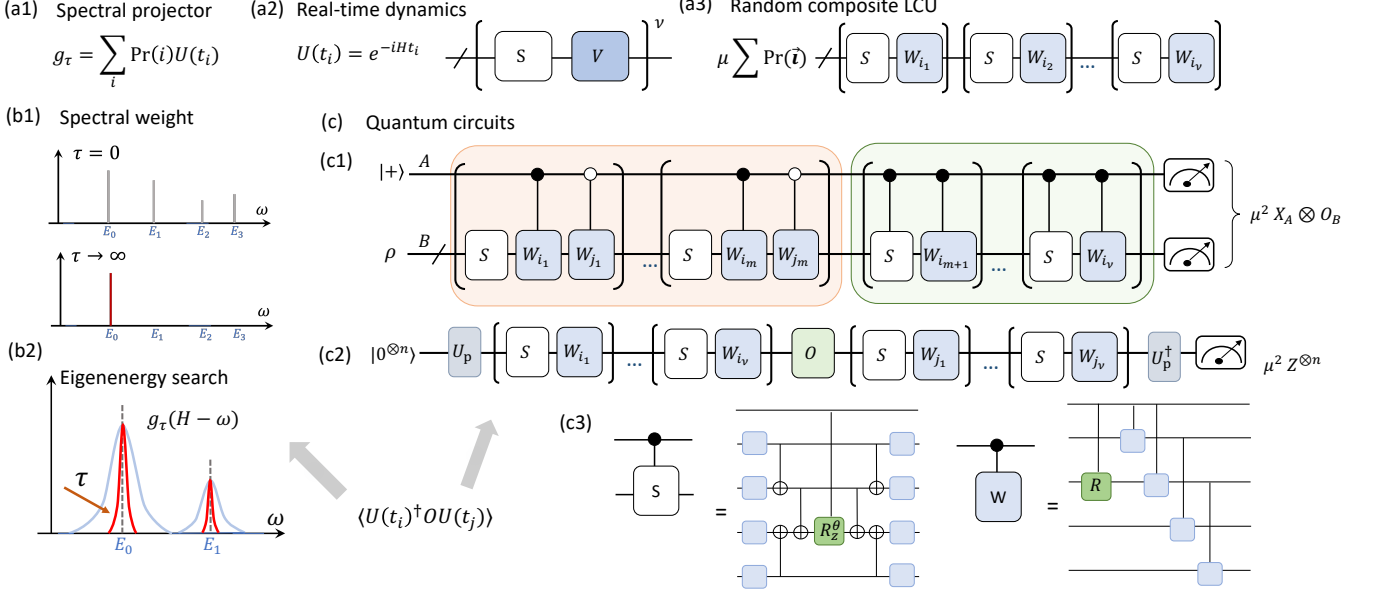


FIG. 1. (a) The random composite LCU formulae components of g_τ . (a1) The spectral filter is decomposed into a combination of real-time evolution $U(t_i) = e^{-iHt_i}$, as described by Eq. (1). (a2) The real-time evolution is divided into ν segments. Each segment with time duration t_i/ν is realised by a Trotter formula S and the Trotter remainder V . The Trotter remainder V can be written into an LCU form in Eq. (3). (a3) A random composite LCU formula of g_τ . The summands of the circuit are shown here (each circuit instance is described by Eq. (35)). In the one-ancilla scheme W_{i_q} ($q \leq \nu$) is composed of a Pauli rotation operator $R = \exp(-i\theta_{i_q} P_{i_q})$ and a tensor product of single-qubit Pauli operators, where P_{i_q} is drawn from a certain probability distribution. The maximum gate count in W_{i_q} is $\text{wt}_m H + n$, where $\text{wt}_m H$ is the largest weight of the Hamiltonian terms. The controlled W operation is shown in (c3). In the ancilla-free measurement scheme illustrated in (c2), W_{i_q} is chosen to be symmetry-conserved operators to conserve the symmetry of the real-time evolution. (b1) The spectral weight of the effectively imaginary-time-evolved state after applying the spectral filter $g_\tau(H - E_0)$ where E_0 is assumed to be known. The y axis represents the spectral weight $\langle u_i | g_\tau(H - E_0) | \psi_0 \rangle$, where $|u_i\rangle$ is the eigenstate with energy E_i . By increasing the imaginary time τ , only the spectral weight on the ground state will be preserved. The contributions from the other eigenstates are suppressed exponentially with τ . (b2) The eigenenergy search using $D_\tau(\omega) = \langle \psi_0 | g_\tau^2(H - \omega) | \psi_0 \rangle$ where $D_\tau(\omega)$ is defined in Eq. (11). By increasing the imaginary time τ , the peaks become sharper (from the blue line to the red line) and the true eigenenergies can be resolved by finding the peaks. The key quantity encountered in (b1) and (b2) is $\langle U^\dagger(t_j) O U(t_i) \rangle$ in Eq. (36). The component in $\langle U^\dagger(t_j) O U(t_i) \rangle$ can be measured using the circuit in (c). There are two extreme cases: Case I: $t_j = 0$, and Case II $t_i = t_j$. When $t_j = 0$, the circuit reduces to the one in the green box. When $t_j = t_i$, the circuit reduces to the one in the orange box. Case I requires more resources than other cases. The resources in other cases with $t_j < t_i$ will be between Case I and Case II. (c2) Ancilla-free measurement scheme for symmetry-conserved cases. U_p is the unitary operator for state preparation $|\psi_0\rangle = U_p |0^{\otimes n}\rangle$ or $\frac{1}{\sqrt{2}}(|\psi_{\text{Ref}}\rangle + |\psi_0\rangle) = U_p |0^{\otimes n}\rangle$ which is discussed in Sec. III D 2. (c3) For general cases in (c1), the controlled S operation takes the form of $\exp(-it_i P/\nu)$ with Pauli operator P , which can be compiled into controlled single-qubit Pauli rotation gates, CNOT gates and single-qubit Pauli gates.

the imaginary-time evolution operator $g_\tau(H) = e^{-\tau H}$ or the Gaussian operator $g_\tau(H) = e^{-\tau^2 H^2}$. For example, by applying $g_\tau(H) = e^{-\tau|H-E_0|}$ to an initial state $|\psi_0\rangle$, the state becomes $|\psi(\tau)\rangle = c(\tau) \sum_i c_i e^{-|E_i - E_0|} |u_i\rangle$ where $c(\tau)$ is the normalisation factor. Provided the assumptions in Problem 1, i.e., a nonvanishing energy gap $\Delta = E_1 - E_0$ and a nonvanishing $c_0 = \eta^{-1/2}$, the spectral weight of the unwanted excited eigenstates is suppressed with increasing τ . In the large τ limit, the unnormalised state becomes $\lim_{\tau \rightarrow \infty} |\psi(\tau)\rangle = c_0 |u_0\rangle$, as illustrated in Fig. 1(b1).

We note that the spectral filter method has been well-established in the existing literature, in particular [20, 22,

24, 29]. In this paper, we introduce a full-stack approach to eigenstate property and energy estimation by random-sampling composite LCU decomposition of a Gaussian operator, and we refer to this full-stack random-sampling LCU approach as our method for simplicity.

Now, let us discuss the construction of the composite LCU formulae. A (μ, ε) -random-sampling linear-combination-of-unitary (RLCU) formula of a general operator g is defined to be

$$\tilde{g} = \mu \sum_i \Pr(i) U_i, \quad (1)$$

such that the spectral norm distance $\|g - \tilde{g}\| \leq \varepsilon$, as illustrated in Fig. 1(a1). Here, $\mu > 0$ is the normalisa-

tion factor, $\Pr(i)$ is a probability distribution associated with an instance specified by i , and $\{U_i\}_i$ is a group of unitaries. Eq. (1) can be extended to a continuous form

$$\tilde{g} = \mu \int_{-x_c}^{+x_c} dx p(x) U(x) \quad (2)$$

where we require that $p(x)$ ($x \in [x_c, x_c]$) is a well-defined probability distribution.

As discussed above, a natural choice for U_i is the real-time evolution $U_i = U(t_i) := e^{-iHt_i}$ with time length t_i because quantum systems in nature evolve governed by the Hamiltonian; for instance, analogue quantum simulators can directly perform $U(t_i)$. The Gaussian spectral filter can be decomposed on the basis of real-time evolution $g(H) = \int_{-\infty}^{\infty} dp(t) e^{-itH}$ with a Gaussian probability distribution $p(t) = \frac{1}{\sqrt{2\pi}} e^{-t^2/4}$. We could truncate the time range and formally express it as $g = \sum_i \Pr(i) e^{-iHt_i}$. Though the Gaussian spectral filter is represented in an integral form, it has a well-defined probability distribution and can be well-characterised by Eq. (1). Therefore, we will mainly discuss the property of composite LCU form in the discretised form, while we use the continuous form when dealing with the Gaussian spectral filter. While most early FTQC algorithms assume that real-time evolution can be implemented perfectly, $U(t_i)$ in general is not directly implementable. An established way to implement $U(t_i)$ without involving other oracles is through Trotter formulae: when the Hamiltonian can be decomposed into Pauli operators, each $U(t_i)$ can be implemented using elementary quantum gates without querying any other oracles and introducing additional gates. However, by using Trotter formulae, the gate complexity will be polynomial in the inverse accuracy [60]. Therefore, any ground-state property estimation protocol based on Trotterisation will lose the advantage of high precision in the first place. The question is how to preserve the logarithmic dependence on the precision.

Given a Trotter formula $S(t_i)$, the Trotter error can be expressed as $V(t_i) = U(t_i)S^\dagger(t_i)$. The problem with the Trotter method is that the remainder of a k th Trotter formula (i.e., Trotter error) is non-negligible, which is polynomial in the order of k . To preserve the high precision property, we choose to implement the Trotter remainder V as well, as opposed to implementing S only in conventional Trotter methods, which is illustrated in Fig. 1(a2,a3). By doing so, we can implement a Trotter-error-free $U(t_i)$. Specifically, we consider dividing the time evolution operator $U(t_i)$ into ν segments, which can be written as $U(t_i) = (S(t_i/\nu)V(t_i/\nu))^\nu$ where $S(t_i/\nu)$ is a Trotter formula and $V(t_i/\nu)$ is the corresponding Trotter error within duration t_i/ν . The key idea of this Trotter error compensation is that the Trotter error can be further decomposed into easy-to-implement unitary operators

$$V = \mu \sum_j \Pr(j) W_j \quad (3)$$

where $\Pr(j)$ is the probability associated with the unitary operator W_j in the decomposition of V , and μ is the normalisation factor. Importantly, the decomposition in Eq. (3) can be explicitly derived by $V = US^\dagger$ using the Taylor expansion. By doing so, we can compensate the Trotter error by sampling W_j according to $\Pr(j)$ in Eq. (3). This effectively realises a Trotter-error-compensated real-time dynamics, with the individual terms illustrated in Fig. 1(a3). In general cases, the elementary operator W_j in Eq. (3) can be chosen as Pauli operators or the exponentiation of Pauli operators, as commonly used in Trotter and LCU methods [49, 61]. However, choosing Pauli operators as the bases may break the symmetry of the real-time evolution. To enable ancilla-free measurement, we choose W_j to be symmetry-conserved operator. Specifically, to conserve the symmetry of either particle number or total spins, W_j is chosen to be SWAP, a tensor product of Pauli-Z operators, and their exponentiation, which will be discussed in Sec. III C.

The spectral filter can now be formally rewritten as

$$\tilde{g} = \sum_i \Pr(i) \left(V\left(\frac{t_i}{\nu}\right) S\left(\frac{t_i}{\nu}\right) \right)^\nu \quad (4)$$

with the aim of being close to the original spectral filter. The spectral filter consists of other LCU formulae in it. We could see that Eq. (4) is a modified version of the original LCU formula given by Eq. (1), which involves hierarchical formulations, as illustrated in Fig. 1(a). Specifically, it adopts a composite structure that integrates both the products of individual LCU components and the summations of LCU components. This work will analyse the propagation of errors and the change of normalisation factors within this composite LCU framework, outlined in Fig. 2.

We will need to introduce a few tools to analyse the properties of the composite form of LCU formulae.

Proposition 1 (Composite LCU formula). *Suppose g_1 takes a (μ_1, ε_1) -LCU formula of g , $g_1 = \mu_1 \sum_i \Pr(i) U(t_i)$ in Eq. (1). Suppose that each of the summands $U(t)$ is real-time evolution and is divided into ν segments, with each segment $U(\delta t)$, $\delta t = t/\nu$. Suppose that $U(\delta t)$ has a (μ_2, ε_2) -LCU formula, $\tilde{U}(\delta t) = \mu_2 \sum_\ell \Pr(\ell) P_\ell$. Then the formula*

$$g_2 = \mu_1 \sum_i \Pr(i) (\tilde{U}(t_i/\nu))^\nu \quad (5)$$

is a (μ, ε) -LCU formula of g , with $\mu := \mu_1 \mu_2^\nu$, and $\varepsilon \leq \varepsilon_1 + \mu_1 \mu_2 \varepsilon_2$.

The proof of Proposition 1 is shown in Appendix A 1. Leveraging Proposition 1, we could calculate the error in the composite LCU form provided the error of each individual LCU approximation.

The key steps of the eigenstate property estimation algorithm and the circuit implementation are summarised in Algorithm 1 below.

Algorithm 1 An overview of the random-sampling algorithm for eigenstate property and eigenenergy estimation described in [Problem 1](#) and [Problem 2](#).

- 1: Construct a composite LCU formula as described in [Proposition 1](#). We first expand a Gaussian spectral filter g into a combination of real-time evolution $U(t_i)$ by [Eq. \(2\)](#). We decompose $U(t_i) = (S_{2k}(t_i/\nu)V_{2k}(t_i\nu))^\nu$ into Pauli operators, which takes a composite LCU form, with the LCU form of V in [Eq. \(3\)](#) and the explicit form in [Eq. \(16\)](#) in [Sec. III](#). Here S_{2k} is the $2k$ th-order Trotter formula and V_{2k} is the Trotter remainder. We consider effectively realising both the Trotter S_{2k} and the Trotter remainder V_{2k} to enable high-precision simulation (where Trotter error is compensated).
- 2: Realise the composite LCU formula by random sampling. We first generate t_i and t_j (at the level of real-time evolution) and \vec{t} and \vec{j} (at the level of gates, see [Eq. \(35\)](#)) by sampling from the corresponding probability distributions, which gives us an explicit form of the circuit in each run (see [Eq. \(35\)](#) and [Eq. \(36\)](#) for example). The circuit for evaluating $N(O)$ and D (in [Eq. \(30\)](#)) is shown in [Fig. 1\(c1,c2\)](#). The ancilla-free scheme is discussed in [Sec. III C](#).
- 3: Estimate the observable expectation value by $\langle O \rangle = \frac{N_\tau(O)}{D_\tau}$, and eigenenergy by $E_j = \arg \max_\omega D_\tau(\omega)$. The estimator of $N_\tau(O)$ and D_τ is given by [Eq. \(40\)](#). The observable expectation on the eigenstate is given by [Eq. \(11\)](#). As illustrated in [Fig. 1\(b\)](#) The eigenenergy could be determined by $\max_\omega D_\tau(\omega)$ where the search process is evaluated by pure classical computation. The eigenenergy can be estimated with $\hat{D}_\tau(E)$ where the search process with different E can be evaluated by pure classical computation.

A. Overview of the results

Our result with random composite LCU can nearly match and, in some cases, outperform the previous best methods for gate complexity with respect to Δ , ε , λ and n , though the sample complexity becomes worse in η . In this section, we provide an overview of the main results of this work. The eigenenergy is first assumed to be known a priori. This is the case for linear algebra tasks, in which the true solution corresponds to the ground state of a constructed Hamiltonian with the eigenenergy being zero. The task with an unknown eigenenergy will be discussed in [Sec. B 5](#). Before diving into the derivations, we first summarise the main theoretical results for generic Hamiltonians.

Theorem 1 (Eigenstate property estimation for generic Hamiltonians). *Suppose we use the method in [Algorithm 1](#) and the conditions and assumptions in [Problem 1](#) hold. Observable estimation ([Problem 1](#)): To achieve the error of observable's expectation on the eigenstate $|u_j\rangle$ within ε , the gate complexity in a single circuit is $\mathcal{O}\left(5^{k-1}L(\lambda\Delta^{-1}\ln(\eta^{-1}\varepsilon^{-1}))^{1+\frac{1}{4k+1}}\right)$ when the number of*

samples is $N_s = \mathcal{O}(\eta^{-2}\varepsilon^{-2}\|O\|_1^2\ln(1/\vartheta))$ with a success probability at least $1 - \vartheta$.

Eigenenergy estimation ([Problem 2](#)): To achieve the eigenenergy estimation error within κ using [Algorithm 1](#), the gate complexity in a single circuit is $\mathcal{O}\left(5^{k-1}L(\lambda\kappa^{-1}\ln(\eta^{-1}))^{1+\frac{1}{4k+1}}\right)$, with number of samples $N_s = \mathcal{O}(\eta^{-2}\ln(1/\vartheta))$ with a success probability at least $1 - \vartheta$, approaching to the Heisenberg limit. Alternatively, by using the methods proposed in [24] and [Algorithm 1](#), the gate complexity in a single circuit is $\mathcal{O}\left(5^{k-1}L(\lambda\Delta^{-1}\ln(\eta^{-1}\kappa^{-1}))^{1+\frac{1}{4k+1}}\right)$ at the cost of more number of samples $N_s = \mathcal{O}(\eta^{-2}\Delta^4\kappa^{-4}(\ln(\kappa^{-2}\eta^{-1}))^2\ln(1/\vartheta))$ with a success probability at least $1 - \vartheta$.

Comparisons of the state-of-the-art ground-state property estimation methods and ground-state energy estimation are shown in [Table I](#) and [Table II](#). We note that in this work, we focus on the application in NISQ or early FTQC, in which circuit depth is more concerned than sample complexity. As in random sampling methods, η only appears in sample complexity and thus η dependence is not included in [Table I](#). As we shall see, the random sampling method has the advantage in system size scaling when qubit connectivity is restricted. However, random sampling methods will require more samples much worse than coherent methods. We leave the comparison of random-sampling methods with coherent methods in the Discussion.

As shown in [Table I](#), our method can achieve polylogarithmic dependence on inverse precision, outperforming the QPE-based method and matching the result by QSP. QETU can achieve near-optimal ground state preparation with a single ancillary qubit by querying real-time evolution. However, QETU hinges on a coherent implementation of e^{-iHt} . That means the Hamiltonian simulation needs to run coherently, ruling out any random sampling method, and thus it is not straightforward to achieve polylogarithmic dependence on inverse precision.

An advantage of our method over QSP is that the commutator relations can be utilised such that it may achieve a better system size dependence. For Heisenberg models, the gate complexity of our method is $\mathcal{O}(n^{1+\frac{2}{4k+1}}\Delta^{-(1+\frac{1}{4k+1})}\varepsilon^{-\frac{1}{4k+1}})$. In contrast, the solution given by QSP [29] is $\mathcal{O}(n^2\Delta^{-1}\log\varepsilon^{-1})$. We summarise the results for the gate complexity for different physical Hamiltonians. These examples include (1) spin-lattice Hamiltonians with nearest-neighbour interactions (e.g., Ising models and Heisenberg models), (2) a second-quantised plane-wave electronic structure with n spin orbitals and $L = \mathcal{O}(n^2)$ terms in the Hamiltonian, which also include the 2D Fermi-Hubbard model, and (3) a general second-quantised quantum chemistry problem with $L = \mathcal{O}(n^4)$ terms.

It is worth comparing our method with the Trotter-based methods. The implementation of time evolution by Trotter methods will undermine the optimal scaling

Methods	Gate complexity	Gate complexity (lattice models)	Extra qubits
QPE + Trotter (2kth-order)	$\mathcal{O}(L\tilde{\Delta}^{-(1+\frac{1}{2k})}\varepsilon^{-(1+\frac{1}{k})})$	$\mathcal{O}(n^{1+\frac{1}{2k}}\Delta^{-(1+\frac{1}{2k})}\varepsilon^{-(1+\frac{1}{k})})$	$\log(\varepsilon^{-1}) + \log(\Delta^{-1})$
QPE + QW [55]	$\tilde{\mathcal{O}}(L\tilde{\Delta}^{-1}\varepsilon^{-1})$	$\mathcal{O}(n^2\Delta^{-1}\varepsilon^{-1})$	$\log(L) + \log(\varepsilon^{-1}) + \log(\Delta^{-1})$
QSP [29]	$\mathcal{O}(L\tilde{\Delta}^{-1}\log\varepsilon^{-1})$	$\mathcal{O}(n^2\Delta^{-1}\log\varepsilon^{-1})$	$\log(L) + \log\log(\varepsilon^{-1}) + \log(\Delta^{-1})$
QETU [48]	$\tilde{\mathcal{O}}(L\tilde{\Delta}^{-(1+\frac{1}{2k})}\varepsilon^{-\frac{1}{2k}})$	$\mathcal{O}(n^2\Delta^{-(1+\frac{1}{2k})}\log\varepsilon^{-1})$	1
This work (2kth-order)	$\mathcal{O}(L(\tilde{\Delta}^{-1}\log\varepsilon^{-1})^{(1+\frac{1}{4k+1})})$	$\tilde{\mathcal{O}}(n^{1+\frac{2}{4k+1}}\Delta^{-(1+\frac{1}{4k+1})}\varepsilon^{-\frac{1}{4k+1}})$	0 or 1
(zeroth-order)	$\mathcal{O}(\tilde{\Delta}^{-2}\log^2\varepsilon^{-1})$	$\mathcal{O}(n^2\Delta^{-2}\log^2\varepsilon^{-1})$	0 or 1

TABLE I. Comparison of observable estimation on the eigenstate of a Hamiltonian (Problem 1). Here we compare the gate complexity of the algorithm in a single coherent run. The results in the second column in the table are based on Algorithm 1 and Theorem 1 using the 2kth-order Trotter error compensation. Here, $\tilde{\Delta} := \lambda/\Delta$. The results in the third column in the table are based on Theorem 2 when the 2kth-order Trotter formula is used. The eigenenergy is assumed to be known a priori and the unknown eigenenergy case is analysed in Sec. B 5. The dependence on η is not included in the table since it only appears in sample complexity for our method. Similar to other random-sampling spectral filter methods (see [19, 22]), the sample complexity with respect to η is $\mathcal{O}(\eta^{-2})$ for which the optimal scaling is $\mathcal{O}(\eta^{-1/2})$ achieved by QSP and QETU with amplitude amplification.

Methods	Gate complexity	Gate complexity (lattice models)	Extra qubits
QPE + Trotter (2kth-order)	$\mathcal{O}(L\lambda^{1+\frac{1}{2k}}\varepsilon^{-(1+\frac{1}{k})})$	$\mathcal{O}(n^{1+\frac{1}{2k}}\varepsilon^{-(1+\frac{1}{k})})$	$\log(\varepsilon^{-1}) + \log(\Delta^{-1})$
QPE + QW [55]	$\tilde{\mathcal{O}}(L\lambda\varepsilon^{-1})$	$\tilde{\mathcal{O}}(n^2\varepsilon^{-1})$	$\log(L) + \log(\varepsilon^{-1}) + \log(\Delta^{-1})$
QSP [29]	$\tilde{\mathcal{O}}(L\lambda\varepsilon^{-1})$	$\tilde{\mathcal{O}}(n^2\varepsilon^{-1})$	$\log(L) + \log\log(\varepsilon^{-1}) + \log(\Delta^{-1})$
QETU [48]	$\tilde{\mathcal{O}}(L\lambda^{1+\frac{1}{2k}}\varepsilon^{-(1+\frac{1}{k})})$	$\tilde{\mathcal{O}}(n^{1+\frac{1}{2k}}\varepsilon^{-(1+\frac{1}{k})})$	1
This work (2kth-order)	$\tilde{\mathcal{O}}(L\lambda^{1+\frac{2}{4k+1}}\varepsilon^{-(1+\frac{1}{4k+1})})$	$\tilde{\mathcal{O}}(n^{1+\frac{2}{4k+1}}\varepsilon^{-(1+\frac{1}{4k+1})})$	0 or 1
(zeroth-order) and [18]	$\tilde{\mathcal{O}}(\lambda^2\varepsilon^{-2})$	$\tilde{\mathcal{O}}(n^2\varepsilon^{-2})$	0 or 1

TABLE II. Gate complexity in eigenenergy estimation up to estimation error ε (Problem 2). Note that this table focuses on the total gate complexity (i.e., sample complexity is included). The dependence on η is not included in the table, as similarly discussed in Table I.

with respect to λ , Δ and ε . Since controlled operations are necessary in QETU (even for the control-free method), it becomes suboptimal when considering the qubit connectivity. Our RLCU method has the following advantages: (1) it has better scaling with respect to λ , Δ and ε , though the dependence on η is much worse than other advanced methods. (2) When restricting the qubit connectivity to nearest neighbours, our method has improved in circuit depth. For the Heisenberg model, QETU has depth $\mathcal{O}(n^{1+\frac{1}{2k}}\varepsilon^{-\frac{1}{2k}})$, while our method has depth $\mathcal{O}(n^{\frac{2}{4k+1}}\varepsilon^{-\frac{1}{4k+1}})$, which shows advantages in the scaling of n and ε .

The result is summarised in Theorem 2 and a comparison with other methods is shown in the third column of Table I.

Theorem 2 (Eigenstate property estimation for lattice Hamiltonians). *For n-qubit Heisenberg Hamiltonians, to estimate the observable on the eigenstate with a precision ε and a success probability $1 - \vartheta$, in a single run, the gate complexity is $\mathcal{O}(n^{1+\frac{2}{4k+1}}\Delta^{-(1+\frac{1}{4k+1})}\varepsilon^{-\frac{1}{4k+1}}\log(\vartheta^{-1}))$. The circuit depth when compiled on qubits with nearest-neighbour geometry is $\mathcal{O}(n^{\frac{2}{4k+1}}\Delta^{-(1+\frac{1}{4k+1})}\varepsilon^{-\frac{1}{4k+1}}\log(\vartheta^{-1}))$.*

The proof idea for Theorem 1 and Theorem 2 is illustrated in Fig. 2 in Sec. III. The proof and a more detailed

version of Theorem 1 can be found in Theorem 3 in Appendix C.

The result can be extended to the simulation of molecules. In the plane-wave dual basis, the second quantised electronic-structure Hamiltonian has the form (see [56, 58, 60])

$$H = \hat{T} + \hat{V} = \sum_{pq} T_{pq} \hat{a}_p^\dagger a_q + \sum_p U_p \hat{n}_p + \sum_{p \neq q} V_{pq} \hat{n}_p \hat{n}_q \quad (6)$$

where \hat{T} and \hat{V} represent the kinetic and potential terms of the fermionic Hamiltonian, respectively, \hat{a} and \hat{a}^\dagger are fermionic creation and annihilation operators and \hat{n}_p is the number operator for the corresponding spin-orbital, and the total number of terms $L = \mathcal{O}(n^2)$. Note that operators are typically indicated by using the hat notation. In this work, to avoid confusion with the estimator, we will only use the hat symbol to denote the fermionic operators and the estimators. Except for the potential terms \hat{V} in molecular Hamiltonians, V denotes the Trotter remainder in this work.

To estimate the eigenstate property of the Hamiltonian described by Eq. (6), the circuit depth scales as $\mathcal{O}(n^{2+\frac{2}{4k+1}})$. When restricted to nearest-neighbour (NN) architecture, the circuit depth by QETU scales as $\Omega(n^{3+\frac{1}{2k}})$. The circuit depth results for different physical Hamiltonians are displayed in Table III. Here, we

Hamiltonians	Ancilla-free method (NN)	QETU (NN) [48]	arbitrary
1D lattice models	$d = \mathcal{O}(n^{\frac{2}{4k+1}} \Delta^{-(1+\frac{1}{4k+1})} \varepsilon^{-\frac{1}{4k+1}})$ $g = \mathcal{O}(n^{1+\frac{2}{4k+1}} \Delta^{-(1+\frac{1}{4k+1})} \varepsilon^{-\frac{1}{4k+1}})$	$d = \mathcal{O}(n^{1+\frac{1}{2k}} \Delta^{-(1+\frac{1}{2k})} \varepsilon^{-\frac{1}{2k}})$ $g = \mathcal{O}(n^{1+\frac{1}{2k}} \Delta^{-(1+\frac{1}{2k})} \varepsilon^{-\frac{1}{2k}})$	$d = \mathcal{O}(n^{\frac{2}{4k+1}} \Delta^{-(1+\frac{1}{4k+1})} \varepsilon^{-\frac{1}{4k+1}})$ $g = \mathcal{O}(n^{1+\frac{2}{4k+1}} \Delta^{-(1+\frac{1}{4k+1})} \varepsilon^{-\frac{1}{4k+1}})$
Electronic structure (Eq. (6))	$d = \mathcal{O}(n^{2+\frac{2}{4k+1}} \Delta^{-(1+\frac{1}{4k+1})} \varepsilon^{-\frac{1}{4k+1}})$ $g = \mathcal{O}(n^{3+\frac{2}{4k+1}} \Delta^{-(1+\frac{1}{4k+1})} \varepsilon^{-\frac{1}{4k+1}})$	$d = \Omega(n^{3+\frac{1}{2k}} \Delta^{-(1+\frac{1}{2k})} \varepsilon^{-\frac{1}{2k}})$ $g = \mathcal{O}(n^{3+\frac{1}{2k}} \Delta^{-(1+\frac{1}{2k})} \varepsilon^{-\frac{1}{2k}})$	$d = \mathcal{O}(n^{2+\frac{2}{4k+1}} \Delta^{-(1+\frac{1}{4k+1})} \varepsilon^{-\frac{1}{4k+1}})$ $g = \tilde{\mathcal{O}}(n^{2+\frac{2}{4k+1}} \Delta^{-(1+\frac{1}{4k+1})} \varepsilon^{-\frac{1}{4k+1}})$

TABLE III. Gate complexity with respect to the maximum simulation time t , target precision ε , and system size n for different Hamiltonians. In the second and third columns, the qubit connectivity is restricted to a linear nearest-neighbour (NN) architecture. The fourth column is the result of our method when there is no restriction on qubit connectivity. In this table, the commutation relation of the Hamiltonian terms is used to improve the system-size scaling. It is worth mentioning that the gate complexity of electronic structure problems studied in this table can be $g = \tilde{\mathcal{O}}(n(\lambda\Delta^{-1}\log\varepsilon^{-1}))^{1+\frac{1}{4k+1}}$ which is nearly linear in n and logarithmic in inverse precision.

note that QSP and methods based on full-order pairing [18] have worse system-size scaling, and thus they are not included in Table III.

The primary contributions of this work are summarised as follows.

1. We provide end-to-end gate complexity analysis of the eigenstate property and energy estimation task, and can achieve nearly logarithmic scaling on inverse precision, with improved scaling on Δ and λ compared to oracle-free methods. The comparison with other methods is shown in Table I and Table II. For electronic structure problems specified in Eq. (6) which is usually compared in the existing literature, the gate complexity for eigenstate property estimation and eigenenergy estimation can be $\tilde{\mathcal{O}}(n(\lambda\Delta^{-1}\log\varepsilon^{-1}))^{1+\frac{1}{4k+1}}$, which is nearly linear in n (excluding the $\log n$ factor) and logarithmic in inverse precision. Note that compared to [51, 55, 56, 62], this result is for the gate count in a single-run circuit with much worse sample complexity.
2. The random sampling approach can exploit the commutation relation of the target Hamiltonian terms to reduce the gate complexity, outperforming QSP for the 1D lattice model. Moreover, our approach favours a linear nearest-neighbour (NN) architecture. When restricted to nearest-neighbour architecture, for the 1D lattice model, the circuit depth scales $d = \mathcal{O}(n^{\frac{2}{4k+1}})$, while the circuit depth in the QETU-Trotter method scales as $d_{\text{QETU}} = \mathcal{O}(n^{1+\frac{1}{2k}})$. For electronic structure problems specified in Eq. (6), when considering the commutation relation and restricting to a NN architecture, the circuit depth is $d = \mathcal{O}(n^{2+\frac{2}{4k+1}})$, while naive implementation of QETU + Trotter requires $d = \Omega(n^{3+\frac{1}{2k}})$. A side product is that controlled $e^{-i\theta H}$ can be implemented by a linear depth circuit $d = \mathcal{O}(n)$ summarised in Proposition 4, comparable to the control-free simulation of electronic problems in [62, 63]. This result could be used as a subroutine in other quantum algorithms.

3. We analyse the actual gate count for typical problems and compare it with the state-of-the-art methods (see Sec. III D for the analytic results and Sec. IV for numerical results).

III. METHODS

In Sec. III A, we first construct the LCU formula for the spectral filter outlined in Fig. 1 and Algorithm 1. The hierarchy of different components in the composite LCU is shown in Fig. 2. Sec. III B shows how errors in observable expectations can be bounded given the approximation error of the composite LCU formula. Sec. III C shows the circuit realisation of the composite LCU form by presenting an explicit form of each circuit instance. An ancilla-free composite LCU formula and measurement scheme is presented for symmetry-conserved cases. Sec. III D analyses the circuit depth and gate complexity for general cases and Hamiltonian-specific cases. Fig. 2 illustrates the proof idea of Theorem 1 and Theorem 2, and shows the connections of different subsections.

A. Composite LCU form of the spectral filter

Now, we show how to construct the composite LCU form of the spectral filter. We mainly consider the Gaussian filter $g_\tau(H) = g(\tau H)$ but present the construction of g in a general form, and hence the results can be readily applied to the investigation of other functions. For the target Hamiltonian H , suppose we want to prepare the j th eigenstate $|u_j\rangle$ with eigenenergy E_j . We consider the spectral filter $g(\tau(H - \omega))$ with $\omega = E_j$, which can be expressed as follows,

$$g(\tau(H - \omega)) = \sum_{i=0}^{N-1} g(\tau(E_i - \omega)) |u_i\rangle \langle u_i|. \quad (7)$$

For an input state $|\psi_0\rangle = \sum_i c_i |u_i\rangle$, the state after applying the spectral filter $g(\tau(H - \omega))$ at a finite τ is given

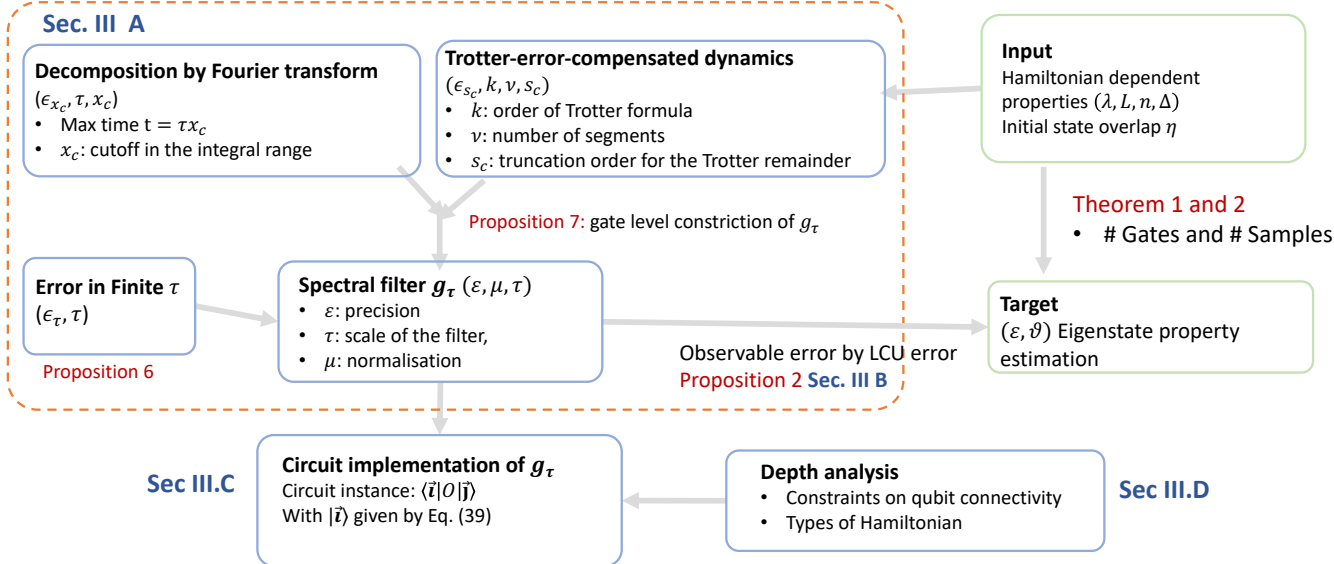


FIG. 2. The diagram illustrates the hierarchy of various components within the composite LCU. The figure shows how different sub-sections in Sec. III connect. This visualisation aids in understanding how the target problem (Problem 1 and Problem 2) can be achieved, specifically, to achieve (ε, ϑ) -eigenstate property estimation. Arrows in the figure indicate direct connections between components. The key parameters relevant to the construction of LCU are highlighted.

by

$$|\psi(\tau)\rangle = \frac{g(\tau(H - \omega)) |\psi_0\rangle}{\|g(\tau(H - \omega)) |\psi_0\rangle\|} = \frac{\sum_i g(\tau(E_i - \omega)) c_i |u_i\rangle}{\sum_i |c_i|^2 g(\tau(E_i - \omega))^2}. \quad (8)$$

It is easy to see that the Gaussian function $g(\tau(E_i - \omega))$ decreases exponentially with τ and $E_i - \omega$. When taking $\omega = E_j$, the amplitudes of the normalised state $|\psi(\tau)\rangle$ concentrate to the eigenstates with energy E_j , and the evolved state asymptotically approximates the eigenstate $|u_j\rangle$ with nonzero $|\langle\psi_0|u_j\rangle|^2 \neq 0$ for sufficiently large τ as $\lim_{\tau \rightarrow \infty} g(\tau(H - E_j)) |\psi_0\rangle \propto |u_j\rangle$.

There are two important parameters τ and ω in the spectral filter $g(\cdot)$, in which τ is a time scaling factor, and $\omega = E_j$ indicates a shift of the original function. We shall see that τ indicates the timescale for the spectral filtering procedure, and larger τ will cool the state closer to the target eigenstate. The shift ω plays an important role in searching the eigenenergies (see Fig. 1(b)) and also the eigenstate property estimation. From the above equation, readers may wonder if we can still get the concentration around the eigenstate $|u_j\rangle$ with energy ω if we do not know the value of E_j a priori. Note that ω only appears in classical post-processing and will not be involved in quantum measurement. In the implementation, we will classically tune ω as a classical variable to find the true eigenenergy while it will not increase any quantum resource cost.

The Gaussian spectral filter can be decomposed into the basis of real-time evolution as

$$g(\tau(H - \omega)) = c \int_{-\infty}^{\infty} dp(x) e^{ix(\omega - H)} \quad (9)$$

with $p(x)$ being a Gaussian distribution. The quantum state given by Eq. (8) becomes

$$|\psi(\tau)\rangle \propto c \int_{-\infty}^{\infty} dp(x) e^{i\tau x \omega} |\phi(x\tau)\rangle, \quad (10)$$

which is now a superposition of real-time evolved states $|\phi(x\tau)\rangle = e^{-ix\tau H} |\psi_0\rangle$ with probability distribution $dp(x) = p(x)dx$.

Instead of preparing the quantum state of Eq. (10), we focus on the goal of obtaining arbitrary observable expectation values. Specifically, we aim to measure any observable O of the evolved state $|\psi(\tau)\rangle$, i.e.,

$$\langle O \rangle_{\psi(\tau)} = \langle \psi(\tau) | O | \psi(\tau) \rangle = \frac{N_\tau(O)}{D_\tau(\omega)}, \quad (11)$$

where

$$D_\tau(\omega) = \langle \psi_0 | g^2(\tau(H - \omega)) | \psi_0 \rangle, \quad (12)$$

$$N_\tau(O) = \langle \psi_0 | g(\tau(H - \omega)) O g(\tau(H - \omega)) | \psi_0 \rangle$$

and we have omitted ω in N_τ to simplify the notation. The denominator is

$$D_\tau(\omega) = c^2 \int_{-\infty}^{\infty} \tilde{p}(x) e^{i\tau x \omega} \langle \psi_0 | e^{-i\tau x H} | \psi_0 \rangle \quad (13)$$

with $d\tilde{p}(x) = \tilde{p}(x)dy$ and $\tilde{p}(x) = \frac{1}{2} \int_{-\infty}^{\infty} p(\frac{z+x}{2})p(\frac{z-x}{2})dz$. The expectation values of the denominator and the numerator can be expressed as $v = \text{Tr}(Og_\tau(H - \omega)\rho_0 g_\tau(H - \omega))$, and the denominator is by taking $O = I$.

For the numerator $N_\tau(O)$, we can efficiently obtain it by sampling the distribution $dp(x, x')$ and then estimating the mean value $\mathbb{E}_{x,x'} \langle \phi(x'\tau) | O | \phi(x\tau) \rangle$, where

each term can be measured by the Hadamard test circuit or using the ancilla-free measurement strategy detailed in Sec. III C. We can similarly obtain the denominator D_τ by estimating $\mathbb{E}_x \langle \psi_0 | e^{-ix\tau H} | \psi_0 \rangle$ with probability $d\tilde{p}(x)$. Therefore, we only need a quantum computer to efficiently estimate the values of state overlaps like $\langle \psi_0 | U | \psi_0 \rangle$ with U being either $e^{ix'\tau H} O e^{-ix\tau H}$ or $e^{-ix\tau H}$. In practice, we also consider a cutoff of the integral from $[-\infty, \infty]$ to $[-x_c, x_c]$ to avoid infinite integration.

The unnormalised eigenstate can be effectively realised by applying a spectral filter $g_{\tau \rightarrow \infty}(H - E_j)$ to an initial state, which holds when the imaginary-time becomes infinity. When $\tau \rightarrow \infty$, one could check that

$$\langle O \rangle = \frac{N_{\tau \rightarrow \infty}(O)}{D_{\tau \rightarrow \infty}}$$

and thus we arrive at the ideal observable expectation. Note that the denominator is nonvanishing $D_{\tau \rightarrow \infty}(E_j) = \eta$ under the assumption. The observable when considering a finite τ is estimated by

$$\langle O \rangle_\tau = \frac{N_\tau(O)}{D_\tau}. \quad (14)$$

Furthermore, to realise the spectral filter with unitary operations, we need to avoid the infinite time length and truncate the time in real-time evolution to a given threshold. Below we discuss the LCU form of g when considering the cutoff.

The Gaussian spectral filter takes an explicit composite LCU form of

$$g_\tau(H - \omega) = c \int_{-x_c}^{+x_c} dx p(x) e^{ix\tau\omega} e^{-ix\tau H} \quad (15)$$

with truncation $[-x_c, x_c]$. The integrand is a real-time evolution with total real-time τx . Suppose that we further use LCU formula to implement $e^{-i\tau x H}$, which takes the form of

$$e^{-i\tau x H} = \mu(x\tau) \sum_{\vec{r} \in \mathcal{K}_x} \Pr(\vec{r}, x\tau, \nu(x\tau)) U_{\vec{r}} \quad (16)$$

where \vec{r} specifies the unitary $U_{\vec{r}}$ involved in the LCU formula of $e^{-i\tau x H}$, $U_{\vec{r}}$ is a unitary operator, and $\Pr(\vec{r}, x\tau, \nu(x\tau))$ represents the normalised decomposition coefficients of $U_{\vec{r}}$. Then, we have

$$\begin{aligned} g_\tau(H - \omega) &= c(\mu) \int_{-x_c}^{+x_c} dx p_\mu(x) e^{i\theta_x} e^{ix\tau\omega} \sum_{\vec{r} \in \mathcal{K}_x} \Pr(\vec{r}, x\tau, \nu(x\tau)) U_{\vec{r}} \\ &\quad (17) \end{aligned}$$

where we defined $c(\mu) := c \int_{-x_c}^{+x_c} p(x) \mu(x\tau) dx$ and $p_\mu(x) = p(x) \mu(x\tau) / c(\mu)$ in a similar vein to Proposition 5.

The central question is how to find the operator $U_{\vec{r}}$ and the corresponding probability distribution, with which the LCU decomposition in Eq. (16) can be determined.

The overall idea is to divide the time evolution into ν segments, and for each segment, we realise both the Trotter evolution and the Trotter error, as proposed in [49]. For evolution time t , let us denote the real-time evolution $U(t) := e^{-iHt} = U_m^\nu$ where $U(m) = e^{imH}$ could be expressed as

$$U(m) = V_{2k}(m) S_{2k}(m), \quad (18)$$

which consists of a deterministic $2k$ th-order Trotter formula S_{2k} and the Trotter remainder V_{2k} . The LCU formula of V_{2k} can be expressed as

$$\tilde{V}_{2k}(m) = \mu(m) \sum_r \Pr(r, m, \nu(m)) W_r \quad (19)$$

where W_k is a unitary operator with the error of the formula $\varepsilon_{2k}(m)$. The overall LCU formula of $U(t)$ is a product of each individual formula

$$U(t) = (U(m))^\nu = \mu(t) \sum_{\vec{r} \in \mathcal{K}_t} \Pr(\vec{r}, t, \nu(t)) U_{\vec{r}} \quad (20)$$

where $\vec{r} := (r_1, r_2, \dots, r_\nu)$ with each U_{r_i} being sampled from the distribution of $\Pr(r, m, \nu(m))$ introduced in Eq. (19) and we denote $\Pr(\vec{r}, t, \nu(t)) := \prod_{i \leq \nu} \Pr(r_i, m, \nu(m))$ and $U_{\vec{r}} := \prod_{i \leq \nu} W_{r_i} S_{2k}$. With some derivation, one can prove that $\mu = \mu(t)^\nu$ and $\varepsilon_{2k}(t) \leq \nu \mu(m) \varepsilon_{2k}(m)$. Eq. (20) shows how $U_{\vec{r}}$ can be sampled and thus how g can be realised. This is illustrated in Fig. 1(a3); in the figure, the index by i is related to the probability $\Pr(i)$ when decomposing g into real-time evolution $U(t_i)$.

Using BCH formula, the $2k$ th-order remainder $V_{2k}(m) := U(m) S_{2k}(m)^\dagger$ has an explicit form of $V_{2k}(m)$ as $V_{2k}(m) = \exp(i \sum_{s=1}^{\infty} E_{2k,s} m^s)$ with Hermitian operators $E_{2k,s}$. Since the $2k$ th-order Trotter error is compensated, we know that $E_{2k,s} = 0$ for $s \leq 2k$. Expanding $V_{2k}(m)$, we have $V_{2k}(m) = \sum_{s=0}^{\infty} F_{2k,s}(m)$ where we group the terms by the order of m , and $F_{1,s}$ denotes the s -order expansion term of $V_{2k}(m)$ with m^s .

Below, we briefly discuss the error in LCU form when considering truncation of s . The truncation error is found to have a quick decrease with an increasing truncation order s_c [49]. Considering of a finite truncation and the vanishing of $F_{2k,s \leq 2k}(m) = 0$, we can rewrite $V_{2k}^{(s_c)}(m)$ as

$$V_{2k}^{(s_c)}(m) = I + \sum_{s=2k+1}^{s_c} F_{2k,s}(m). \quad (21)$$

Given the truncation, the LCU formula for $U(m)$ is

$$U_{2k}^{(s_c)}(m) = V_{2k,s}(m) S_{2k}(m), \quad (22)$$

which consists of a deterministic second-order Trotter formula and the Trotter error compensation term. The overall LCU formula for $U(t)$ is to repeat the sampling of $\tilde{U}_{2k}(m)$ for ν times, $U_{2k}^{(s_c)}(t) = (U_{2k}^{(s_c)}(m))^\nu$ with $\nu = t/m$.

[Eq. \(17\)](#) is a composite LCU formula; more specifically, it is a $(c(\mu), 0)$ LCU formula. When we consider a finite x_c, s_c , it will introduce some errors. When considering a finite s_c , the spectral filter becomes

$$g_{\tau, x_c, s_c}(H - \omega) = c \int_{-x_c}^{x_c} dx p(x) e^{ix\tau\omega} U_{2k}^{(s_c)}(x\tau, \nu(x\tau)) \quad (23)$$

It is easy to check that $\|g_{\tau, x_c, s_c}(H - \omega)\| \leq c(1 + \varepsilon_{s_c})$. The operator distance between g_{τ, x_c} and g_{τ, x_c, s_c} due to finite s_c is

$$\begin{aligned} & \|g_{\tau, x_c} - g_{\tau, x_c, s_c}\| \\ & \leq c \int_{-x_c}^{x_c} dx p(x) e^{ix\tau\omega} \|U(x\tau) - U_{2k}^{(s_c)}(x\tau, \nu(x\tau))\| \leq \varepsilon_{s_c} \end{aligned} \quad (24)$$

when $\|U - U_{2k}^{(s_c)}(x\tau, \nu(x\tau))\| \leq \varepsilon_{s_c}/c$. In order to achieve an additive error of the approximation

$$\|U(t) - U_{2k}^{(s_c)}(t)\| \leq \varepsilon_{s_c} \quad (25)$$

[Lemma 1](#) in the Appendix gives the required segment numbers ν given the truncation order s_c .

With the above result, the total error of the spectral filter g can be bounded by each individual error term. This process is illustrated within the orange box of [Fig. 2](#). Specifically, we can bound the error in spectral filter construction by comparing the operator distance between

$$\|g_{\tau, x_c, s_c} - g_{\tau, x_c, s_c \rightarrow \infty}\|, \quad (26)$$

which gives an upper bound for the numerator and the denominator. Using the triangular inequality, the operator error between g_τ and g_{τ, x_c, s_c} defined in [Eq. \(B26\)](#) is

$$\|g_\tau - g_{\tau, x_c, s_c}\| \leq \varepsilon_{x_c} + \varepsilon_{s_c}. \quad (27)$$

In [Theorem 3](#) in [Sec. B](#), we show that when the segment number is of the order

$$\nu = \mathcal{O}((\lambda\tau x_c)^{1+\frac{1}{4k+1}}) \quad (28)$$

it suffices to ensure the LCU construction error up to ε . Similarly, [Theorem 5](#) in Appendix [Sec. B](#) shows the required segment number for eigenenergy estimation. Together with [Proposition 3](#) in Appendix [Sec. IID](#), one can prove [Theorem 1](#). For the lattice model's eigenstate property estimation, the segment number can be further reduced to $\nu = \mathcal{O}(n^{\frac{2}{4k+1}}(\lambda\tau x_c)^{1+\frac{1}{4k+1}}\varepsilon^{-\frac{1}{4k+1}})$. With this result, one can prove [Theorem 2](#).

B. Observable estimation

Here, we discuss the eigenstate property estimation when the state is filtered under the constructed LCU formula discussed above. We first discuss how to measure the expectation value of observable O . Denote the initial

state on which the spectral operator acts as ρ . The expectation value of observable O on the normalised state can be expressed by

$$\langle O \rangle = \frac{N(O)}{D} = \frac{\text{Tr}(g\rho g^\dagger O)}{\text{Tr}(g\rho g^\dagger)}. \quad (29)$$

We have

$$N(O) = \mu^2 \sum_{ij} \Pr(i) \Pr(j) e^{i(t_i - t_j)\omega} \text{Tr}(U(t_i)\rho U^\dagger(t_j)O). \quad (30)$$

Since $U(t_i)$, $U(t_j)$ are independent, readers may group it and take the symmetric estimator as $\text{Tr}(U(t_i)\rho U(t_j)^\dagger O) + \text{Tr}(U(t_i)\rho U(t_j)^\dagger O)$ to save measurement resources. However, this symmetric estimator is not applicable to dealing with general cases. In the later discussion, we shall see that there is an additional phase factor associated with $U(t_i)$ such that the imaginary part of $\text{Tr}(U(t_i)\rho U(t_j)^\dagger O)$ matter for the final result. For the sake of consistency, we will focus on the discussion on the asymmetric estimator.

Denote the expectation value of the estimator of the numerator over measurement outcomes with $U(t_i)$ and $U(t_j)$, $\text{Tr}(U(t_i)\rho U(t_j)^\dagger O)$, as $\bar{N}_{ij}(O)$. The expectation value of $N(O)$ is given by sampling over the distribution

$$\bar{N}(O) = \mu^2 \mathbb{E}_{ij} \bar{N}_{ij}(O) \quad (31)$$

As random sampling is used in our method, we cannot prepare the state deterministically. However, in terms of the expectation of observables, our scheme owns a similar function to the other schemes.

When considering finite gate complexity and sample complexity, the eigenstate property is estimated by

$$\hat{O}_{\tau, x_c, s_c} = \frac{\hat{N}_{\tau, x_c, s_c}(O)}{\hat{D}_{\tau, x_c, s_c}}. \quad (32)$$

The selection of τ, x_c, s_c can be determined by analysing the error of \hat{O}_{τ, x_c, s_c} compared to the ideal value, which can be analysed using the operator distance detailed in the above section. [Proposition 2](#) shows the error in observable estimation when we are given a (μ, ε) random sampling formula of g . The proof is shown in the Appendix.

Proposition 2 (Observable estimation using the composite LCU formula). *For a target operator g and its (μ, ε) -random-sampling formula defined in [Eq. \(1\)](#), if we estimate the value on the unnormalised state $N_g(O) := \text{Tr}(g\rho g^\dagger O)$ with an initial state ρ and observable O , then the distance between the mean estimator value \hat{O} and the true value $N_g(O)$ is bounded by*

$$\varepsilon_N := |\hat{N}_g(O) - N_g(O)| \leq \|O\|(2\mu^2\varepsilon + \varepsilon_n), \quad (33)$$

with a success probability $1 - \vartheta$. Here, we use the variant of the Hadamard test circuit for $N = \mu^4 \ln(2/\vartheta)/\varepsilon_n^2$ times and $\|O\|$ is the spectral norm of O . The error for the

denominator is bounded as $\varepsilon_D := |\hat{D}_{\bar{g}} - D_g| \leq 2\mu^2\varepsilon + \varepsilon_n$. Given the error ε_D and ε_N , the error for the normalised observable expectation $\langle O \rangle_g = N_g(O)/D_g$ is

$$\left| \frac{\hat{N}_{\bar{g}}(O)}{\hat{D}_{\bar{g}}} - \frac{N_g(O)}{D_g} \right| \leq \frac{1}{D_g} ((\langle O \rangle + 1)\varepsilon_D + \varepsilon_N). \quad (34)$$

Given [Proposition 2](#), the error of the observables can be bounded given the RLCU form. We remark that the random sampling algorithm is not a deterministic state preparation that cannot prepare the target state σ . However, when we focus on the property estimation of the target state, the estimator owns similar performance to the normal Hamiltonian simulation methods: the sample complexities of the former algorithms and RLCU algorithm to learn the observable properties of the state are similar, as long as the norm of the estimator is a constant. This is guaranteed by [Proposition 2](#).

Using these results of error propagation in the LCU form, we can determine the required segment number ν_c in order to achieve the desired accuracy as shown in [Eq. \(28\)](#). [Theorem 3](#) in Appendix [Sec. B](#) and [Theorem 5](#) in Appendix [Sec. C](#) present the required segment number ν_c and the gate count (with the prefactors included) for achieving desired accuracy for two tasks, which will be used to estimate the actual gate numbers needed for physical Hamiltonians.

The total gate count is determined by multiplying ν_c and the gate count for realising S_{2k} and V_{2k} within each segment, denoted by g hereafter. The gate count for lattice models is straightforward $g = \mathcal{O}(n)$. For electronic structure problem in [Eq. \(6\)](#), a naive realisation of S_{2k} and V_{2k} will result in the cost $g = \mathcal{O}(n^3)$. However, we could bring down the scaling by considering the properties of fermions. The kinetic operator is quadratic and thus can be diagonalised by an efficient circuit transformation, either by Givens rotations or fermionic fast Fourier transform (FFFT) [58, 62, 63]. By using the results in [64], $e^{-im\hat{T}}$ and $e^{-im\hat{V}}$ can be implemented with $\mathcal{O}(n \log n)$ gates with m being the time length. The compensation term will cost $\mathcal{O}(n)$ gates. Therefore, we have $g = \mathcal{O}(n \log n)$ and the total gate count for electronic structure problem is $g_{\text{tot}} = \tilde{\mathcal{O}}(n(\lambda\Delta^{-1})^{1+\frac{1}{4k+1}} \log \varepsilon^{-1})$.

C. Estimation by quantum circuits: general strategy and ancilla-free strategy

In this section, we discuss the circuit realisation for [Algorithm 1](#). For symmetry-conserved cases, we introduce an ancilla-free LCU construction strategy and the corresponding measurement strategy. To estimate an observable, a quantum computer is only used for estimating the quantity involving real-time evolution $\langle U^\dagger(t_j)OU(t_i) \rangle$, where $U(t_i) = e^{-iHt_i}$. As that $U(t_i)$ is implemented by a Trotter-LCU formula in [Eq. \(18\)](#), involving the Trotter operator S_{2k} and the Trotter error compensation term

$V_{2k}^{(s)}$, the unitary can be expressed in an explicit LCU form as

$$U(t_i) = \mu \sum_{\vec{i}} \Pr(\vec{i}) \prod_{q=1}^{\nu} W_{i_q} S \quad (35)$$

where $\vec{i} = (i_1, i_2, \dots, i_\nu)$. The observable expectation is

$$\langle U^\dagger(t_j)OU(t_i) \rangle = \mu^2 \sum_{\vec{i}, \vec{j}} \Pr(\vec{i}) \Pr(\vec{j}) \langle \vec{j} | O | \vec{i} \rangle \quad (36)$$

where we denote $|\vec{i}\rangle := \prod_{q=1}^{\nu} W_{i_q} S |\psi_0\rangle$.

To measure $\langle \vec{j} | O | \vec{i} \rangle$, we can use the Hadamard test circuit with an extra ancillary qubit. For Hamiltonians with certain symmetries, we do not need this ancillary qubit and thus do not require any controlled operation. Below, we first introduce the general cases by introducing an ancillary qubit. Then we discuss the ancilla-free composite LCU formula and the corresponding measurement schemes.

1. General cases

There are two extreme cases: Case I $t_i = 0$ (or $t_j = 0$) and Case II $t_i = t_j$. For $t_j = 0$, each component in [Eq. \(36\)](#) $\langle \psi_0 | O | \vec{i} \rangle$ can be measured using a Hadamard test circuit, which is the circuit depicted in the green box in [Fig. 1\(c\)](#).

For $0 < t_j < t_i$, suppose that $U(t_j)$ is divided into m segments and $U(t_i)$ is divided into ν segments with the first m segments being set the same as that of $U(t_i)$. The quantum circuit that can measure $\langle \vec{j} | O | \vec{i} \rangle$ is shown in [Fig. 1](#). After post-selecting $|+\rangle$ on the ancillary qubit (but before measurements on B), the circuit on system B outputs

$$\frac{1}{2} \left(\prod_{q=1}^m W_{i_q} S + \prod_{q=1}^{\nu} W_{i_q} S \right) |\psi_0\rangle \quad (37)$$

The case of $t_i = t_j$ is a special case in [Fig. 1\(c1\)](#) by only implementing the circuits in the orange box.

Here, we can use a single-shot measurement strategy to estimate $N(O)$ in [Eq. \(30\)](#). Suppose that the sequence of the unitary operators has been obtained from sampling. To measure $\langle \vec{j} | O | \vec{i} \rangle$, we can use the circuit in [Fig. 1\(c1\)](#). We first prepare the state $|\psi_0\rangle$ and an extra ancillary qubit prepared on $|+\rangle$. Afterwards, we perform a C-U gate from ancillary to $|\psi_0\rangle$. If we directly measure the ancillary qubit on the X-basis, the outcome a will be 0 with a probability of $\Pr(a=0) = \frac{1}{2}(1 + \text{Re}(\langle \vec{j} | O | \vec{i} \rangle))$ and 1 with a probability of $\Pr(a=1) = \frac{1}{2}(1 - \text{Re}(\langle \vec{j} | O | \vec{i} \rangle))$. Then we add a phase gate $S = R_z(\frac{\pi}{2})$ before measurement. The outcome b will be 0 with a probability of $\Pr(b=0) = \frac{1}{2}(1 + \text{Im}(\langle \vec{j} | O | \vec{i} \rangle))$ and 1 with a probability of $\Pr(b=1) = \frac{1}{2}(1 - \text{Im}(\langle \vec{j} | O | \vec{i} \rangle))$.

We consider the estimator as

$$\hat{d} = (-1)^a + i(-1)^b \quad (38)$$

based on the measurement outcome a and b obtained from the above circuit. \hat{d} is an unbiased estimator of $\langle \vec{j}|O|\vec{i}\rangle$. One can verify that

$$\mathbb{E}_a(-1)^a = \text{Re}(\langle \vec{j}|O|\vec{i}\rangle), \quad \mathbb{E}_b(-1)^b = \text{Im}(\langle \vec{j}|O|\vec{i}\rangle) \quad (39)$$

and thus $\mathbb{E}_{a,b}\hat{d} = \langle \vec{j}|O|\vec{i}\rangle$.

We take an estimator as

$$\hat{v} = c^2(\mu)e^{i\omega(t_i-t_j)}\hat{d} \quad (40)$$

The estimator \hat{v} defined in Eq. (40) is an unbiased estimator of $\langle \psi_0|g_\tau(H-\omega)Og_\tau(H-\omega)\psi_0\rangle$,

$$\mathbb{E}_{t_i,t_j,\vec{i},\vec{j}}\mathbb{E}_{a,b}\hat{v} = \langle \psi_0|g_\tau(H-\omega)Og_\tau(H-\omega)\psi_0\rangle. \quad (41)$$

By analysing the error dependence on the finite τ , x_c , segment number ν in Eq. (28), we arrive at the result of property estimation in Theorem 1 (see detailed description in Theorem 3 and Theorem 5). More detailed proof can be found in Appendix Sec. B and Sec. C.

2. Ancilla-free composite LCU formula and the corresponding measurement scheme for symmetry conserved systems

In the above section, given a sampled configuration $(t_i, t_j, \vec{i}, \vec{j})$, the real and imaginary part of $\langle \vec{j}|O|\vec{i}\rangle$ can be obtained by the circuit in Fig. 1(c). In cases of the Heisenberg model and electronic structure problems (Eq. (6)), the target problem has certain symmetries S satisfying $[H, S] = 0$. For symmetry-conserved systems with $[U, S] = 0$, it is possible to estimate the expectation value of a unitary $\langle \psi_0|U|\psi_0\rangle$ without ancilla, as proposed in [42, 65, 66]. However, the issue here is that as the unitary operator is realised by a Trotter-LCU expansion in Eq. (35), at least there exists a Pauli operator W_{i_q} that does not commute with S . In this section, we first briefly introduce how to measure $\langle \psi_0|U|\psi_0\rangle$ without ancilla, where the unitary is either $U = e^{-iHt}$ or $U = e^{-iHt_1}\hat{O}e^{-iHt_2}$. Then we show how to design the unitary in Eq. (35) such that $[U, S] = 0$.

The expectation value $\langle \psi_0|U|\psi_0\rangle$ can be expressed as $\langle \psi_0|U|\psi_0\rangle = re^{i\theta}$. If $|\psi_0\rangle$ is a product state, or can be prepared as $|\psi_0\rangle = U_p|0\rangle^{\otimes n}$, the amplitude of the expectation value $r = |\langle \psi_0|U|\psi_0\rangle|$ can be obtained by measuring $U_p^\dagger U U_p|0\rangle^{\otimes n}$ in the computational basis. The next step is to obtain the phase θ , for which we can make use of the fact that the unitary operation conserves the symmetry of S , $[U, S] = 0$. To do so, we need to introduce a reference state $|\psi_{\text{Ref}}\rangle$, which lies in a different sector of the initial state, such that $\langle \psi_{\text{Ref}}|U|\psi_0\rangle = 0$. We assume that $\langle \psi_{\text{Ref}}|U|\psi_{\text{Ref}}\rangle$ can be computed classically. In addition, the following state can be prepared

$$|\phi_0\rangle = U_p|\psi_0\rangle = \frac{1}{\sqrt{2}}(|\psi_{\text{Ref}}\rangle + |\psi_0\rangle).$$

As $r_s = |\langle \psi_0|U_p^\dagger U U_p|\psi_0\rangle|$ can be measured on a computational basis, the phase θ can be computed.

The requirements of this protocol include the preparation of the superposition state and efficient computation of $\langle \psi_{\text{Ref}}|U|\psi_{\text{Ref}}\rangle$. Let us take the fermionic Hamiltonian as an example (note that the Heisenberg model can be regarded as a 1D Fermi-Hubbard model after the Jordan-Wigner transformation). If the reference state is the vacuum state with the number of particles being zero, then $\langle \psi_{\text{Ref}}|U|\psi_{\text{Ref}}\rangle$ can be computed classically. The Hartree-Fock state takes the simple product-state form $|\psi_0\rangle = |1\rangle^{\otimes N_e}|0\rangle^{\otimes N-N_e} \in \{|N_e\rangle\}$, where the first N_e qubits are prepared in the $|1\rangle$ states and the rest of the qubits remain in the $|0\rangle$ states. To prepare the target superposition state, $|\phi_0\rangle$, the Hadamard gate is applied to the first qubit, followed by a ladder of CNOT gates applied up to the N_e th qubit, resulting in a total of $N_e - 1$ CNOT gate operations.

To measure $\langle \vec{j}|O|\vec{i}\rangle$, we can use the circuit in Fig. 1(c) to generate

$$U_p^\dagger \left(\prod_{q=1}^{\nu} W_{i_q} S \right)^\dagger O \prod_{q=1}^m W_{i_q} S U_p |\psi_0\rangle, \quad (42)$$

and then measure on a computational basis.

In our case, we need to implement the Trotter formula S and the Trotter remainder V . For the implementation of S , we need to pair the terms to ensure each individual term does not break the symmetry. Take the quantum chemistry problems, $H = \hat{T} + \hat{V}$, for example. We group the term $\hat{T}_{ij} = h_{ij}(\hat{a}_i^\dagger \hat{a}_j + \hat{a}_j^\dagger \hat{a}_i)$ in the kinetic term \hat{T} , which conserve the particle number. Its exponentiation $e^{-i\theta \hat{T}_{ij}}$ can be directly implemented, which is similar to the implementation for the Heisenberg model case. For the potential V , we can group $g_{ijkl}(\hat{a}_i^\dagger \hat{a}_j^\dagger \hat{a}_k \hat{a}_l + \hat{a}_l^\dagger \hat{a}_k^\dagger \hat{a}_j \hat{a}_i)$ and implement its exponentiation similarly.

The issue is that if we expand the Trotter remainder into Pauli bases, then applying each individual Pauli term will break the symmetry. One may think of expanding it into

$$V(m) = US^\dagger = \sum_{k,l,i,j} \hat{T}_i^k \hat{V}_j^l m^{k+l} \quad (43)$$

where \hat{T}_i and \hat{V}_j are components of the kinetic and potential terms, respectively. Although each term conserves the symmetry, the issue is that \hat{T}_i or \hat{V}_j is not unitary, and cannot be implemented directly. To address this issue, we decompose the Hamiltonian into SWAP and tensor products of Pauli-Z operators rather than Pauli operators. Let us give an example of the 1D Fermi-Hubbard model, which after the Jordan-Wigner Transformation takes the form of

$$H = J_1 \sum_i X_i X_{i+1} + Y_i Y_{i+1} + J_2 \sum_i Z_i Z_{i+1} + h_z \sum_i Z_i \quad (44)$$

which is the XXZ Heisenberg Hamiltonian. We reformulate it into the following

$$H = 4J_1 \sum_i \text{SWAP}_{i,i+1} + (J_2 - J_1) \sum_i Z_i Z_{i+1} + h_z \sum_i Z_i. \quad (45)$$

Note that the identity term in the Hamiltonian is a trivial term, so it is always removed in the Hamiltonian in this work for simplicity. Now, each individual term is unitary, and commutes with the particle number operator.

For electronic problems in Eq. (6) or more general cases, the Hamiltonian can be reformulated with SWAP and Pauli Z operators. The kinetic term, $\hat{T}_{ij} = \frac{h_{ij}}{2}(X_i X_j \otimes_{k=i+1}^{j-1} Z_k + Y_i Y_j \otimes_{k=i+1}^{j-1} Z_k)$ can be reformulated as

$$\hat{T}_{ij} = h_{ij}(2 \text{SWAP}_{i,j} \otimes_{k=i+1}^{j-1} Z_k - \frac{1}{2} \otimes_{k=i}^j Z_k).$$

The potential term \hat{V}_{ijkl} can be similarly reformulated such that each individual term commutes with the particle number operator.

We note that although we reformulate the Hamiltonian in the basis of SWAP and Pauli Z operators, the implementation of the Trotter formulae remains the same as that in the Pauli basis. Only the compensation term will be different compared to the case with one ancillary qubit. As shown in Sec. IIID2, the ancilla-free measurement strategy shows advantages when qubit connectivity is restricted.

D. Analysis of circuit depth and gate complexity

We first discuss the gate complexity for general Hamiltonians in Sec. IIID1. In Sec. IIID2, we analyse the circuit depth and gate complexity for various Hamiltonians of physical relevance when using either our method or other early fault-tolerant quantum algorithms. A comparison with a focus on circuit depth for each elementary block is shown in Table IV which supports the results in Table III.

1. Gate complexity for general cases

The maximum resource appears in the case when $t_j = 0$, in which case we need to implement one controlled Trotter formula plus two controlled compensation terms specified by V_i . The minimum resource appears in the case when $t_j = t_i$, in which case we need to implement the Trotter formula plus two controlled compensation terms specified by V_i . This is because a controlled Trotter is more costly than a controlled compensation operation, as analysed in Proposition 3. The resources in other cases with $t_j < t_i$ will be between Case I and Case II.

We define the following characters of the Hamiltonian,

$$\begin{aligned} \text{wt}(H) &:= \sum_{l=1}^L \text{wt}(P_l) \\ \text{wt}_m(H) &:= \max_l \text{wt}(P_l) \end{aligned} \quad (46)$$

Here, $\text{wt}(P_l)$ indicates the weight of the Pauli operator P_l , i.e., the number of $\{X, Y, Z\}$ terms in P_l . The following result gives

Proposition 3 (Gate complexity analysis). *Suppose the composite LCU is realised by Algorithm 1 and the Hamiltonian dynamics $U = e^{-iHt}$ is realised by Eq. (35) with the maximum segment number ν . The gate complexity of the circuit instance in eigenstate property estimation is the following: CNOT gate number: $\nu(4 \times 5^{k-1} \text{wt}(H) + 4 \text{wt}_m(H) + 2 \min(n, s_c \text{wt}_m)) - 2L$, single-qubit Pauli rotation gate number: $(2L + 4)\nu$.*

We give more details in the following. Overall, the circuit within each segment consists of one controlled Trotter plus controlled compensation terms. Each of the components within the Trotter formula takes the form of e^{-iHm} with evolution time $m = t/\nu$. The cost by Trotter is given in Lemma 3.

Note that a controlled-Pauli-rotation gate, $\text{Ctrl-exp}(-iP\theta/2)$ with Pauli operator P , can be realised by $2(\text{wt}(H) - 1)$ CNOT gates, a controlled single-qubit Z -axis Pauli rotation gate $R_z(\theta)$ with rotation angle θ , and some single-qubit Clifford gates. Furthermore, we can decompose the controlled single-qubit Pauli rotation gate into two single-qubit Z -axis rotation gates and two CNOT gates. Therefore, the cost for the controlled Trotter operator $\text{Ctrl-}S_{2k}(m)$, in each segment, the number of CNOT gates are $2 \times 5^{k-1}(2 \text{wt}(H) - 2L)$ and $2L$ controlled single-qubit Pauli rotations.

The compensation term V consists of a controlled multi-qubit Pauli rotation operator and some controlled Pauli operators. The controlled multi-qubit Pauli rotation operator can be realised by $2 \text{wt}_m(H)$ CNOT gates and two single-qubit Pauli rotations. The Pauli gates are randomly drawn from $\{P_l\}_l$ according to the corresponding probability distribution. In the worst case, the gate sequence length is the truncated value s_c , and thus the CNOT gate number is bounded by $s_c \text{wt}_m(H)$. There is a saturation when the number of the compensation Pauli operations reaches n . To sum up, for the compensation term, the number of CNOT gates is upper bounded by

$$2 \text{wt}_m(H) + \min(n, s_c \text{wt}_m) \leq 3n \quad (47)$$

and 2 single-qubit Pauli rotations. We note that since there is a saturation of the gate count for the Trotter-error-compensation indicated by Eq. (47), we take s_c to be infinity in deriving the asymptotic scaling in gate complexity in Theorem 1 and Theorem 2.

With the above results, it is easy to check that Case I is more costly than Case II in Fig. 1. For observable

Hamiltonians	NN (ancilla-free)	NN (1-ancilla)	QETU [48]	arbitrary
Heisenberg model	$\mathbf{d} = \mathcal{O}(1)$ $g = \mathcal{O}(n)$	$d = \mathcal{O}(n)$ $g = \mathcal{O}(n)$	$d = \mathcal{O}(n)$ $g = \mathcal{O}(n)$	$d = \mathcal{O}(1)$ $g = \mathcal{O}(n)$
Electronic structure (Eq. (6))	$\mathbf{d} = \mathcal{O}(n)$ $g = \mathcal{O}(n^2)$ $\mathbf{d} = \mathcal{O}(n)$ ([$n/2$] ancilla)	$d = \Omega(n^2)$ $g = \mathcal{O}(n^3)$	$d = \Omega(n^2)$ $g = \mathcal{O}(n^3)$	$d = \mathcal{O}(n)$ $g = \mathcal{O}(n \log n)$
Molecular Hamiltonians (Eq. (50))	$d = \mathcal{O}(n^2)$ $g = \mathcal{O}(n^3)$	$d = \Omega(n^3)$ $g = \mathcal{O}(n^4)$	$d = \Omega(n^3)$ $g = \mathcal{O}(n^4)$	$d = \mathcal{O}(n^2)$ $g = \mathcal{O}(n^2 \log n)$

TABLE IV. Circuit depth d and gate count g in each segment when using our scheme. We consider the restricted qubit structure with nearest-neighbour architecture or arbitrary architecture (which has all-to-all connectivity). We compare the ancilla-free or the 1-ancilla schemes. Note that when considering the all-to-all connectivity, both schemes have the same gate and depth complexity. We compare our method with the QETU. Note that the control-free version of QETU has the same depth scaling as the controlled scheme.

dynamics described in Eq. (36), there are two compensation terms, but simply one controlled Trotter Ctrl- S_{2k} , as illustrated in Fig. 1(c1). Together with the cost for the Trotter formula, the number of CNOT gates is upper bounded by

$$\nu(4 \times 5^k \text{wt}(H) - 2L + 4 \text{wt}_m(H) + 2 \min(n, s_c \text{wt}_m)). \quad (48)$$

The number of single-qubit Pauli rotations is $(2L + 4)\nu$.

The gate complexity of the ancilla-free measurement strategy can be analysed in a similar way. We emphasise that the advantage of the ancilla-free measurement scheme is that it allows the compilation with nearest-neighbour coupling only, which is discussed in Sec. III D 2 in detail.

2. Circuit compilation for typical Hamiltonians and circuit depth analysis

In this section, we show the circuit depth for typical Hamiltonians including (1) Heisenberg models, (2) electronic structure in the plane wave dual basis in Eq. (6), and (3) second-quantised molecular Hamiltonian which takes the following form

$$H = \sum_{i,j=1}^n h_{ij} \hat{a}_i^\dagger \hat{a}_j + \frac{1}{2} \sum_{i,j,k,l=1}^n V_{ijkl} \hat{a}_i^\dagger \hat{a}_j^\dagger \hat{a}_k \hat{a}_l, \quad (49)$$

where n is the number of spin orbitals of the molecular system; \hat{a}_i^\dagger and \hat{a}_i are the fermionic creation and annihilation operators, respectively; h_{ij} and V_{ijkl} are the corresponding coefficients for the one-body and two-body interactions, respectively. For quantum chemistry Hamiltonians, there has been considerable progress [55, 67] in efficiently representing the Hamiltonians with fewer terms and low weights, such as single factorisation [57] and double factorisation [68]. A common strategy is to reformulate the two-body fermionic operators as a sum of squared one-body operators by the Cholesky decom-

position [67], reformulated as

$$H = \hat{K} + \frac{1}{2} \sum_{\ell}^{\Gamma} \hat{L}_{\ell}^2, \quad (50)$$

where \hat{K} and \hat{L}_{ℓ} are the one-body terms, the number of terms is $\Gamma = \mathcal{O}(n)$ [55], and the constant has been removed.

We analyse the circuit depth for the task of eigenstate property estimation with nearest-neighbour architecture. We will consider two scenarios: (1) the qubit connectivity is restricted to a linear nearest-neighbour architecture; (2) arbitrary connectivity is allowed. We will analyse the circuit depth and gate complexity for typical Hamiltonians using either the ancilla-free scheme or the one-ancilla scheme.

Within each segment, the circuit consists of two parts: the implementation of the Trotter formula S and the Trotter remainder V . As aforementioned, the implementation of S is the same for either the ancilla-free scheme or the one-ancilla scheme. The only difference is the compensation term, which uses the symmetry-conserved gates as the elementary gates, i.e., SWAP, Pauli-Z gates and their exponentiations. However, we observe that the compensation term requires at most $d = \mathcal{O}(n)$ and $g = \mathcal{O}(n)$ in the worse case, which is fewer than the implementation of the Trotter formula in all cases. In Table IV, we show the gate complexity (including both two-qubit Clifford gates and non-Clifford gates) within each segment when taking the qubit connectivity into account. Below, we elaborate on these results.

We first discuss the Heisenberg-type Hamiltonians given by Eq. (44). Each component $e^{-im(J_1 X_i X_{i+1} + J_1 Y_i Y_{i+1} + J_2 Z_i Z_{i+1})}$ with time duration m can be realised by 3 CNOT gates and 3 single-qubit Pauli rotation gates as proposed by [69]. When restricted to a linear nearest-neighbour architecture, $d_{\text{Trotter}} = \mathcal{O}(1)$. In the ancilla-free scenario, the compensation term is SWAP $_{i,i+1}$, Pauli-Z operators and the exponentiations, resulting in $d = \mathcal{O}(1)$ and $g = \mathcal{O}(n)$. In the one-ancilla scenario, since we need to implement controlled

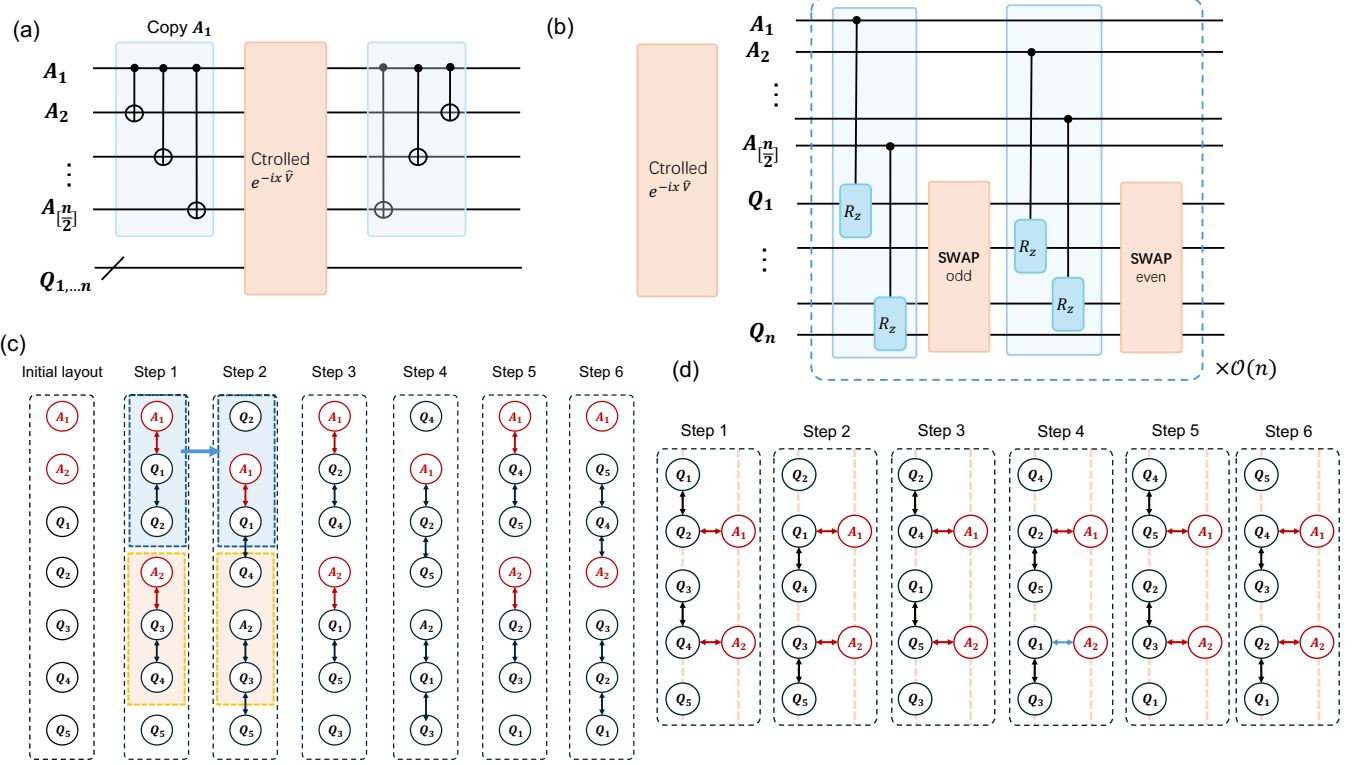


FIG. 3. An example of how to use $[\frac{n}{2}]$ extra ancillary qubits to realise controlled exponentiation of potential terms $\text{Ctrl-}e^{-ix\hat{V}}$ with a NN architecture. $[\frac{n}{2}]$ ancillary qubits are introduced to reduce the depth from $\mathcal{O}(n^3)$ to $\mathcal{O}(n)$. (a) Copy the data on the qubit A_1 to $A_2, \dots, A_{[\frac{n}{2}]}$, and the undo the copy operation. This circuit is equivalent to using A_1 as the single-controlled qubit to control all the other physical qubits Q_1 to Q_n . The advantage of introducing the copy operation is that all the controlled rotation (shaded blue box in (b)) can be realised by nearest-neighbour gates. (b) The circuit block controlled $e^{-ix\hat{V}}$ consists of exponentiation of of nearest-neighbour operations $e^{-iZ_i Z_{i+1}}$ followed by $[\frac{n}{2}]$ SWAP operations. The circuit block in (b) is repeated $\mathcal{O}(n)$ times. An example is shown in (c). The CNOT operations are omitted in the sub-figure. (c) 1D linear architecture. Q_i represents the n th physical qubit (encoding the n th spin orbitals), and A_i represents the i th ancillary qubit. The ancillary qubits A_i $i = 1, 2, \dots, [\frac{n}{2}]$ and actual qubits Q_i $i = 1, 2, \dots, n$ can be placed in the way shown in Step 1 in $\mathcal{O}(n)$ depth. The red arrow connecting A_i and Q_j is used to represent to perform the exponentiation of $e^{-iZ_j Z_k}$ where Q_j and Q_k are adjacent qubits. The black arrow connecting different qubits Q_j and Q_k is used to represent to perform the corresponding CNOT operation as a subroutine in the exponentiation of $e^{-iZ_j Z_k}$, followed by a SWAP operation. The transformation from the shaded blue and orange boxes in Step 1 to Step 2 can be realised by 2 SWAP gates (cyclic swap operation). The rest of the transformation is realised in the same way. (d) 2D planer architecture. The qubit connectivity is represented by the orange dashed line.

two-qubit Pauli rotations, when restricted to linear nearest-neighbour architecture, we need to swap the ancillary qubit sequentially to qubit $1, \dots, n$ and then perform the controlled rotation. Then, we need to undo the swap to change back the ordering of the qubits. The compensation term can be done when the ancillary qubit is adjacent to the target controlled qubit. Compared to the ancilla-free scheme, we cannot do it in parallel, resulting in $d = \mathcal{O}(n)$ and $g = \mathcal{O}(n)$. When removing the restriction of the qubit connectivity, both scenarios have $d = \mathcal{O}(1)$ and $g = \mathcal{O}(n)$.

For the electronic structure problem in Eq. (6), it can be grouped into $H = \hat{T} + \hat{V}$. Below, we discuss the cost for the ancilla-free scheme and the one-ancilla scheme with a linear nearest-neighbour architecture. The kinetic term is a non-interacting term which can be di-

agonised as $\hat{T} = \hat{C}(\sum_i \alpha_i \hat{n}_i)\hat{C}^\dagger$. For the implementation of $e^{-i\theta\hat{T}}$, a NN architecture requires $d = \mathcal{O}(n)$ and $g = \mathcal{O}(n^2)$. For the interacting potential term $e^{-i\theta\hat{V}}$ which consists of $\mathcal{O}(n^2)$ terms, a NN architecture requires $d = \mathcal{O}(n)$ and $g = \mathcal{O}(n^2)$. Therefore, $d_{\text{Trotter}} = \mathcal{O}(n)$ and $g_{\text{Trotter}} = \mathcal{O}(n^2)$. For the compensation term, since there is only one term in the form of $\text{SWAP}_{i,j} \otimes_{k=i+1}^{j-1} Z_k$ or $\otimes_{k=i+1}^{j-1} Z_k$ or $\otimes_{k=i}^j Z_k$, which can be implemented at most $d_{\text{Remainder}} = \mathcal{O}(n)$ and $g_{\text{Remainder}} = \mathcal{O}(n)$. We note that for the 2D Fermi-Hubbard model, which is a special case of Eq. (6), the compensation term can be implemented with $d_{\text{Remainder}} = 1$ given a planer nearest-neighbour architecture. To sum up, a NN architecture requires $d = \mathcal{O}(n)$ and $g = \mathcal{O}(n^2)$.

For the one-ancilla scheme, the first observation is that

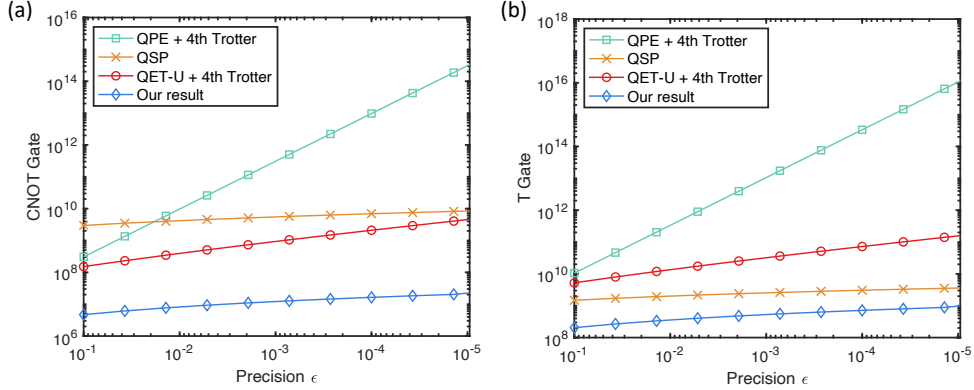


FIG. 4. Resource estimation (the number of CNOT gates and T gates) for the eigenstate property estimation for the 50-site 1D Heisenberg Hamiltonian with different target precision. The energy gap is fixed as $\Delta = 0.5$. We compare the gate count involved in different methods. The commutation relations are taken into account. The second-order paired Taylor series method is used in our result.

we do not need to implement controlled \hat{C} . The rest of the diagonal part is similar to the case of the Heisenberg model, which requires $d = \mathcal{O}(n)$ and $g = \mathcal{O}(n)$. The implementation of $e^{-i\theta\hat{T}}$ requires $d = \mathcal{O}(n)$ and $g = \mathcal{O}(n^2)$. However, the implementation of $e^{-i\theta\hat{V}}$ requires $d = \Omega(n^2)$ and $g = \Omega(n^2)$ in a NN architecture. The challenge of realising the controlled \hat{V} with one control qubit is that at each time, the control qubit can only control one rotation $R_z(\theta_{ij})$ given a pair of (i, j) . Therefore, the controlled rotation cannot be realised in parallel. Naively, we could first apply a cyclic swap operation and then realise each individual $R_z(\theta_{ij})$, with the total depth $d = \mathcal{O}(n^3)$. A lower bound of the depth complexity of realising the controlled \hat{V} is $\Omega(n^2)$. The compensation term requires at most $d = \mathcal{O}(n)$ and $g = \mathcal{O}(n)$. Therefore, a NN architecture requires $d = \mathcal{O}(n^2)$ and $g = \mathcal{O}(n^2)$.

The depth can be reduced to $\mathcal{O}(n)$ provided $[n/2]$ ancillary qubits. The result is summarised in [Proposition 4](#).

Proposition 4. *When restricted to linear nearest-neighbour qubit connectivity, a controlled exponentiation $\text{Ctrl-}e^{i\theta H}$ with electronic problems' Hamiltonian H in [Eq. \(6\)](#) and an angle θ can be realised in depth $\mathcal{O}(n)$ with $[n/2]$ ancillary qubits. The circuit implementation is illustrated in [Fig. 3](#). When restricted to only one ancillary qubit, the circuit depth is $\Omega(n^2)$.*

A graphic proof is shown in [Fig. 3](#). [Fig. 3\(a,b\)](#) shows the overall structure of the circuit with $\mathcal{O}(n)$ depth. [Fig. 3\(a\)](#) shows how to copy the information of A_1 to the rest of ancilla and finally give it back to A_1 . By using the circuit illustrated in [Fig. 3\(c\)](#) for 1D architecture and [Fig. 3\(d\)](#) for 2D architecture, the controlled- H can be realised with only NN operations.

When considering an arbitrary architecture, the gate count can be further reduced from $\mathcal{O}(n^2)$ to $\mathcal{O}(n \log n)$ using the results in [\[64\]](#). The exponentiation of $e^{-ix\hat{T}}$ can be implemented by FFT, $\text{FFFT}e^{-i\sum_i t_i \hat{n}_i} \text{FFFT}^\dagger$, which can be implemented with $g = \mathcal{O}(n \log n)$ and

$d = \mathcal{O}(\log n)$. The exponentiation of $e^{-ix\hat{V}}$ can be implemented with $d = \mathcal{O}(n)$ and $g = \mathcal{O}(n \log n)$. In addition, we discuss the case of molecular Hamiltonians in [Eq. \(50\)](#) when Cholesky decomposition is applied. The dominant cost comes from the potential terms. We summarise the results in [Table IV](#).

Our method shows advantages in circuit depth when considering a linear NN architecture. We emphasise that the circuit depth and gate complexity of our ancilla-free scheme match the complexity of implementing Trotter formulae, even though the eigenstate task is more complicated than the dynamics problem. [Table III](#) displays the total gate and depth complexity concerning both CNOT and T gates, which can be obtained by using the cost within each segment shown in [Table IV](#).

QETU method requires one ancillary qubit because of the phase iteration. For certain Hamiltonians, if there exists a single Pauli operator K_j such that it anticommutes with each component of H , then the evolution can be implemented in a control-free way. For example, for Heisenberg models, we can divide the Hamiltonian into three terms $H = H_X + H_Y + H_Z$ where H_X, H_Y, H_Z contains tensor products of Pauli X, Y, Z , respectively. For H_X , we can choose $K_1 = \otimes_{i \in \text{odd}} X_i \otimes_{i \in \text{even}} Y_i$. However, the controlled- K operations still need depth $d_K = \mathcal{O}(n)$, as opposed to $d = \mathcal{O}(1)$ in our ancilla-free scheme. For electronic structure problems, to reduce the Trotter error and implement the operations in parallel, we can group the Hamiltonian into \hat{T} and \hat{V} , in which case it is difficult to find a Pauli operation K such that it commutes with the grouped term. If the Hamiltonian is not grouped, then the circuit depth will be increased to $d = \mathcal{O}(n^3)$ in a naive way of implementing each individual term.

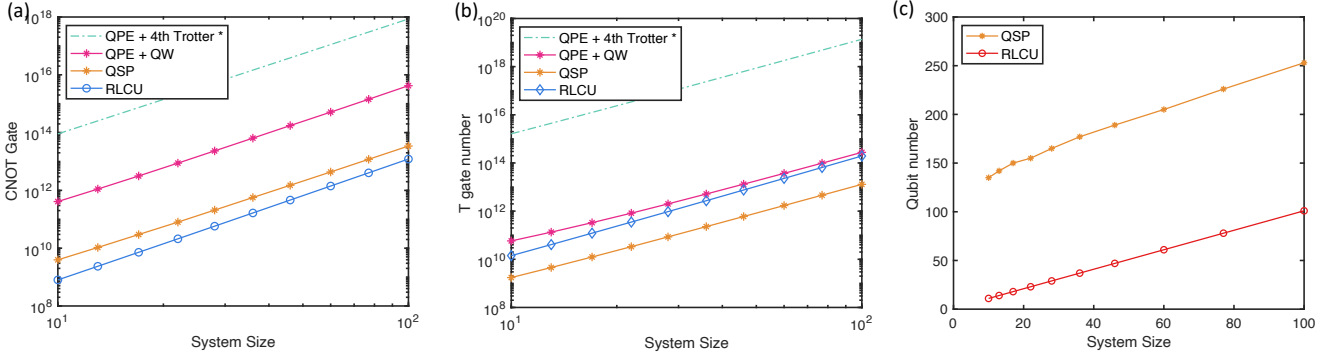


FIG. 5. Resource estimation (the number of CNOT gates and T gates) for the eigenstate property estimation for the 2-local Hamiltonian, $H = \sum_{i,j} X_i X_j + \sum_i Z_i$, in which case the commutator relation between different Hamiltonian summands is ignored. Here 4th-order random Trotter formula is used, which is marked by an asterisk alongside Trotter in the legend. We compare the gate count involved in different methods.

IV. RESOURCE ESTIMATIONS

In this section, we compare the resource costs associated with different algorithms, focusing on the number of qubits, CNOT gate count, and non-Clifford gate count across various models. We will consider the one-dimensional Heisenberg model with NN coupling, 2-local spin model, and molecules. The algorithms compared in this section include QPE, QSP, and QETU. The QPE method relies on Hamiltonian simulation, which can be realised by the Trottersation or qubitised quantum walk (QW), with the latter having a better ε scaling though with a larger overhead. We find that the fourth-order (random) Trotter result is tested that performs the best among all the Trotter methods, which is consistent with the results in [61]. For our RLCU method, we consider the Hamiltonian simulation using the $2k$ th-order paring with $k = 0, 1$ or 2 . To estimate the gate costs of the RLCU algorithm, we set the normalisation factor $\mu = 2$ to ensure that the sample complexity of the RLCU algorithm is similar to other quantum algorithms.

The quantum circuit is synthesised to CNOT gates, single-qubit Clifford gates and non-Clifford gates (including single-qubit Z-axis rotation R_z gates and T gates). The requirements for the gate number in the representative algorithms are estimated. Since the central objective is for the application in the early FTQC or NISQ era, we mainly focus on the circuit depth in a single-run experiment. Therefore, the amplitude amplification is not considered in the algorithms, which can deterministically prepare the state closer to the true ground state yet at the cost of a deeper circuit. Our algorithm requires single-qubit Pauli rotation gate $R_z(\theta)$, which has a circuit compilation overhead when it is compiled into T gates. The optimal ancilla-free gate synthesis algorithm in Ref. [70], which requires $3\log_2(1/\varepsilon) + \mathcal{O}(\log\log(1/\varepsilon))$ T-gates to approximate the $R_z(\theta)$ gate to a precision ε . It is worth noting that $R_z(\theta)$ can be virtually implemented with real physical devices. For superconducting devices, $R_z(\theta)$ in-

deed does not have to be implemented physically, but rather it can be implemented by changing the phase of the reference frame defined by the multi-level rotating frame. That is, $R_z(\theta)$ is a virtual gate, and therefore, there is no physical error in implementing $R_z(\theta)$.

The elementary operations in the block encoding of H is the Select and Prepare operations. In the Appendix, we discuss the cost for these two operations in detail, such that the cost for algorithms based on block encoding of H can be analysed. When we consider a real physical model, such as quantum chemistry problems, the coefficient of the Hamiltonian is constructed by calculating the integral and represents the feature of the quantum system. Due to finite precision, there will be an amplitude encoding error when we perform the PREP operation. To ensure that the amplitude encoding error is less than a threshold, we require more qubits to encode the coefficient. However, for the toy models, the absolute value of the coefficient may not be essentially relevant for the actual physics. For instance, we can manually set the interaction strength when we study the phase transition. In this work, we include the amplitude encoding error in our analysis when aiming for a realistic application. That is why we require more qubits for the algorithm involving amplitude amplification.

For lattice Hamiltonians, the resource cost can be largely reduced by considering the commutation relations of the Hamiltonian terms. First, we show the gate number estimation for Heisenberg models with different target precisions shown in Fig. 4. Our method shows advantages in both the CNOT gates and the T gates. It is worth noting that although the logarithmic scaling does not persist when taking account of the worst-case commutator bound, the actual performance may be better. The precision dependence is similar to QSP. Fig. 6 clearly shows that our method has a better system size dependence than QSP, both the gate count and the asymptotic scaling. In the numerics, we set the energy gap $\Delta = 0.01$ and the lower bound of the initial state overlap $\eta = 0.5$.

Next, we show the gate number estimation for spin

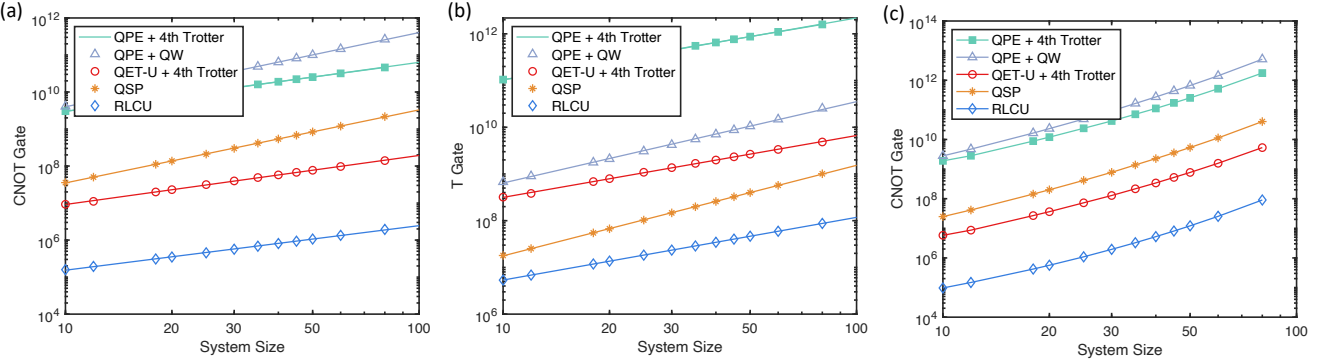


FIG. 6. Resource estimation (the number of CNOT gates and T gates) for the eigenstate property estimation for the 1D lattice Heisenberg Hamiltonian. Commutation relations are considered. We compare the gate count involved in different methods with a constant gap in (a,b). For QSP, the CNOT gate count's system size dependence is $\mathcal{O}(n^{1.97})$. Our method's system size dependence is $\mathcal{O}(n^{1.20})$. QETU's system size dependence is $\mathcal{O}(n^{1.32})$. (c) The number of CNOT gates for the eigenstate property estimation for the 1D lattice Heisenberg Hamiltonian in Eq. (51). The energy gap is fitted by an exponential decaying function.

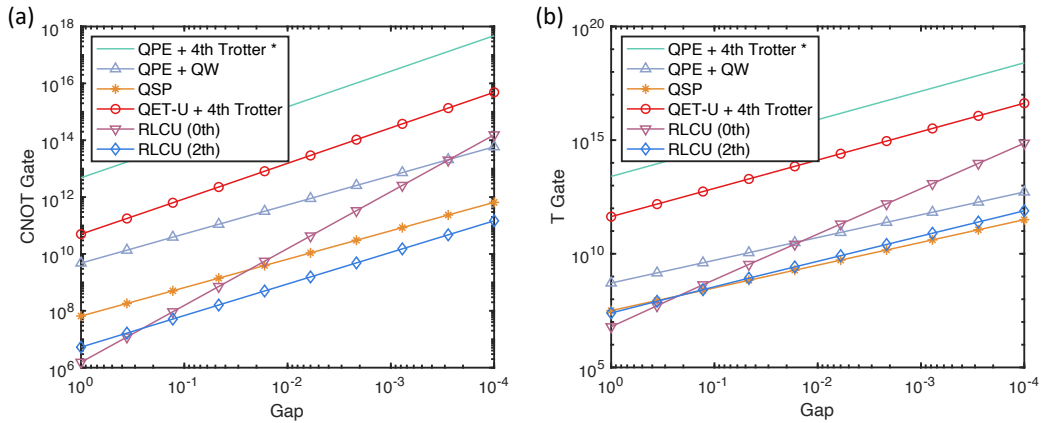


FIG. 7. The number of CNOT and T gates for the eigenstate property estimation for the P450 molecules with the A-type active space specified in [52]. The simulation of fermionic dynamics with Trotterisation is not optimised in this work. The total weight $\text{wt}(H) = 591$.

models with an increasing system size. We consider the XXZ Hamiltonian

$$H = - \sum_{i=1}^n (J_x X_i X_{i+1} + J_y Y_i Y_{i+1} + J_z Z_i Z_{i+1}) + h_x \sum_{i=1}^n X_i + \sqrt{c^2 - 1} (Z_1 - Z_n) \quad (51)$$

with the periodic boundary condition and the coupling strengths being $J_x = J_y = 1$ and $J_z = c J_x$. When $h_x = 0$, it has a gap $\Delta(c) = 4(c-1)$ when the system size is infinity. For $J_z = 2$ and $h_x = 0$, it has an energy gap $\Delta = 4$, and the degeneracy is $n+1$. When h_x increases, more excited states will emerge. For $n \leq 100$, the energy gap is not very small, which can be fitted by an exponential decay function, $\Delta = b \exp(-n^a)$. We found that $a = 1/2$ agrees quite well with the actual gap. The energy gap could be obtained by fitting, and we have $\Delta(20) = 0.382$,

$\Delta(50) = 0.124$, $\Delta(100) = 0.041$. The results considering the energy gaps are shown in Fig. 6(c).

For general Hamiltonians without considering commutation relation, our method may require more T gates than QSP because our method requires R_z gates, which have a large overhead when they are synthesised into T gates. To verify this point, we consider the two-local Hamiltonian. The results are shown in Fig. 5. It is worth noting that our method only requires rotation gates $R_z(\theta)$ with the rotation angles being identical and small. Therefore, further reductions may be made by exploiting the protocols in [71, 72] and [58], and we leave it to future work.

We give the resource cost for the cytochrome enzyme (P450) molecule with the A active space [52]. We use the circuits in [73] for compiling the single- and double-excitation operators, which saves gate count compared to naive implementing each Trotterised operation of the fermionic operator. However, we did not optimise the

cost for Trotterisation in every step, in which each term is nonlocal which is why the cost is quite large. The methods for simulating fermionic Hamiltonians can be directly used [58, 60, 74]. We leave the resource estimations incorporating these fermion simulation methods to future work.

V. OUTLOOK AND DISCUSSION

In this work, we provide a full-stack quantum algorithm based on random composite LCU for eigenstate property and eigenenergy estimation. Previous works have established near-optimal query complexity by querying either the block encoding of the Hamiltonian H (QSP) or the time evolution e^{-iHt} (QETU). Here, we show that the random sampling algorithm can achieve high precision and good system size scaling when considering gate complexity. We present an ancilla-free strategy by choosing the elementary operators to be symmetry-conserved operators (SWAP and Pauli-Z operators). Our method can be implemented with linear NN architecture, under which constraints, our method shows advantages over other existing schemes. This is particularly useful for implementation on NISQ or early FTQC devices since, for most algorithms, due to the restriction of connectivity, there could be a large overhead when compiling it into the nearest-neighbour operation. We show a concrete gate count analysis for various physical models on the CNOT gate and T gate concerning the circuit synthesis. It shows advantages in both the asymptotic scaling and the actual gate counts. Our result provides a clear illustration of the resource requirements for physical systems of interest, such as the Ising model, the Hubbard model, and molecular systems, with a focus on the application of quantum computing in the NISQ and early FTQC era.

Similar to other spectral filter methods, our method cannot overcome the fundamental limitations set up by the initial state and the energy gap. Ref. [6] numerically investigated its scaling for a few examples, possibly exponentially vanishing with increasing system size, aligning with the complexity conjecture. However, on the other side, even if we are given a sufficiently good

initial state with η close to 1, it is BQP-hard to prepare the ground state of 2-local Hamiltonians (known as the guided local Hamiltonian problem) [75, 76]. Therefore, it does not rule out the possibility of quantum speedup over classical computing. Similar to other random-sampling spectral filter methods ([19, 22]), the sample complexity with respect to η is $\mathcal{O}(\eta^{-2})$ for which the optimal scaling is $\mathcal{O}(\eta^{-1/2})$ achieved by QSP or QETU with amplitude amplification [29], though amplitude amplification also introduces a large circuit compilation cost. However, the random sampling method does bring some non-trivial advantages. When considering qubit connectivity, the depth complexity is nearly independent of the system size, which cannot be achieved with protocols relying on coherent implementations, particularly QSP or QETU. Our method is useful in the NISQ or early FTQC eras where the major issue is the maximum gate (depth) complexity.

Finally, we remark that recent works consider preparing the ground state by simulation of an open system dynamics described by Lindbladins [33] or a thermal process [34], which may partially overcome the limitations set up by the initial state [6]. Though they consider simulating the open system dynamics, a fundamental building block of the method in [33] is querying the real-time evolution. The resource cost can be analysed using the methods developed in this work. We leave a detailed comparison between the spectral filter methods and the one using open system dynamics for future work.

ACKNOWLEDGMENTS

J.S. would like to thank Xiao Yuan for early discussion on the project and Yukun Zhang, Andrew Green for useful related discussions on the manuscript. J.S. would like to express gratitude to Georg Schusteritsch for providing the molecular Hamiltonians used in this work. J.S. and M.S.K. thank the UK EPSRC through EP/Y004752/1, EP/W032643/1, and the KIST Open Research Program. T.G. thanks UKRI MR/S031545/1, and EPSRC EP/X018180/1 and EP/W032635/1. J.S. would like to thank Imperial Faculty Researcher Mobility Grant and Schmidt AI in Science Fellowship.

-
- [1] Kishor Bharti, Alba Cervera-Lierta, Thi Ha Kyaw, Tobias Haug, Sumner Alperin-Lea, Abhinav Anand, Matthias Degroote, Hermanni Heimonen, Jakob S. Kottmann, Tim Menke, Wai-Keong Mok, Sukin Sim, Leong-Chuan Kwek, and Alán Aspuru-Guzik. Noisy intermediate-scale quantum (nisq) algorithms, 2021.
- [2] Sam McArdle, Suguru Endo, Alan Aspuru-Guzik, Simon C Benjamin, and Xiao Yuan. Quantum computational chemistry. *Reviews of Modern Physics*, 92(1):015003, 2020.
- [3] Bela Bauer, Sergey Bravyi, Mario Motta, and Garnet Kin-Lic Chan. Quantum algorithms for quantum chemistry and quantum materials science. *Chemical Reviews*, 120(22):12685–12717, 2020.
- [4] Alexander M Dalzell, Sam McArdle, Mario Berta, Przemysław Bienias, Chi-Fang Chen, András Gilyén, Connor T Hann, Michael J Kastoryano, Emil T Khabiboulline, Aleksander Kubica, et al. Quantum algorithms: A survey of applications and end-to-end complexities. *arXiv preprint arXiv:2310.03011*, 2023.
- [5] Julia Kempe, Alexei Kitaev, and Oded Regev. The complexity of the local hamiltonian problem. *Siam journal*

- on computing*, 35(5):1070–1097, 2006.
- [6] Seunghoon Lee, Joonho Lee, Huachen Zhai, Yu Tong, Alexander M Dalzell, Ashutosh Kumar, Phillip Helms, Johnnie Gray, Zhi-Hao Cui, Wenyuan Liu, et al. Evaluating the evidence for exponential quantum advantage in ground-state quantum chemistry. *Nature Communications*, 14(1):1952, 2023.
- [7] A Yu Kitaev. Quantum measurements and the abelian stabilizer problem. *arXiv preprint quant-ph/9511026*, 1995.
- [8] Brendon L Higgins, Dominic W Berry, Stephen D Bartlett, Howard M Wiseman, and Geoff J Pryde. Entanglement-free heisenberg-limited phase estimation. *Nature*, 450(7168):393–396, 2007.
- [9] Emanuel Knill, Gerardo Ortiz, and Rolando D Somma. Optimal quantum measurements of expectation values of observables. *Physical Review A*, 75(1):012328, 2007.
- [10] Patrick Rall. Faster coherent quantum algorithms for phase, energy, and amplitude estimation. *Quantum*, 5:566, 2021.
- [11] Richard Meister and Simon C Benjamin. Resource-frugal hamiltonian eigenstate preparation via repeated quantum phase estimation measurements. *arXiv preprint arXiv:2212.00846*, 2022.
- [12] John M Martyn, Zane M Rossi, Andrew K Tan, and Isaac L Chuang. Grand unification of quantum algorithms. *PRX Quantum*, 2(4):040203, 2021.
- [13] Zhiyan Ding and Lin Lin. Even shorter quantum circuit for phase estimation on early fault-tolerant quantum computers with applications to ground-state energy estimation. *PRX Quantum*, 4(2):020331, 2023.
- [14] Yimin Ge, Jordi Tura, and J. Ignacio Cirac. Faster ground state preparation and high-precision ground energy estimation with fewer qubits. *Journal of Mathematical Physics*, 60(2):022202, 2019.
- [15] Trevor Keen, Eugene Dumitrescu, and Yan Wang. Quantum algorithms for ground-state preparation and green’s function calculation. *arXiv preprint arXiv:2112.05731*, 2021.
- [16] Dong An, Jin-Peng Liu, and Lin Lin. Linear combination of hamiltonian simulation for nonunitary dynamics with optimal state preparation cost. *Physical Review Letters*, 131(15):150603, 2023.
- [17] Yongdan Yang, Bing-Nan Lu, and Ying Li. Accelerated quantum monte carlo with mitigated error on noisy quantum computer. *PRX Quantum*, 2(4):040361, 2021.
- [18] Kianna Wan, Mario Berta, and Earl T. Campbell. A randomized quantum algorithm for statistical phase estimation, 2021.
- [19] Lin Lin and Yu Tong. Heisenberg-limited ground state energy estimation for early fault-tolerant quantum computers, 2021.
- [20] Pei Zeng, Jinzhao Sun, and Xiao Yuan. Universal quantum algorithmic cooling on a quantum computer. *arXiv preprint arXiv:2109.15304*, 2021.
- [21] Sirui Lu, Mari Carmen Bañuls, and J. Ignacio Cirac. Algorithms for quantum simulation at finite energies. *PRX Quantum*, 2:020321, May 2021.
- [22] Ruizhe Zhang, Guoming Wang, and Peter Johnson. Computing ground state properties with early fault-tolerant quantum computers. *Quantum*, 6:761, 2022.
- [23] Mingxia Huo and Ying Li. Shallow trotter circuits fulfil error-resilient quantum simulation of imaginary time, 2021.
- [24] Guoming Wang, Daniel Stilck França, Ruizhe Zhang, Shuchen Zhu, and Peter D Johnson. Quantum algorithm for ground state energy estimation using circuit depth with exponentially improved dependence on precision. *Quantum*, 7:1167, 2023.
- [25] Zhiyan Ding, Haoya Li, Lin Lin, HongKang Ni, Lexing Ying, and Ruizhe Zhang. Quantum multiple eigenvalue gaussian filtered search: an efficient and versatile quantum phase estimation method. *arXiv preprint arXiv:2402.01013*, 2024.
- [26] Min-Quan He, Dan-Bo Zhang, and ZD Wang. Quantum gaussian filter for exploring ground-state properties. *Physical Review A*, 106(3):032420, 2022.
- [27] Guoming Wang, Daniel Stilck França, Gumaro Rendon, and Peter D Johnson. Faster ground state energy estimation on early fault-tolerant quantum computers via rejection sampling. *arXiv preprint arXiv:2304.09827*, 2023.
- [28] Samson Wang, Sam McArdle, and Mario Berta. Qubit-efficient randomized quantum algorithms for linear algebra. *PRX Quantum*, 5(2):020324, 2024.
- [29] Lin Lin and Yu Tong. Near-optimal ground state preparation. *Quantum*, 4:372, 2020.
- [30] Lin Lin and Yu Tong. Optimal polynomial based quantum eigenstate filtering with application to solving quantum linear systems. *Quantum*, 4:361, 2020.
- [31] András Gilyén, Yuan Su, Guang Hao Low, and Nathan Wiebe. Quantum singular value transformation and beyond: exponential improvements for quantum matrix arithmetics. In *Proceedings of the 51st Annual ACM SIGACT Symposium on Theory of Computing*, pages 193–204, 2019.
- [32] Toby S Cubitt. Dissipative ground state preparation and the dissipative quantum eigensolver. *arXiv preprint arXiv:2303.11962*, 2023.
- [33] Zhiyan Ding, Lin Lin, et al. Single-ancilla ground state preparation via lindbladians. *arXiv preprint arXiv:2308.15676*, 2023.
- [34] Chi-Fang Chen, Hsin-Yuan Huang, John Preskill, and Leo Zhou. Local minima in quantum systems. *arXiv preprint arXiv:2309.16596*, 2023.
- [35] Jarrod R McClean, Jonathan Romero, Ryan Babbush, and Alán Aspuru-Guzik. The theory of variational hybrid quantum-classical algorithms. *New Journal of Physics*, 18(2):023023, feb 2016.
- [36] Marco Cerezo, Andrew Arrasmith, Ryan Babbush, Simon C Benjamin, Suguru Endo, Keisuke Fujii, Jarrod R McClean, Kosuke Mitarai, Xiao Yuan, Lukasz Cincio, et al. Variational quantum algorithms. *Nature Reviews Physics*, 3(9):625–644, 2021.
- [37] Yihao Liu, Min-Quan He, and ZD Wang. Variational quantum eigensolvers with quantum gaussian filters for solving ground-state problems in quantum many-body systems. *arXiv preprint arXiv:2401.13459*, 2024.
- [38] William J Huggins, Bryan A O’Gorman, Nicholas C Rubin, David R Reichman, Ryan Babbush, and Joonho Lee. Unbiasing fermionic quantum monte carlo with a quantum computer. *Nature*, 603(7901):416–420, 2022.
- [39] Jia-Jin Feng and Biao Wu. Escaping local minima with quantum circuit coherent cooling. *Physical Review A*, 109(3):032405, 2024.
- [40] Lucas K Kovalsky, Fernando A Calderon-Vargas, Matthew D Grace, Alicia B Magann, James B Larsen, Andrew D Baczewski, and Mohan Sarovar. Self-healing of trotter error in digital adiabatic state preparation. *Phys-*

- ical Review Letters*, 131(6):060602, 2023.
- [41] Mario Motta, Chong Sun, Adrian TK Tan, Matthew J O'Rourke, Erika Ye, Austin J Minnich, Fernando GSL Brandão, and Garnet Kin-Lic Chan. Determining eigenstates and thermal states on a quantum computer using quantum imaginary time evolution. *Nature Physics*, 16(2):205–210, 2020.
- [42] Xiaosi Xu and Ying Li. Quantum-assisted monte carlo algorithms for fermions. *Quantum*, 7:1072, 2023.
- [43] Yukun Zhang, Yifei Huang, Jinzhao Sun, Dingshun Lv, and Xiao Yuan. Quantum computing quantum monte carlo. *arXiv preprint arXiv:2206.10431*, 2022.
- [44] Kasra Hejazi, Mario Motta, and Garnet Kin Chan. Adiabatic quantum imaginary time evolution. *arXiv preprint arXiv:2308.03292*, 2023.
- [45] Amara Katabarwa, Katerina Gratsea, Athena Caesura, and Peter D Johnson. Early fault-tolerant quantum computing. *arXiv preprint arXiv:2311.14814*, 2023.
- [46] Dhruv Devulapalli, Eddie Schoute, Aniruddha Bapat, Andrew M. Childs, and Alexey V. Gorshkov. Quantum routing with teleportation, 2022.
- [47] Note that Ref. [20] extends to eigenstate property estimation.
- [48] Yulong Dong, Lin Lin, and Yu Tong. Ground state preparation and energy estimation on early fault-tolerant quantum computers via quantum eigenvalue transformation of unitary matrices. *arXiv preprint arXiv:2204.05955*, 2022.
- [49] Pei Zeng, Jinzhao Sun, Liang Jiang, and Qi Zhao. Simple and high-precision hamiltonian simulation by compensating trotter error with linear combination of unitary operations. *arXiv preprint arXiv:2212.04566*, 2022.
- [50] Isaac H Kim, Ye-Hua Liu, Sam Pallister, William Pol, Sam Roberts, and Eunseok Lee. Fault-tolerant resource estimate for quantum chemical simulations: Case study on li-ion battery electrolyte molecules. *Physical Review Research*, 4(2):023019, 2022.
- [51] Markus Reiher, Nathan Wiebe, Krysta M Svore, Dave Wecker, and Matthias Troyer. Elucidating reaction mechanisms on quantum computers. *Proceedings of the national academy of sciences*, 114(29):7555–7560, 2017.
- [52] Joshua J Goings, Alec White, Joonho Lee, Christofer S Tautermann, Matthias Degroote, Craig Gidney, Toru Shiozaki, Ryan Babbush, and Nicholas C Rubin. Reliably assessing the electronic structure of cytochrome p450 on today's classical computers and tomorrow's quantum computers. *Proceedings of the National Academy of Sciences*, 119(38):e2203533119, 2022.
- [53] Dave Wecker, Bela Bauer, Bryan K Clark, Matthew B Hastings, and Matthias Troyer. Gate-count estimates for performing quantum chemistry on small quantum computers. *Physical Review A*, 90(2):022305, 2014.
- [54] Earl Campbell. Random compiler for fast hamiltonian simulation. *Physical review letters*, 123(7):070503, 2019.
- [55] Joonho Lee, Dominic W Berry, Craig Gidney, William J Huggins, Jarrod R McClean, Nathan Wiebe, and Ryan Babbush. Even more efficient quantum computations of chemistry through tensor hypercontraction. *PRX Quantum*, 2(3):030305, 2021.
- [56] Ryan Babbush, Craig Gidney, Dominic W Berry, Nathan Wiebe, Jarrod McClean, Alexandru Paler, Austin Fowler, and Hartmut Neven. Encoding electronic spectra in quantum circuits with linear t complexity. *Physical Review X*, 8(4):041015, 2018.
- [57] Dominic W Berry, Craig Gidney, Mario Motta, Jarrod R McClean, and Ryan Babbush. Qubitization of arbitrary basis quantum chemistry leveraging sparsity and low rank factorization. *Quantum*, 3:208, 2019.
- [58] Ian D Kivlichan, Craig Gidney, Dominic W Berry, Nathan Wiebe, Jarrod McClean, Wei Sun, Zhang Jiang, Nicholas Rubin, Austin Fowler, Alán Aspuru-Guzik, et al. Improved fault-tolerant quantum simulation of condensed-phase correlated electrons via trotterization. *Quantum*, 4:296, 2020.
- [59] Earl T Campbell. Early fault-tolerant simulations of the hubbard model. *Quantum Science and Technology*, 7(1):015007, 2021.
- [60] Andrew M Childs, Yuan Su, Minh C Tran, Nathan Wiebe, and Shuchen Zhu. Theory of trotter error with commutator scaling. *Physical Review X*, 11(1):011020, 2021.
- [61] Andrew M Childs, Dmitri Maslov, Yunseong Nam, Neil J Ross, and Yuan Su. Toward the first quantum simulation with quantum speedup. *Proceedings of the National Academy of Sciences*, 115(38):9456–9461, 2018.
- [62] Ryan Babbush, Nathan Wiebe, Jarrod McClean, James McClain, Hartmut Neven, and Garnet Kin-Lic Chan. Low-depth quantum simulation of materials. *Physical Review X*, 8(1):011044, 2018.
- [63] Ian D Kivlichan, Jarrod McClean, Nathan Wiebe, Craig Gidney, Alán Aspuru-Guzik, Garnet Kin-Lic Chan, and Ryan Babbush. Quantum simulation of electronic structure with linear depth and connectivity. *Physical review letters*, 120(11):110501, 2018.
- [64] Guang Hao Low and Nathan Wiebe. Hamiltonian simulation in the interaction picture. *arXiv preprint arXiv:1805.00675*, 2018.
- [65] Thomas E O'Brien, Stefano Polla, Nicholas C Rubin, William J Huggins, Sam McArdle, Sergio Boixo, Jarrod R McClean, and Ryan Babbush. Error mitigation via verified phase estimation. *PRX Quantum*, 2(2):020317, 2021.
- [66] Cristian L Cortes and Stephen K Gray. Quantum krylov subspace algorithms for ground-and excited-state energy estimation. *Physical Review A*, 105(2):022417, 2022.
- [67] Mario Motta, Erika Ye, Jarrod R McClean, Zhendong Li, Austin J Minnich, Ryan Babbush, and Garnet Kin-Lic Chan. Low rank representations for quantum simulation of electronic structure. *npj Quantum Information*, 7(1):83, 2021.
- [68] Vera von Burg, Guang Hao Low, Thomas Häner, Damian S Steiger, Markus Reiher, Martin Roetteler, and Matthias Troyer. Quantum computing enhanced computational catalysis. *Physical Review Research*, 3(3):033055, 2021.
- [69] Adam Smith, MS Kim, Frank Pollmann, and Johannes Knolle. Simulating quantum many-body dynamics on a current digital quantum computer. *npj Quantum Information*, 5(1):106, 2019.
- [70] Neil J Ross and Peter Selinger. Optimal ancilla-free clifford+ t approximation of z-rotations. *Quantum Inf. Comput.*, 16(11&12):901–953, 2016.
- [71] Earl T Campbell and Joe O'Gorman. An efficient magic state approach to small angle rotations. *Quantum Science and Technology*, 1(1):015007, 2016.
- [72] Guillaume Duclos-Cianci and David Poulin. Reducing the quantum-computing overhead with complex gate distillation. *Physical Review A*, 91(4):042315, 2015.

- [73] Yordan S Yordanov, David RM Arvidsson-Shukur, and Crispin HW Barnes. Efficient quantum circuits for quantum computational chemistry. *Physical Review A*, 102(6):062612, 2020.
- [74] Yuan Su, Hsin-Yuan Huang, and Earl T Campbell. Nearly tight trotterization of interacting electrons. *Quantum*, 5:495, 2021.
- [75] Sevag Gharibian and François Le Gall. Dequantizing the quantum singular value transformation: hardness and applications to quantum chemistry and the quantum pcp conjecture. In *Proceedings of the 54th Annual ACM SIGACT Symposium on Theory of Computing*, pages 19–32, 2022.
- [76] Sevag Gharibian, Ryu Hayakawa, François Le Gall, and Tomoyuki Morimae. Improved hardness results for the guided local hamiltonian problem. *arXiv preprint arXiv:2207.10250*, 2022.
- [77] Yukun Zhang, Yifei Huang, Jinzhao Sun, Dingshun Lv, and Xiao Yuan. Quantum computing quantum monte carlo. *arXiv preprint arXiv:2206.10431*, 2022.
- [78] Alex Bocharov, Martin Roetteler, and Krysta M Svore. Efficient synthesis of universal repeat-until-success quantum circuits. *Physical review letters*, 114(8):080502, 2015.
- [79] Guang Hao Low and Isaac L Chuang. Hamiltonian simulation by qubitization. *Quantum*, 3:163, 2019.
- [80] Guang Hao Low and Isaac L Chuang. Optimal hamiltonian simulation by quantum signal processing. *Physical review letters*, 118(1):010501, 2017.
- [81] Michele Mosca and Priyanka Mukhopadhyay. A polynomial time and space heuristic algorithm for t-count. *Quantum Science and Technology*, 7(1):015003, 2021.
- [82] Dmitri Maslov. Advantages of using relative-phase toffoli gates with an application to multiple control toffoli optimization. *Physical Review A*, 93(2):022311, 2016.
- [83] Andrew M Childs, Aaron Ostrander, and Yuan Su. Faster quantum simulation by randomization. *Quantum*, 3:182, 2019.
- [84] Michael A Nielsen and Isaac Chuang. Quantum computation and quantum information, 2002.

CONTENTS

I. Introduction	1
II. Framework and main results	3
A. Overview of the results	6
III. Methods	8
A. Composite LCU form of the spectral filter	8
B. Observable estimation	11
C. Estimation by quantum circuits: general strategy and ancilla-free strategy	12
1. General cases	12
2. Ancilla-free composite LCU formula and the corresponding measurement scheme for symmetry conserved systems	13
D. Analysis of circuit depth and gate complexity	14
1. Gate complexity for general cases	14
2. Circuit compilation for typical Hamiltonians and circuit depth analysis	15
IV. Resource estimations	18
V. Outlook and discussion	20
Acknowledgments	20
References	20
A. Construction of the spectral filter	25
1. Composite LCU formulae for decomposing a nonunitary operator	25
2. Spectral filter by composite LCU formulae	26
B. Eigenstate property estimation	27
1. Estimator	27
2. Error analysis	28
3. Proof of Theorem 1 (Problem 1)	32
a. Gate complexity analysis	34
4. Discussions on molecular Hamiltonians	35
5. Effect of energy error on eigenstate property expectation estimation	36
6. Discretised version	37
C. Eigenenergy estimation (Problem 2)	38
D. Circuit compilation and gate cost for block-encoding-based methods	40
1. Stage Setting	40
2. Gate cost	41
a. The index enumeration circuit	41
3. The amplitude encoding, select gates, and reflection gates	41
4. Gate cost for Trotter methods	43
E. Ground state property estimation by quantum signal processing proposed by Lin and Tong	44
1. Overview	44
F. Ground state property estimation with phase estimation	46
1. Complexity of phase estimation	46
2. Hamiltonian simulation by Trotterisation	46
3. Hamiltonian simulation by qubitised quantum walk	47

In Sec. A, we discuss the construction of the spectral filter with composite LCU. We discuss the error in observation estimation when given an LCU form. In Sec. B, we discuss the building blocks of the eigenstate property estimation algorithm outlined in Algorithm 1. We will follow the proof idea illustrated in Fig. 2 and Sec. III to prove the main theorems for eigenstate property estimation in the main text. In Sec. C, we prove the result for eigenenergy estimation

in the main text. Sec. D analyses the circuit compilation cost for block-encoding-based methods. Sec. E and Sec. F discuss the cost when using QSP and QPE.

Appendix A: Construction of the spectral filter

1. Composite LCU formulae for decomposing a nonunitary operator

In the main text, we have introduced a few tools to analyse the property of the composite form of an LCU formula. Proposition 1 shows how to bound the error of a composite LCU formula written in the discretised form. We provide the proof here.

Proof. (of Proposition 1)

Recall that the LCU formula of g can be written as

$$g_2 = \mu_1 \sum_i \Pr(i) (U(t_i/\nu))^\nu. \quad (\text{A1})$$

Given the LCU formula of $U(t_i/\nu)$, g_2 can be written as

$$g_2 = \mu_1 \mu_2^\nu \sum_i \Pr(i) \left(\sum_{i_\ell} \Pr(i_\ell) P_{i_\ell} \right)^\nu = \mu_1 \mu_2^\nu \sum_i \Pr(i) \sum_{\{i_\ell\}} \prod_{q=1}^{\nu} \Pr(i_{\ell_q}) \prod_{q=1}^{\nu} P_{i_{\ell_q}} \quad (\text{A2})$$

with some abuse of notation.

Given a (μ_2, ε_2) -LCU form of $U(\delta t)$, one can prove that the product of LCU formula $U(\delta t)^\nu$ has a normalisation factor $\mu'_2 = \mu_2^\nu$ and an error $\varepsilon'_2 \leq \nu \mu'_2 \varepsilon_2$. We can prove the result by using the triangle inequality

$$\|g_2 - g\| \leq \|g_1 - g\| + \|g_2 - g_1\| \leq \varepsilon_1 + \nu \mu_1 \mu'_2 \varepsilon_2,$$

which completes the proof. \square

To implement LCU in practice, we could consider either a discretised form or a continuous form. As shown in the main text, the Fourier transform gives an explicit form for decomposing the spectral filter into unitary operators in a continuous form. When the integral form of a spectral filter has a well-defined probability distribution, it can be well-characterised by Eq. (1). Therefore, we use the continuous form for the Gaussian spectral filter. We provide a discretised version of the spectral filter in Sec. B 6 and show that the discretisation error for the Gaussian spectral filter can be sufficiently small.

We provide the composite LCU formula in a continuous form for completeness.

Proposition 5 (Composite LCU formula in a continuous form). *Suppose g_1 is a (μ_1, ε_1) -LCU formula of g ,*

$$g_1 = \mu_1 \int dx p(x) U(x) \quad (\text{A3})$$

Suppose that each of the summand $U(x)$ has a (μ_2, ε_2) -LCU formula,

$$\tilde{U}(x) = \mu_2(x) \int dy q(x, y) V(x, y) \quad (\text{A4})$$

Then the formula

$$g_2 = \mu_1 \int dx p(x) \tilde{U}(x) \quad (\text{A5})$$

is a (μ, ε) -LCU formula of g , with $\mu := \mu_1 \int_{-\infty}^{\infty} p(x) \mu_2(x) dx$, and $\varepsilon = \varepsilon_1 + \mu_1 \varepsilon_2$.

Proof. (of Proposition 5)

The formula of g_2 can be written as

$$g_2 = \mu_1 \int dx p(x) \mu_2(x) \int dy q(x, y) V(x, y) \quad (\text{A6})$$

We define

$$p_\mu(x) = \mu_1 \mu_2(x) p(x) / \mu \quad (\text{A7})$$

with $\mu := \mu_1 \int_{-\infty}^{\infty} p(x) \mu_2(x) dx$. Then g_2 takes the form of

$$g_2 = \mu \int dx p_\mu(x) \int dy q(x, y) V(x, y). \quad (\text{A8})$$

The proof is straightforward by using the triangle inequality $\|g_2 - g\| \leq \|g_1 - g\| + \|g_2 - g_1\| \leq \varepsilon_1 + \mu_1 \varepsilon_2$. Note that $p_\mu(x)$ and $q(x, y)$ (for given x) are both normalised and can thus be regarded as probability distributions. Therefore, g_2 can be realised in a random-sampling way by sampling from the distribution $p_\mu(x)$ and then $q(x, y)$. \square

[Eq. \(A8\)](#) is a general (μ, ε) composite LCU form of g . As we shall see in the later discussion, to reduce the maximum evolution time (related to x) we usually set a truncation of x in the integral, i.e.,

$$g_1 = \mu_1 \int_{-x_c}^{x_c} dx p(x) U(x) \quad (\text{A9})$$

with $\tilde{\varepsilon}_1 = \varepsilon_1 + \varepsilon_c$ and ε_c being a small truncation error. Then we may set the constant μ_2 to be $\mu_2 = \max_x \mu_2(x)$ in the LCU formula of $U(x)$, $\tilde{U}(x) = \mu_2 \int dy q(x, y) V(x, y)$. Then the LCU formula of g could be simplified as

$$g_2 = \mu \int dx p(x) \int dy q(x, y) V(x, y), \quad (\text{A10})$$

with $\mu = \mu_1 \mu_2$.

2. Spectral filter by composite LCU formulae

Recall that we choose a Gaussian spectral filter $g_\tau(H) = e^{-\tau^2 H^2}$. Below, we elaborate on a few properties of the spectral filter. A general matrix function acting on the Hamiltonian is defined as

$$g(H) := \sum_{i=0}^{N-1} g(E_i) |u_i\rangle \langle u_i|. \quad (\text{A11})$$

where $g(h) : \mathbb{R} \rightarrow \mathbb{C}$ is a generic continuous-variable function determining the transformation of the spectrum of the Hamiltonian. As a spectral filter, the function $g(h)$ is required to satisfy strictly non-increasing absolute value, $|g(h')| < |g(h)|$, $\forall |h'| > |h|$, and vanishing asymptotic value, $\lim_{\tau \rightarrow \infty} |g(\tau h')/g(\tau h)| = 0$, $\forall |h'| > |h|$, and is an even function, $g(h) = g(-h)$. In this work, we choose the Gaussian function $g(h) = e^{-h^2}$, corresponding to a generalised imaginary-time evolution $g(\tau H) = e^{-\tau^2 H^2}$. As shown in the main text, the Gaussian spectral filter is decomposed into the basis of real-time evolution and is further decomposed into elementary operations, either Pauli operators for general cases or symmetry-conserved operators for ancilla-free consideration.

Given an LCU form of g , [Proposition 2](#) shows the error in observable estimation. Below we provide the proof of [Proposition 2](#).

Proof. (of [Proposition 2](#))

Suppose \tilde{g} is a (μ, ε) -RLCU formula of g . We first have

$$N_{\tilde{g}}(O) = \text{Tr}(\tilde{g}_\tau(H - E_0) O \tilde{g}_\tau(H - E_0)) \quad (\text{A12})$$

we have

$$\begin{aligned} |N_{\tilde{g}}(O) - N_g(O)| &= |\text{Tr}(\tilde{g}_\tau(H - E_0) O \tilde{g}_\tau(H - E_0)) - \text{Tr}(g_\tau(H - E_0) O g_\tau(H - E_0))| \\ &\leq \varepsilon(\|\tilde{g}_\tau\| + \|g_\tau\|) \|O\|_\infty \\ &\leq 2\mu^2 \varepsilon \|O\|_\infty \end{aligned} \quad (\text{A13})$$

Here, we have used the fact that $\|\rho\| \leq 1$, $\|\tilde{g}_\tau\| \leq \mu^2$, and $g = g^\dagger$.

Suppose we have the estimator $\hat{N}_{\tilde{g}}(O)$ defined in Eq. (40). The expectation range is $[-\sqrt{2}\mu^2\|O\|_\infty, \sqrt{2}\mu^2\|O\|_\infty]$. Using the Hoeffding bound, we have the following probability tail bound for the mean estimator $\hat{N}_{\tilde{g}}(O)$,

$$\Pr(|\hat{N}_{\tilde{g}}(O) - N_{\tilde{g}}(O)|) \leq 2 \exp\left(-\frac{Ns\varepsilon_n^2}{\mu^4}\right) \quad (\text{A14})$$

By setting $N := \mu^4 \ln(2/\vartheta)/\varepsilon_n^2$, we have the estimation error

$$\varepsilon_N := |\hat{N}_{\tilde{g}}(O) - N_g(O)| \leq \|O\|(2\mu^2\varepsilon + \varepsilon_n), \quad (\text{A15})$$

with a success probability $1 - \vartheta$.

The result for the denominator can be similarly derived since

$$D_{\tilde{g}} := \langle \tilde{g}_\tau^2(H - E_0) \rangle = N_{\tilde{g}}(I). \quad (\text{A16})$$

We have

$$\varepsilon_D := |\hat{D}_{\tilde{g}} - D_g| \leq 2\mu^2\varepsilon + \varepsilon_n. \quad (\text{A17})$$

The error for the normalised observable expectation is

$$\begin{aligned} \left| \frac{\hat{N}_{\tilde{g}}(O)}{\hat{D}_{\tilde{g}}} - \frac{N_g(O)}{D_g} \right| &= \left| \frac{(\hat{N}_{\tilde{g}}(O)D_g - N_g(O)D_g) + (N_g(O)D_g - \hat{D}_{\tilde{g}}(O)N_g)}{\hat{D}_{\tilde{g}}D_g} \right| \\ &\leq \left| \frac{N_g(O)\varepsilon_D + D_g\varepsilon_N}{\hat{D}_{\tilde{g}}D_g} \right| \\ &\leq \left| \frac{(D_g + N_g(O))\varepsilon_D + D_g\varepsilon_N}{D_g^2} \right| = \frac{1}{D_g}((\langle O \rangle_g + 1)\varepsilon_D + \varepsilon_N) \end{aligned} \quad (\text{A18})$$

□

The performance of our method in eigenstate property estimation can be estimated by the error in the construction of the RLCU formula. One can thus compare our method with the other deterministic schemes at the same level.

Appendix B: Eigenstate property estimation

In this section, we provide error analysis for eigenstate property estimation described in Problem 1. We will provide the proof of gate complexity (Theorem 1) in the main text.

1. Estimator

Recall that the task in Problem 1 is to estimate the observable expectation on the target eigenstate $|u_j\rangle$ up to a certain precision ε , which is characterised by

$$\langle O \rangle = \frac{N(O)}{D} = \frac{\langle u_i | O | u_i \rangle}{\langle u_i | u_i \rangle} \quad (\text{B1})$$

where the denominator D and the numerator N is defined in respect to the eigenstate $|u_i\rangle$. The unnormalised eigenstate can be effectively realised by applying a spectral filter $g_{\tau \rightarrow \infty}(H - \omega)$ to an initial state, which holds when $\omega = E_j$ and the imaginary-time becomes infinity. In this section, the eigenenergy is first assumed to be known a priori. The task with an unknown eigenenergy will be discussed in Sec. B 5.

It is easy to see that we arrive at the ideal observable expectation when $\tau \rightarrow \infty$,

$$\langle O \rangle = \frac{N_{\tau \rightarrow \infty}(O)}{D_{\tau \rightarrow \infty}}, \quad (\text{B2})$$

given a nonvanishing denominator, which is $D_{\tau \rightarrow \infty}(E_j) = |c_j|^2 = \eta$. Note that we assume that the spectral weight $\langle u_i | \psi_0 \rangle$ is nonvanishing. The observable when considering a finite τ is estimated by

$$\langle O \rangle_\tau = \frac{N_\tau(O)}{D_\tau}. \quad (\text{B3})$$

The denominator and the numerator have the same definition in Eq. (11). In practice, when considering finite gate complexity and sample complexity, the eigenstate property is estimated by

$$\hat{O}_{\tau, x_c, s_c} = \frac{\hat{N}_{\tau, x_c, s_c}(O)}{\hat{D}_{\tau, x_c, s_c}}. \quad (\text{B4})$$

The selection of τ, x_c, s_c can be determined by analysing the error of \hat{O}_{τ, x_c, s_c} compared to the ideal value. As shown in Proposition 1, the spectral filter can be written as an RLCU formula. The spectral filter takes an explicit form of

$$g_{\tau}(H - \omega) = c \int_{-\infty}^{\infty} dx p(x) e^{ix\tau\omega} e^{-i\tau x H} \quad (\text{B5})$$

The integrand is a real-time evolution with total real-time τx . Suppose we further use LCU formula to implement $e^{-i\tau x H}$, which takes the form of

$$e^{-i\tau x H} = \mu(x\tau) \sum_{\vec{r} \in \mathcal{K}_x} \Pr(\vec{r}, x\tau, \nu(x\tau)) U_{\vec{r}} \quad (\text{B6})$$

where we have follow the definition in Eq. (17): k specifies the unitary $U_{\vec{r}}$ involved in the LCU formula of $e^{-i\tau x H}$, $\Pr(\vec{r}, x\tau, \nu(x\tau))$ represents the normalised decomposition coefficients of $U_{\vec{r}}$. Then, we have

$$g_{\tau}(H - \omega) = c(\mu) \int_{-\infty}^{\infty} dx p_{\mu}(x) e^{i\theta_x} e^{ix\tau\omega} \sum_{\vec{r} \in \mathcal{K}_x} \Pr(\vec{r}, x\tau, \nu(x\tau)) U_{\vec{r}}. \quad (\text{B7})$$

2. Error analysis

Now, we discuss the errors when considering finite τ, x_c, s_c . Note that Eq. (B7) is a composite LCU formula, more specifically, it is a $(c(\mu), 0)$ -LCU formula. When we consider a finite x_c, s_c , it will introduce some errors. The key idea of analysing the errors is to compare the operator distance between

$$\|g_{\tau, x_c, s_c} - g_{\tau, x_c, s_c \rightarrow \infty}\| \quad (\text{B8})$$

which will gives a bound for the numerator and the denominator.

a. Error due to finite τ . The imaginary-time τ determines the strength of the spectral filter. The spectral weight on the unwanted eigenstates, namely those energies away from the pre-set parameters E , will be exponentially suppressed. In the infinite time limit, g will effectively project out all the spectral weights on the unwanted eigenstates, given that the initial state has a nonvanishing spectral weight on the target eigenstate. The error of the denominator and numerator can be analysed by considering the operator distance between g_{τ} and $g_{\tau \rightarrow \infty}$. In this section, we choose $\omega = E_j$ and omit ω when there is no ambiguity.

Proposition 6 (Error due to a finite τ). *When $\tau \geq \frac{1}{\Delta} \sqrt{\ln(2/\varepsilon_{\tau})}$, the error of the denominator and the numerator that are defined in Eq. (11) when compared with those defined with respect to the ideal eigenstates in Eq. (B1) satisfy $|D_{\tau} - D| \leq \varepsilon_{\tau}$, $|N_{\tau}(O) - N(O)| \leq \varepsilon_{\tau} \|O\|$.*

Proof. The distance between $g_{\tau}(H - E_j)$ and $g_{\tau \rightarrow \infty}(H - E_j)$ can be bounded by

$$g_{\tau}(H - E_j) - g_{\tau \rightarrow \infty}(H - E_j) = \sum_{i \neq j} g_{\tau}(E_i - E_j) |u_i\rangle \langle u_i| \quad (\text{B9})$$

where $g_{\tau}(H - \omega)$ is defined in Eq. (B7). According to the definition of g_{τ} , when $\tau \geq \frac{1}{\Delta} \sqrt{\ln(2/\varepsilon_{\tau})}$, it is easy to check that

$$g_{\tau}(E_i - E_j) \leq \varepsilon_{\tau}/2, \quad \forall i \neq j \quad (\text{B10})$$

and thus we have

$$\|g_{\tau}(H - E_j) - g_{\tau \rightarrow \infty}(H - E_j)\| \leq \varepsilon_{\tau}/2 \quad (\text{B11})$$

Using the result in Proposition 2, the error of the numerator can be bounded by

$$N_{\tau}(O) - N(O) \leq \varepsilon \|O\| \quad (\text{B12})$$

The error of the denominator can be obtained straightforwardly by taking $O = I$. \square

b. *Error due to finite truncation in real-time evolution.* Then we analyse the error due to finite x_c and s_c . In practice when the integral is truncated to from infinite range $[-\infty, \infty]$ a finite time length $[-x_c, x_c]$, $g_\tau(H - \omega)$ becomes

$$g_{\tau, x_c}(H - \omega) = c \int_{-x_c}^{x_c} dx p(x) e^{ix\tau\omega} e^{-i\tau x H}. \quad (\text{B13})$$

Using the property of the Gaussian tail, it is easy to verify that the truncation error of g_τ with a finite x_c is given by

$$\|g_\tau - g_{\tau, x_c}\| \leq \varepsilon_{x_c} \quad (\text{B14})$$

when $x_c \geq 2\sqrt{\ln(1/\varepsilon_{x_c})}$.

As shown in the main text, we consider dealing with the real-time evolution using Trotter-LCU expansion. For evolution time t , let us denote the real-time evolution $U(t) := e^{-iHt} = U_m^\nu$ where

$$U(m) = e^{imH} = \mu(m)\mu(m) \sum_r \Pr(r, m, \nu(m)) W_r$$

is a short time dynamics during the time interval $m = t/\nu$. In a $2k$ th-order Trotter-LCU algorithm, the overall LCU formula for $U(m)$ is

$$U(m) = V_{2k}(m) S_{2k}(m), \quad (\text{B15})$$

which consists of a deterministic $2k$ th-order Trotter formula S_{2k} and the Trotter error compensation term V_{2k} . We consider a truncated Trotter-LCU formula to realize a (μ, ε) -LCU formula for $U(t) = e^{-iHt}$ based on ν segments of \tilde{U}_{2k} in Eq. (18).

We will use the results established in [49] to analyse the segment number ν to control the error to a certain level. The complexity of the zeroth-order leading-order-pairing algorithm scales quadratically to t , which is undesirable for simulation with a long time. If we apply $2k$ th-order Trotter formula $S_{2k}(m)$ in each segment, the $2k$ th-order remainder is $V_{2k}(m) := U(m)S_{2k}(m)^\dagger$. Using BCH formula, we can have an explicit form of $V_{2k}(m)$

$$V_{2k}(m) = \exp(i \sum_{s=2k+1}^{\infty} E_{2k,s} m^s) = \sum_{s=0}^{\infty} F_{2k,s}(m) = \sum_{s=0}^{\infty} \|F_{2k,s}(m)\| V_{2k}^{(s)}(m) \quad (\text{B16})$$

where we group the terms by the order of m , and $F_{1,s}$ denotes the s -order expansion term of $V_{2k}(m)$ with m^s . Here, $\|F_{2k,s}(m)\|_1$ is the 1-norm of the s -order expansion formula $F_{2k,s}(m)$ and $V_{2k,s}(m)$ is the normalised LCU formula for the s -order terms. It is easy to see that

$$F_{2k,s}(m) = im^s E_{2k,s}, \quad s \in [2k+1, 4k+1] \quad (\text{B17})$$

Formally, we can express

$$E_{2k,s} = \lambda_r \sum_r \Pr(r|s) P_{2k}(r). \quad (\text{B18})$$

By pairing the s th order expansion term with the identity I , the order of $F_{2k,s}(m)$ can be doubled as

$$I + F_{2k,s}(m) = \lambda_r \sqrt{1+m^{2s}} \sum_r \Pr(r|s) \exp(i \arctan(m^{2s}) P_{2k}(r)). \quad (\text{B19})$$

Therefore, the norm of $F_{2k,s}$ decreases from $\mathcal{O}(1+m^s)$ to $\mathcal{O}(1+m^{2s})$. Here we note that this holds for the symmetry-conserved LCU decomposition where the elementary operations are SWAP and Pauli Z operators.

The error can be shown to have a quick decrease with an increasing truncation order s_c . Considering of a finite truncation and the vanishing of $F_{2k,j \leq 2k}(m) = 0$, we can rewrite $V_{2k}^{(s)}(m)$ as

$$V_{2k}^{(s)}(m) = I + \sum_{s=2k+1}^{s_c} F_{2k,s}(m). \quad (\text{B20})$$

Given the truncation, the LCU formula for $U(m)$ is

$$U_{2k}^{(s_c)}(m) = V_{2k,s}(m) S_{2k}(m). \quad (\text{B21})$$

The overall LCU formula for $U(t)$ is to repeat the sampling of $\tilde{U}_{2k}(x)$ for ν times. The overall LCU formula for time t is

$$U_{2k}^{(s_c)}(t) = \left(U_{2k}^{(s_c)}(m) \right)^\nu \quad (\text{B22})$$

with $\nu = t/m$. Here $U_{2k}^{(s_c)}(t)$ denotes the RLCU formula of U when truncating it to s_c orders and t is the total evolution time, and $U_{2k}^{(s_c)}(t)$ is a $(\mu_{2k,tot}(t), \varepsilon_{2k,tot}(t))$ -LCU formula of $U(t)$ with

$$\mu_{2k,tot}(t) = \mu(m)^\nu, \quad \varepsilon_{2k,tot}(t) \leq \nu \mu_{2k,tot}(t) \varepsilon_{2k}(m) \quad (\text{B23})$$

The key component is to analyse the quantum resources needed to achieve an additive error of the approximation given by Eq. (22)

$$\|U(t) - U_{2k}^{(s_c)}(t)\| \leq \varepsilon_{s_c}. \quad (\text{B24})$$

Lemma 1 in [49] gives the Hamiltonian simulation error ε_{s_c} when using 2kth-order paired Taylor-series compensation with finite s_c .

Lemma 1 (Hamiltonian simulation error using 2kth-order paired Taylor-series compensation (Theorem 1 in the Appendix in [49])). *In a 2kth-order Trotter-LCU algorithm, if the segment number ν and the truncation order s_c satisfy*

$$\begin{aligned} \nu &\geq \left(\frac{2(e + c_k) \lambda t}{\ln \mu} \right)^{\frac{1}{4k+1}} 2\lambda t, \\ s_c &\geq \max \left\{ \left\lceil \frac{\ln(\frac{\mu}{\varepsilon} \nu_{2k}(t))}{W_0(\frac{1}{2e\lambda t} \nu_{2k}(t) \ln(\frac{\mu}{\varepsilon} \nu_{2k}(t)))} - 1 \right\rceil, 4k + 1 \right\}, \end{aligned} \quad (\text{B25})$$

we can then realize a (μ, ε) -LCU formula for $U(t) = e^{-iHt}$, i.e., $\|U(t) - U_{2k}^{(s_c)}(t)\| \leq \varepsilon_{s_c}$, based on ν segments of \tilde{U}_{2k} in Eq. (18). Here, c_k is defined as $c_k := \frac{1}{2} \left(\frac{e}{2k+1} \right)^{4k+2}$.

When considering a finite s_c , the spectral filter becomes

$$g_{\tau, x_c, s_c}(H - \omega) = c \int_{-x_c}^{x_c} dx p(x) e^{ix\tau E} U_{2k}^{(s_c)}(x\tau, \nu(x\tau)) \quad (\text{B26})$$

It is easy to check that $\|g_{\tau, x_c, s_c}(H - \omega)\| \leq c(1 + \varepsilon_{s_c})$. The operator distance between g_{τ, x_c} and g_{τ, x_c, s_c} due to finite s_c is

$$\|g_{\tau, x_c} - g_{\tau, x_c, s_c}\| \leq c \int_{-x_c}^{x_c} dx p(x) e^{ix\tau\omega} \|U(x\tau) - U_{2k}^{(s_c)}(x\tau, \nu(x\tau))\| \leq \varepsilon_{s_c} \quad (\text{B27})$$

when $\|U - U_{2k}^{(s_c)}(x\tau, \nu(x\tau))\| \leq \varepsilon_{s_c}/c$.

Using the triangular inequality, the operator error between g_τ and g_{τ, x_c, s_c} defined in Eq. (B26) is

$$\|g_\tau - g_{\tau, x_c, s_c}\| \leq \varepsilon_{x_c} + \varepsilon_{s_c} \quad (\text{B28})$$

With the error due to a finite time when evaluating the integral Eq. (B14) and the truncation order s_c Eq. (B27), we arrive at the following **Proposition 7**.

Proposition 7 (Error due to finite time length and truncation). *When $x_c \geq 2\sqrt{\ln(2/\varepsilon_{x_c})}$, ν_c and s_c satisfying Eq. (B25), we have $|D_{\tau, x_c, s_c} - D_\tau| \leq 3\varepsilon_c$, $|N_{\tau, x_c, s_c}(O) - N_\tau(O)| \leq 3\varepsilon_c \|O\|$ with $\varepsilon_c = \varepsilon_{x_c} + \varepsilon_{s_c}$*

Proof. The estimator

$$\begin{aligned} |N_\tau(O) - N_{\tau, x_c, s_c}(O)| &= |\langle \psi_0 | g_\tau(H - \omega) O g_\tau(H - \omega) | \psi_0 \rangle - \langle \psi_0 | g_{\tau, x_c, s_c}(H - \omega) O g_{\tau, x_c, s_c}(H - \omega) | \psi_0 \rangle| \\ &\leq |\langle \psi_0 | g_\tau(H - \omega) O g_\tau(H - \omega) | \psi_0 \rangle - \langle \psi_0 | g_{\tau, x_c, s_c}(H - \omega) O g_\tau(H - \omega) | \psi_0 \rangle| \\ &\quad + |\langle \psi_0 | g_{\tau, x_c, s_c}(H - \omega) O g_\tau(H - \omega) | \psi_0 \rangle - \langle \psi_0 | g_{\tau, x_c, s_c}(H - \omega) O g_{\tau, x_c, s_c}(H - \omega) | \psi_0 \rangle| \\ &\leq \varepsilon_c (\|g_\tau\| + \|g_{\tau, x_c, s_c}\|) \|O\| \leq 3\varepsilon_c \|O\| \end{aligned} \quad (\text{B29})$$

where $\varepsilon_c := \varepsilon_{x_c} + \varepsilon_{s_c}$. In the third inequality, we have used the inequality by Eq. (B28). \square

The gate complexity of the overall algorithm can then be estimated. To construct controlled- $U(t)$, we split it to ν segments. In each segment, we need to implement k th-order Trotter circuits and random Taylor-series sampling circuits. The number of gates in the random Taylor-series sampling circuit is $\mathcal{O}(s_c)$. Therefore, the gate complexity of the overall algorithm using K th Trotter formula ($K = 0, 1, 2k$) is given by

$$N_K = \mathcal{O}(\nu(\kappa_K L + s_c)), \quad (\text{B30})$$

where

$$\kappa_K = \begin{cases} K, & K = 0, 1 \\ 2 \cdot 5^{K/2-1}, & K = 2k, k \in \mathbb{N}_+. \end{cases} \quad (\text{B31})$$

c. *Unbiased estimator.*

Proposition 8. *The estimator \hat{v} defined in Eq. (40) is an unbiased estimator of $\langle \psi_0 | g_\tau(H - \omega) O g_\tau(H - \omega) \psi_0 \rangle$.*

Proof. Taking an average over a, b, r we have

$$\mathbb{E}_{a,b,r} \hat{v} = c^2(\mu) e^{i\tau\omega(t_i-t_j)} \mathbb{E}_{a,b,r} \hat{d} = c^2(\mu) e^{i\tau\omega(t_i-t_j)} = c^2(\mu) e^{i\tau\omega(t_i-t_j)} \langle \vec{\mathbf{j}} | O | \vec{\mathbf{i}} \rangle \quad (\text{B32})$$

Taking an average of $t_i, t_j, \vec{i}, \vec{j}$, we have

$$\begin{aligned} \mathbb{E}_{t_i, t_j, \vec{i}, \vec{j}} \mathbb{E}_{a, b, r} \hat{v} &= c^2(\mu) \mathbb{E}_{t_i, t_j} e^{i\tau\omega(t_i-t_j)} \mathbb{E}_{\vec{i}, \vec{j}} \langle \vec{\mathbf{j}} | O | \vec{\mathbf{i}} \rangle \\ &= c^2(\mu) \sum_{i,j} \Pr(i) \Pr(j) e^{i\tau\omega(t_i-t_j)} \sum_{\vec{i}, \vec{j}} \Pr(\vec{i}, \tau t_i, \nu) \Pr(\vec{j}, \tau t_j, \nu) \langle \vec{\mathbf{j}} | O | \vec{\mathbf{i}} \rangle \\ &= \langle \psi_0 | g_\tau(H - \omega) O g_\tau(H - \omega) \psi_0 \rangle = N_\tau(O). \end{aligned} \quad (\text{B33})$$

□

In the other case, where $O = \sum_l o_l P_l$ is composed of many terms as described in Problem 1, an importance sampling method can be used to estimate the observable. Compared to measuring each term separately, the measurement cost using importance sampling is independent of L . In particular, we sample the observables's index l from the probability distribution $o_l/\|O\|_1$. Given a sampled l , we define the estimator, \hat{d}_l , in the same way as Eq. (38). It is easy to see that \hat{d}_l is an unbiased estimator of $\langle \vec{\mathbf{j}} | O | \vec{\mathbf{i}} \rangle$ as

$$\mathbb{E}_{a,b,l} r_l = \langle \vec{\mathbf{j}} | O | \vec{\mathbf{i}} \rangle. \quad (\text{B34})$$

Similarly, we define the estimator as

$$\hat{v}_l = c^2(\mu) e^{i\tau\omega(t_i-t_j)} \hat{d}_l \quad (\text{B35})$$

Taking the average of $t_i, t_j, \vec{i}, \vec{j}, a, b, r, l$, we have

$$\mathbb{E}_{t_i, t_j, \vec{i}, \vec{j}, a, b, r, l} \hat{v}_l = N_\tau(O). \quad (\text{B36})$$

The range of the estimator is $[-\sqrt{2}c^2(\mu)\|O\|_1, \sqrt{2}c^2(\mu)\|O\|_1]$. Using Hoeffding inequality, the estimation error can be bounded

$$\begin{aligned} |\hat{D}_{\tau, x_c, s_c} - D_{\tau, x_c, s_c}| &\leq \varepsilon_n \\ |\hat{N}_{\tau, x_c, s_c}(P_l) - D_{\tau, x_c, s_c}(P_l)| &\leq \varepsilon_n \|O\|_1 \end{aligned} \quad (\text{B37})$$

with a success probability of $1 - \vartheta$ when the number of measurements $N_s \geq 2c^4(\mu) \frac{1}{\varepsilon_n^2} \ln(1/\vartheta)$. In this work, we will set $c(\mu) = 2$. We have the following result.

Proposition 9 (Error due to finite measurements using Hadamard test). $|\hat{D}_{\tau, x_c, s_c} - D_{\tau, x_c, s_c}| \leq \varepsilon_n$ and $|\hat{N}_{\tau, x_c, s_c}(O) - N_{\tau, x_c, s_c}(O)| \leq \varepsilon_n$ has a success probability of $1 - \vartheta$ when the number of measurements $N_s \geq 2c^4(\mu) \frac{\|O\|_1^2}{\varepsilon_n^2} \ln(1/\vartheta)$.

d. *Measurement strategy* To measure $\langle \vec{j} | O | \vec{i} \rangle$, we can use the circuit in Fig. 1(c) to generate

$$U_p^\dagger \left(\prod_{q=1}^{\nu} W_{i_q} S \right)^\dagger O \prod_{q=1}^m W_{i_q} S U_p |\psi_0\rangle, \quad (\text{B38})$$

and then measure on a computational basis.

In many practical cases, such as Heisenberg models and electronic structure problems (Eq. (6)), the target problem has certain symmetries S satisfying $[H, S] = 0$. Consequently, the state can be divided into state spaces with different symmetry sectors. For instance, for fermionic problems, the Hamiltonian has particle number symmetry, $[H, \hat{N}] = 0$ with $\hat{N} = \sum_i a_i^\dagger a_i$. In this case, the state can be divided into different sectors in the Hilbert space with different particle numbers, $\mathcal{H} : \text{span}\{|i\rangle\}$ with $|i\rangle$ representing the state with i particles. We can use the ancilla-free measurement strategy in Fig. 1(c2). Note that in this case, the operator W_{i_q} must be symmetry preserving.

3. Proof of Theorem 1 (Problem 1)

When τ is taken as a finite value, g_τ can be regarded a $(1, \varepsilon_\tau)$ -RLCU formula of g . The integral is evaluated within a finite time range,

$$g_{\tau, x_c} = \int_{-x_c}^{x_c} dx p(x) U(x\tau) \quad (\text{B39})$$

One can check that g_{τ, x_c} is a $(1, \varepsilon_{x_c})$ -RLCU formula of g_τ defined in Eq. (9), and is a $(1, \varepsilon_{x_c} + \varepsilon_\tau)$ -RLCU formula of $g_{\tau \rightarrow \infty}$. Each of the integrand $U(x\tau)$ in g_{τ, x_c} is approximated by $U_{2k}^{(s_c)}(x\tau)$ defined in Eq. (18). According to Proposition 7 and Lemma 1, when considering a segment number ν_c and the truncation order s_c defined in Eq. (B45), $U_{2k}^{(s_c)}(x\tau)$ is a $(\mu_2(x), \varepsilon_x)$ -LCU formula, where upper bounds of μ_2 and ε_x can be obtained by Proposition 1.

According to Proposition 1, g_{τ, x_c, s_c} , which is defined as

$$g_{\tau, x_c, s_c} = \int_{-x_c}^{x_c} dx p(x) \tilde{U}(x\tau) \quad (\text{B40})$$

is a (μ, ε) -LCU formula of g , with $\mu := \int_{-\infty}^{\infty} p(x) \mu_2(x) dx \leq \max_x \mu_2(x)$, and $\varepsilon = \varepsilon_c + \varepsilon_\tau + \varepsilon_{s_c}$.

Next, we analyse the error due to finite measurements. In the case where we can directly measure in the eigenbases of the observable O , we can take the estimator in Eq. (40). Then the error of the expectation value of observable can be bounded by directly using Proposition 2. The error distance can be bounded in a similar fashion to Proposition 2. For the case with observables composed of many Pauli terms. Suppose we measure it using importance sampling; the only difference is the amplification of the prefactor by $\|O\|_1$.

Equipped with all these results, we arrive at the following result of eigenstate property estimation

Theorem 3 (Eigenstate property estimation for generic Hamiltonians). *Suppose the conditions and assumptions in Problem 1 hold. Suppose we use the method in Algorithm 1 where we choose the time-segment number function $\nu_c = \mathcal{O}\left((\lambda \Delta^{-1} \ln(\eta^{-1} \varepsilon^{-1}))^{1+\frac{1}{4k+1}}\right)$ for realising the real-time evolution (in Eq. (B44)) and the truncation order $s_c = \mathcal{O}(\ln(\nu_c/\varepsilon_c)/\ln \ln(\nu_c/\varepsilon_c))$. We can achieve the error of observable's expectation on the eigenstate $|u_j\rangle$ within ε , $|\hat{v} - \langle u_j | O | u_j \rangle| \leq \varepsilon$ when the sampling number is $N_s = \mathcal{O}(\eta^{-2} \varepsilon^{-2} \|O\|_1^2 \ln(1/\vartheta))$ (in Eq. (B47)), where \hat{v} is the estimator defined in Eq. (40) with a success probability at least $1 - \vartheta$.*

Proof. We set the imaginary-time as

$$\tau \geq \frac{1}{\Delta} \sqrt{\ln \frac{2}{\varepsilon_\tau}} \quad (\text{B41})$$

and set truncation time x_c

$$x_c \geq 2\sqrt{\ln(2/\varepsilon_c)}. \quad (\text{B42})$$

The maximum real-time is

$$t_c = \tau x_c = \frac{2}{\Delta} \sqrt{\ln(2/\varepsilon_\tau)} \sqrt{\ln(2/\varepsilon_c)} \quad (\text{B43})$$

According to [Proposition 7](#), when the segment number is set as

$$\nu_c = 2 \left(\frac{2(e + c_k)}{\ln 2} \right)^{\frac{1}{4k+1}} (\lambda \tau x_c)^{1+\frac{1}{4k+1}} = 4 \left(\frac{4(e + c_k)}{\ln 2} \right)^{\frac{1}{4k+1}} \left(\frac{\lambda}{\Delta} \sqrt{\ln(2/\varepsilon_\tau) \ln(2/\varepsilon_c)} \right)^{1+\frac{1}{4k+1}} \quad (\text{B44})$$

and set

$$s_c = \mathcal{O} \left(\frac{\ln \left(\frac{4\nu_c}{\varepsilon_{s_c}} \right)}{\ln \left(\nu_c^{\frac{1}{4k+2}} \ln \left(\frac{4\nu_c}{\varepsilon_{s_c}} \right) \right)} \right) \quad (\text{B45})$$

$U_{2k}^{(s_c)}(t_i)$ is a $(2, \varepsilon_{s_c})$ -LCU formula of $U(t_i)$, and the approximation error is given by

$$\max_{t_i} \|U_{2k}^{(s_c)}(t_i) - U(t_i)\| \leq \varepsilon_{s_c}. \quad (\text{B46})$$

According to [Proposition 7](#), we have $|D_{\tau, x_c, s_c} - D_\tau| \leq \varepsilon_c$, $|N_{\tau, x_c, s_c}(O) - N_\tau(O)| \leq \varepsilon_c \|O\|$ with $\varepsilon_c = 3(\varepsilon_{x_c} + \varepsilon_{s_c})$. We set the sampling number as

$$N_s = \frac{2c^4(\mu) \|O\|_1^2}{\varepsilon_n^2} \ln(1/\vartheta). \quad (\text{B47})$$

According to [Proposition 9](#), $|\hat{D}_{\tau, x_c, s_c} - D_{\tau, x_c, s_c}| \leq \varepsilon_n$ and $|\hat{N}_{\tau, x_c, s_c}(O) - N_{\tau, x_c, s_c}(O)| \leq \varepsilon_n$ has a success probability of $1 - \vartheta$ when the number of measurements $N_s \geq 32 \frac{\|O\|_1^2}{\varepsilon_n^2} \ln(1/\vartheta)$. Using the triangular inequality, we have

$$\begin{aligned} \varepsilon_N &:= |\hat{N}_{\tau, x_c, s_c}(O) - N_{\tau \rightarrow \infty}(O)| \leq \|O\|(\varepsilon_\tau + \varepsilon_c) + \|O\|_1 \varepsilon_n, \\ \varepsilon_D &:= |\hat{D}_{\tau, x_c, s_c} - D_{\tau \rightarrow \infty}| \leq \varepsilon_\tau + \varepsilon_c + \varepsilon_n, \end{aligned} \quad (\text{B48})$$

The observable's error in respect to ε_τ , ε_c and ε_n is given by

$$\begin{aligned} |\langle \hat{O} \rangle_{\tau, x_c, s_c} - \langle O \rangle| &= \left| \frac{\hat{N}_{\tau, x_c, s_c}(O)}{\hat{D}_{\tau, x_c, s_c}} - \frac{N(O)}{D} \right| \\ &= \left| \frac{D \hat{N}_{\tau, x_c, s_c}(O) - N(O) \hat{D}_{\tau, x_c, s_c}}{D \hat{D}_{\tau, x_c, s_c}} \right| \\ &\leq \left| \frac{D(N(O) + \varepsilon_N(O)) - N(O)(D - \varepsilon_D)}{D(D - \varepsilon_D)} \right| \\ &= \left| \frac{D\varepsilon_N(O) + N(O)\varepsilon_D}{D^2 - D\varepsilon_D} \right| \\ &\leq \left| \frac{D\varepsilon_N(O) + (N(O) + D)\varepsilon_D}{D^2} \right| \\ &= \eta^{-1} ((\varepsilon_\tau + \varepsilon_c) \|O\| + \varepsilon_n \|O\|_1) + \eta^{-1} (\langle O \rangle + 1) (\varepsilon_\tau + \varepsilon_c + \varepsilon_n) \\ &\leq \eta^{-1} (2 \|O\| + 1) (\varepsilon_\tau + \varepsilon_c) + \eta^{-1} (\|O\| + \|O\|_1 + 1) \varepsilon_n. \end{aligned} \quad (\text{B49})$$

If we set the precision for each component

$$\begin{aligned} \varepsilon_\tau &= \varepsilon_c = \frac{1}{3} \eta \varepsilon \left(\frac{1}{2 \|O\|_\infty + 1} \right), \\ \varepsilon_n &= \frac{1}{3} \eta \varepsilon \frac{1}{\|O\|_\infty + \|O\|_1 + 1}, \end{aligned} \quad (\text{B50})$$

then we have

$$|\langle \hat{O} \rangle_{\tau, x_c, s_c} - \langle O \rangle| \leq \varepsilon \quad (\text{B51})$$

for observable O with a success probability bounded by $1 - \vartheta$.

Under the precision requirement in Eq. (B50), we know from Eq. (B44) that the segment number scales as

$$\nu_c = \mathcal{O}\left((\lambda\Delta^{-1}\ln(\eta^{-1}\varepsilon^{-1}))^{1+\frac{1}{4k+1}}\right) \quad (\text{B52})$$

and the sampling number scales as

$$N_s = \mathcal{O}(\eta^{-2}\varepsilon^{-2}\|O\|_1^2\ln(1/\vartheta)). \quad (\text{B53})$$

□

The actual quantum resources can be estimated by Eq. (B44) and Eq. (B50) (and thus Eq. (B57)) and Eq. (B47).

a. Gate complexity analysis

Using the results in Proposition 3 and Theorem 3, we have the following result for generic Hamiltonians.

Theorem 4 (Gate complexity for generic Hamiltonians' eigenstate property estimation). *Suppose we are given the same condition in Theorem 3. Suppose we synthesise the circuit to CNOT gates, single-qubit Clifford gates and single-qubit Z rotation gates, we have gate count*

$$C_{\text{CNOT}} = \mathcal{O}(\text{wt}(H)\nu_c), \quad C_{R_z} = \mathcal{O}(L\nu_c) \quad (\text{B54})$$

with ν_c given by Eq. (B57).

Proof. We can calculate the maximum required evolution time based on Theorem Theorem 3 with Gaussian function if we want to estimate an observables O with an accuracy ε .

For the ground state preparation, the maximum real-time is given by Eq. (B43). Suppose we divide the time slice into ν segments and use $2k$ th order Trotterisation, in this context, the segment number ν can be chosen as

$$\nu_c = \mathcal{O}((\lambda\Delta^{-1}\ln(\eta^{-1}\varepsilon^{-1}))^{1+\frac{1}{4k+1}}). \quad (\text{B55})$$

We note that since there is a saturation of the gate count for the Trotter-error-compensation indicated by Eq. (47), we take s_c to be infinity in deriving the asymptotic scaling and the gate count is less or at the same order of L or $\text{wt}(H)$. Therefore, the gate complexity in each sample is given by Eq. (B54). In cases where we could implement each e^{-iH_it} , then the gate complexity in each single run is

$$\mathcal{O}(L(\lambda\Delta^{-1}\ln(\eta^{-1}\varepsilon^{-1}))^{1+\frac{1}{4k+1}}). \quad (\text{B56})$$

Thus far, we have completed the proof of Theorem 1.

□

Suppose O is simply a Pauli operator, $\|O\| = 1$. A more explicit form for the segment number can be obtained using Eq. (B50), which is

$$\nu_c = 4\left(\frac{4(e+c_k)}{\ln 2}\right)^{\frac{1}{4k+1}}\left(\frac{\lambda}{\Delta}\ln\left(\frac{9}{\eta\varepsilon}\right)\right)^{1+\frac{1}{4k+1}}, \quad (\text{B57})$$

and can be used to carry out resource estimations when given the parameters of the Hamiltonian.

Theorem 3 gives an upper bound on the gate complexity required for estimating generic Hamiltonians' eigenstate properties in relation to λ , L , and $\text{wt}(H)$. For physical Hamiltonians, we could reduce the gate complexity by using the properties of the Hamiltonians. As shown in Theorem 2 in the Appendix of [49], the segment number can be reduced to

$$\nu_c = \mathcal{O}(n^{\frac{2}{4k+1}}(\Delta^{-1}\ln(\eta^{-1}\varepsilon^{-1}))^{1+\frac{1}{4k+1}}). \quad (\text{B58})$$

Using Proposition 3, we can obtain the gate complexity for lattice models. In short, by using the commutation relation of the Hamiltonian terms in real-time evolution, the gate complexity for eigenstate property estimation using Algorithm 1 scales $\mathcal{O}(n^{1+\frac{2}{4k+1}})$. When using the ancilla-free LCU formulae and the corresponding measurement strategy, the gate operations within each segment can be implemented in parallel, as discussed in Sec. III D 2. Therefore, the depth complexity is $\mathcal{O}(n^{\frac{2}{4k+1}})$. As such, we have completed the proof of Theorem 2 in the main text

4. Discussions on molecular Hamiltonians

The following discusses the resource cost for fermionic problems with the Hamiltonian Eq. (6) and its qubit form given by Eq. (B59). Note that each term in the expansion of V_i is a Pauli operator. Therefore, at each segment, δt , the gates that effectively implement the remainder will merge into a single Pauli operator. This means that the gate count for Trotter-error compensation will saturate to n , regardless of the truncation order s_c .

The Trotter formula will be implemented in a split-operator way. The nonlocal kinetic term will be converted to local terms with an additional cost for implementing the diagonalisation. However, to derive the remainder, we still need to expand all the terms in the Pauli basis. The second-quantised Hamiltonian given by Eq. (6) can be mapped by the Jordan-Wigner transform to a qubit Hamiltonian of the form

$$H = \hat{T} + \hat{V} = \sum_{pq} \tilde{T}_{pq} (X_p Z_{r_i} Z_{r_{i+1}} \cdots Z_{r_{i+k}} X_q + Y_p Z_{r_i} Z_{r_{i+1}} \cdots Z_{r_{i+k-1}} Z_{r_{i+k}} Y_q) + \sum_p \tilde{U}_p Z_p + \sum_{pq} \tilde{V}_{pq} Z_p Z_q \quad (\text{B59})$$

A direct application of our zeroth-order method gives CNOT gate count: $\text{wt}_m(H)(s_c + 2)\nu = \mathcal{O}(n(s_c + 2)\nu) = \mathcal{O}(n(s_c + 2)(\lambda t)^2)$, and 2kth order CNOT gate count gives $(\text{wt}_m(H)s_c + 2 \text{wt}(H))\nu = \mathcal{O}(n^3(\lambda t)^{1+\frac{1}{4k+1}})$ with $\text{wt}(H) = nL = n^3$. However, the kinetic operator is quadratic and thus can be diagonalised by an efficient circuit transformation C

$$\hat{T} = C \left(\sum_p T_p Z_p \right) C^\dagger \quad (\text{B60})$$

The second-order Trotterised time evolution is

$$S_2 = (e^{-iT_x/2} e^{-iV_x} e^{-iT_x/2})^\nu = (Ce^{-iT_x/2} C^\dagger e^{-iV_x} Ce^{-iT_x/2} C^\dagger)^\nu \quad (\text{B61})$$

We denote that the rotation circuit C is composed of C_{CNOT} CNOT gates and the diagonal circuit with the kinetic terms is composed of T_{CNOT} single-qubit rotation gates. For the error compensation term, the gate cost shown in Eq. (47) has a saturation, which is upper bounded by $3n$. The dominant cost is from the Trotterisation.

For Hamiltonian in Eq. (6), we can use the fermionic swap network to simulate the Hamiltonian dynamics with depth $\mathcal{O}(n)$ and gate count $\tilde{\mathcal{O}}(n)$ in each segment. Using the results in Table III and [49], we can estimate the gate complexity for molecular systems in Eq. (6).

Corollary 1 (Eigenstate property estimation for molecular systems). *Suppose we aim to estimate the observable O on the eigenstate $|u_i\rangle$ of an n -qubit molecular Hamiltonian specified in Eq. (6), $\langle u_i | \hat{O} | u_i \rangle$. To achieve an estimation error within ε , it is sufficient to have the gate count of $\tilde{\mathcal{O}}(n^2(\Delta^{-1})^{1+\frac{1}{4k+1}} \log(\eta^{-1}\varepsilon^{-1}) \log(\vartheta^{-1}))$ and a success probability $1 - \vartheta$.*

For quantum molecular systems, the Hamiltonian H takes the following form

$$H := \hat{T} + \frac{1}{2} \hat{V} + C = \sum_{i,j=1}^n h_{ij} \hat{a}_i^\dagger \hat{a}_j + \frac{1}{2} \sum_{i,j,k,l=1}^n V_{ijkl} \hat{a}_i^\dagger \hat{a}_j^\dagger \hat{a}_k \hat{a}_l, \quad (\text{B62})$$

where n is the number of spin orbitals of the molecular system; \hat{a}_i^\dagger and \hat{a}_i are the fermionic generation and annihilation operators, respectively; h_{ij} and V_{ijkl} are the corresponding coefficients for the one-body and two-body interactions, respectively. Note that the identity term in the Hamiltonian is a trivial term, so it is removed in the Hamiltonian in this work for simplicity. For quantum chemistry Hamiltonians, there has been considerable progress in efficiently representing the Hamiltonians with fewer terms and low weights.

These results, such as single factorisation [57] and double factorisation [68], can be directly applied to reduce the cost. A common strategy is to reformulate the two-body fermion operators as a sum of squared one-body operators by Cholesky decomposition, as has been used in AFQMC. The Hamiltonian is reformulated as

$$H = \hat{K} + \hat{V} := \hat{K} + \frac{1}{2} \sum_{\ell}^{\Gamma} \hat{L}_{\ell}^2, \quad (\text{B63})$$

with $\hat{K} := \sum_{i,j=1}^n \left[h_{ij} - \frac{1}{2} \sum_{\ell=1}^{\Gamma} \sum_{k=1}^n L_{(ik)\ell} L_{(jk)\ell}^* \right] \hat{a}_i^\dagger \hat{a}_j$, and $\hat{L}_{\ell} := \sum_{i,l=1}^n L_{(il)\ell} \hat{a}_i^\dagger \hat{a}_l$. Here, the constant is removed and Γ is the number of \hat{L}_{ℓ} .

Below, we use the first-order Trotter formula as an example to analyse the cost within each Trotter segment

$$e^{-iHt} \approx e^{-i\hat{K}t} \prod_{\ell=1}^{\Gamma} e^{-\frac{it}{2} U_{\ell} \sum_p (f_p \hat{n}_p)^2} U_{\ell}^{\dagger} = e^{-i\hat{K}t} \prod_{\ell=1}^{\Gamma} U_{\ell} e^{-\frac{it}{2} \sum_p (f_p \hat{n}_p)^2} U_{\ell}^{\dagger} \quad (\text{B64})$$

In the first line, Trotterisation is used, and thus, this is an approximation with some Trotter errors up to the second order. In the second line, some derivations have been abbreviated and the key facts that we used are $[U_{\ell} \hat{n}_p U_{\ell}^{\dagger}, U_{\ell} \hat{n}_q U_{\ell}^{\dagger}] = 0$ and $e^{-itU_{\ell}\hat{n}_p} U_{\ell}^{\dagger} = U_{\ell} e^{-it\hat{n}_p} U_{\ell}^{\dagger}$.

$$O_a \bigotimes_i |n_i\rangle |0\rangle_o \rightarrow \bigotimes_i |n_i\rangle |\sum_i f_i n_i\rangle \rightarrow \bigotimes_i |n_i\rangle |(\sum_i f_i n_i)^2\rangle \rightarrow \bigotimes_i |n_i\rangle e^{-i(\sum_i f_i n_i)^2} |(\sum_i f_i n_i)^2\rangle \quad (\text{B65})$$

the addition operation may be A very inefficient way to implement the above process may be like this. We first compute Z_j by applying a controlled NOT gate and store the information on the ancillary qubit $|j_1\rangle \dots |j_n\rangle$. We require the following circuit oracle

$$O_a |j_1\rangle \dots |j_n\rangle |0\rangle_r = |j_1\rangle \dots |j_n\rangle |(-1)^{j_1} + (-1)^{j_2} + \dots + (-1)^{j_n}\rangle_r. \quad (\text{B66})$$

$$O_{\vec{A}} |j\rangle |0\rangle_o |0\rangle_{\text{garb}} = |j\rangle |A_j\rangle_o |g(j)\rangle_{\text{garbage}} \quad (\text{B67})$$

with $A_j = j^2$. Then

$$|j\rangle |0\rangle_o |0\rangle_{\text{garb}} |0\rangle \xrightarrow{O_{\vec{A}}} |j\rangle |A_j\rangle_o |g(j)\rangle_{\text{garb}} |0\rangle \xrightarrow{\text{PHASE}} e^{-iA_j t} |j\rangle |A_j\rangle_o |g(j)\rangle_{\text{garb}} |0\rangle \xrightarrow{O_{\vec{A}}^{\dagger}} e^{-iA_j t} |j\rangle |0\rangle_o |0\rangle_{\text{garb}} |0\rangle \quad (\text{B68})$$

The implementation of $e^{-\frac{it}{2} \sum_p (f_p \hat{n}_p)^2}$ can be done by using qubit SWAP gate with $\mathcal{O}(n)$ depth. Therefore, $e^{-\frac{it}{2} \sum_p (f_p \hat{n}_p)^2}$ requires $\mathcal{O}(n)$ depth circuit. Therefore in total, for each time segment, we require $L \times \mathcal{O}(n) = \mathcal{O}(n^2)$ depth circuit.

5. Effect of energy error on eigenstate property expectation estimation

Suppose the energy has an estimation error $\kappa := |\hat{E}_j - E_j| \leq \Delta$. The observable expectation will become

$$\hat{O}_{\tau, x_c, s_c}(\hat{E}_j) = \frac{\hat{N}_{\tau, x_c, s_c}(O, \hat{E}_j)}{\hat{D}_{\tau, x_c, s_c}(\hat{E}_j)}. \quad (\text{B69})$$

In the presence of estimation error $E \neq E_j$, $g_{\tau}(H - \omega)$ will tend to be zero $\|g_{\tau \rightarrow \infty}(H - \omega)\| = 0$. In such a case, we consider the projector $\hat{P}_j = |u_i\rangle \langle u_i|$. Eq. (B9) will need to be modified a little. For a general E , we have

$$g_{\tau}(H - \omega) = \sum_i g_{\tau}(E_i - \omega) \hat{P}_i \quad (\text{B70})$$

When $\tau \geq \frac{1}{\Delta} \sqrt{\ln(2/\varepsilon_{\tau})}$, we have

$$\|g_{\tau}(H - \omega) - g_{\tau}(E_j - \omega) \hat{P}_j\| \leq \varepsilon_{\tau}/2 \quad (\text{B71})$$

The error of the numerator can be bounded by

$$|N_{\tau}(O, E) - g_{\tau}^2(E_j - \omega) N(O)| \leq \varepsilon_{\tau} \|O\| \quad (\text{B72})$$

Compared to the result with an accurate estimation, the only difference is that $N(O)$ and D is coupled with an additional factor $g_{\tau}^2(\kappa)$.

Recall that the objective is to estimate $N(O)$. Therefore, we put the factor $g_{\tau}^{-2}(\kappa)$ coupled with N_{τ} , and denote

$$\varepsilon_N := |g_{\tau}^{-2}(\kappa) N_{\tau}(O, E) - N(O)|. \quad (\text{B73})$$

Since $g_{\tau}^{-2} > 1$, the error ε_N compared to the previous estimation error of the numerator is amplified.

The results concerning a finite cutoff and number of samples can be derived similarly to that in [Theorem 3](#).

$$\begin{aligned}
|\langle \hat{O} \rangle_{\tau, y_c, s_c} - \langle O \rangle| &= \left| \frac{\hat{N}_{\tau, y_c, s_c}(O, \omega)}{\hat{D}_{\tau, y_c, s_c}(\omega)} - \frac{N(O, \omega)}{D(\omega)} \right| \\
&= \left| \frac{D(\omega) \hat{N}_{\tau, y_c, s_c}(O, \omega) - N(O, \omega) \hat{D}_{\tau, y_c, s_c}(\omega)}{D(\omega) \hat{D}_{\tau, y_c, s_c}(\omega)} \right| \\
&\leq \frac{1}{|D(\omega) \hat{D}_{\tau, y_c, s_c}(\omega)|} \left(\left| D(\omega) \hat{N}_{\tau, y_c, s_c}(O) - \frac{\hat{N}_{\tau, y_c, s_c}(O, \omega) \hat{D}_{\tau, y_c, s_c}(\omega)}{g_\tau^2(\kappa)} \right| \right. \\
&\quad \left. + \left| \frac{\hat{N}_{\tau, y_c, s_c}(O, \omega) \hat{D}_{\tau, y_c, s_c}(\omega)}{g_\tau^2(\kappa)} - N(O, \omega) \hat{D}_{\tau, y_c, s_c}(\omega) \right| \right) \\
&\leq \frac{|D(\omega) \varepsilon_N(O, \omega) + N(O, \omega) \varepsilon_D|}{g_\tau^2(\kappa) (D(\omega)^2 - D(\omega) \varepsilon_D)} \\
&\leq \frac{|D(\omega) \varepsilon_N(O, \omega) + (N(O, \omega) + D(\omega)) \varepsilon_D|}{g_\tau^2(\kappa) D^2} \\
&\leq g_\tau^2 \eta^{-1} (2 \|O\| + 1) (\varepsilon_\tau + \varepsilon_c) + g_\tau^2 \eta^{-1} (\|O\| + \|O\|_1 + 1) \varepsilon_n.
\end{aligned} \tag{B74}$$

Compared to the case with known eigenenergy, the observable estimation error ε will be amplified by a factor $g_\tau^{-2}(\kappa) = \exp(2\tau^2 \kappa^2)$.

To ensure the estimation is nonvanishing, we require $\tau \kappa \leq c$, which indicates the energy precision needs to satisfy

$$\kappa \leq c \mathcal{O}(\Delta \log^{-1}((\eta \varepsilon)^{-1})). \tag{B75}$$

6. Discretised version

For the Gaussian-type spectral filter, we show a deterministic version of the LCU decomposition of the spectral filter in [Eq. \(8\)](#). Using the Gaussian integral, also known as the Hubbard-Stratonovich transformation which is widely used in the field theories and auxiliary-field quantum Monte Carlo [[38](#), [43](#)], we have

$$g_\tau(H) = e^{-\tau^2 H^2} = \frac{1}{\sqrt{2\pi}} \int dx e^{-x^2/4} e^{-i\tau x H}. \tag{B76}$$

By converting the integral into a summation, we define a discretised version of $g_{\tau, x_c}^{(D)}(H - \omega)$ with a maximum evolution time x_c as

$$g_{\tau, x_c}^{(D)}(H - \omega) = \frac{1}{\sqrt{2\pi}} \sum_{j=-N_m}^{N_m} b e^{-y_j^2/4} e^{i\tau y_j (H - \omega)} \tag{B77}$$

with total number of steps N_m , the step size $b = x_c/N_m$, and $y_j = jb$, a superscript D denoting a discretised version. An infinite sum of $g_{\tau, x_c}^{(D)}(H - \omega)$ is given by

$$g_\tau^{(D)}(H - \omega) = \frac{1}{\sqrt{2\pi}} \sum_{j=-\infty}^{\infty} b e^{-y_j^2/4} e^{i\tau y_j (H - \omega)} \tag{B78}$$

with total number of steps N_m , the step size $b = x_c/N_m$, and $y_j = jb$.

The discretisation error can be bounded by

$$\varepsilon_{d, x_c} := |g_{\tau, x_c} - g_{\tau, x_c}^{(D)}| \leq |g_\tau - g_\tau^{(D)}| + |g_\tau - g_{\tau, x_c}| + |g_\tau^{(D)} - g_{\tau, x_c}^{(D)}| \tag{B79}$$

We define the discretisation error with an infinite expansion as $\varepsilon_d = |g_\tau - g_\tau^{(D)}|$ the truncation error $\varepsilon_{x_c} := |g_\tau - g_{\tau, x_c}|$ and its discretisation as $\varepsilon_{x_c}^{(D)} := |g_\tau^{(D)} - g_{\tau, x_c}^{(D)}|$

Since e^{-x^2} is a monotonic function, the discretisation form is less than the integral. From the definition of $g_{\tau,x_c}^{(D)}$ Eq. (B77), we can check that $\varepsilon_{x_c}^{(D)} \leq \varepsilon_{x_c}$. From Proposition 7, we know that $\varepsilon_{x_c} \leq \exp(-x_c^2/2)$ and thus $\varepsilon_{x_c}^{(D)}$ is bounded by $\exp(-x_c^2/2)$ as well. With the result derived in [15], ε_d can be bounded by

$$\varepsilon_d \leq \exp\left(\left(\frac{2\pi}{b} - \tau\right)/2\right)^2 \quad (\text{B80})$$

For an equal distribution of error, we choose to set $\varepsilon_d = \varepsilon_{x_c} = \varepsilon/3$. When the stepsize is set as $b = 2\pi/(x_c + \tau) = \mathcal{O}(\Delta(\ln(\varepsilon^{-1}))^{-1/2})$, the total error is bounded by ε . The total number of steps is

$$N_m = x_c(x_c + \tau)/2\pi \leq \frac{2}{\pi\Delta} \ln \frac{2}{\varepsilon_\tau} = \mathcal{O}(\Delta^{-1} \ln(\varepsilon^{-1})) \quad (\text{B81})$$

with ε_τ defined in Eq. (B50).

Appendix C: Eigenenergy estimation (Problem 2)

In this section, we discuss the gate complexity of eigenenergy estimation described in Problem 2. We provide a proof for the second part of Theorem 1. We first discuss how to use the denominator to estimate the eigenenergy E_j . Intuitively, we can find that $D_\tau(\omega)$ indeed shows a coarse-grained energy spectrum. For the initial state $|\psi_0\rangle = \sum_i c_i |u_i\rangle$, the spectrum of the initial state can be characterised by

$$P(E) = \sum_i |c_i|^2 \delta(\omega - E_i). \quad (\text{C1})$$

One can prove that $D_\tau(E) = [g_\tau^2 \star P](E)$ where \star denotes the convolution of two functions.

Suppose we have a prior knowledge of $E_j \in [E_j^L, E_j^R]$. It is worth noting that we cannot distinguish eigenenergies that are very close to each other. The eigenenergies that are close to each other could be merged and regarded as a broadened eigenenergy. Here, we assume that the target resolution is less than the energy gap, i.e., $\kappa < \Delta$, and $E_j^R < E_j + \Delta/2$, $E_j^L > E_j - \Delta/2$. Given this range, the j th eigenenergy can be searched by

$$E_j = \arg \max_{\omega \in [E_j^L, E_j^R]} \hat{D}_\tau(\omega). \quad (\text{C2})$$

The maximum of $D_\tau(\omega)$ within the range $[E_j^L, E_j^R]$ gives us an estimate of eigenenergy E_j .

In practice, we can only obtain an estimation $\hat{D}_\tau^{(x_c)}(E)$ of $D_\tau(E)$, when considering finite cutoff time x_c , segment number ν_c , truncation s_c and number of samples N_s . The eigenenergy is determined by

$$\hat{E}_j := \arg \max_{\omega \in [E_j^L, E_j^R]} \hat{D}_{\tau, x_c, s_c}(\omega). \quad (\text{C3})$$

Similar to property estimation in Sec. B, the error sources include a finite imaginary time, a finite cutoff of real-time evolution, discretization error, and the statistical error due to Hamiltonian simulation and finite number of samples

$$\hat{D}_{\tau, x_c, s_c}(\hat{E}_j) - D_\tau(E_j) \leq \varepsilon_\tau + \varepsilon_{x_c} + \varepsilon_{s_c} + \varepsilon_n \quad (\text{C4})$$

Based on the error dependence, we can estimate the resource requirements (i.e., circuit depth and number of samples) for eigenenergy estimation. Compared to Sec. B, the only difference is that the denominator is a function of ω in energy estimation, while we take $\omega = E_j$ in property estimation in Sec. B. The following lemma establishes the error due to a finite τ .

Lemma 2 (Error due to a finite τ (Proposition 3 in [20])). *When $\tau \geq \frac{2}{\Delta} \sqrt{\ln(2/\varepsilon_\tau)}$, $|D_\tau(\omega) - \eta g_\tau^2(\omega - E_j)| \leq \varepsilon_\tau$.*

The rest of the proof is nearly identical to Sec. B. We give the result here.

Theorem 5 (Eigenenergy estimation for generic Hamiltonians). *Suppose the conditions and assumptions in Problem 2 hold.*

Case I: Suppose that \hat{E}_j is determined by Eq. (C3) and we use the method in Algorithm 1 where we choose the time-segment number function $\nu_c = \mathcal{O}\left((\lambda\kappa^{-1} \ln(\eta^{-1}))^{1+\frac{1}{4k+1}}\right)$ for realising the real-time evolution (in and the truncation

order $s_c = \mathcal{O}(\ln(\nu_c)/\ln\ln(\nu_c))$. We can achieve the error of eigenenergy estimation within κ , $|\hat{E}_j - E_j| \leq \kappa$ with a success probability at least $1 - \vartheta$ when the number of samples is $N_s = \mathcal{O}(\eta^{-2}\ln(1/\vartheta))$.

Case II: Suppose that \hat{E}_j is determined by Eq. (C3) and we use the method proposed by [77]. When we choose the time-segment number function $\nu_c = \mathcal{O}((\lambda\Delta^{-1}\ln(\eta^{-1}\kappa^{-1}))^{1+\frac{1}{4k+1}})$ for realising the real-time evolution, we can achieve the error of eigenenergy estimation within κ , $|\hat{E}_j - E_j| \leq \kappa$ with a success probability at least $1 - \vartheta$ when the number of samples is $N_s = \mathcal{O}(\eta^{-2}\Delta^4\kappa^{-4}(\ln(\kappa^{-2}\eta^{-1}))^2\ln(1/\vartheta))$.

Proof. We start by proving the result in Case I. From Eq. (C3), we have

$$\hat{D}_{\tau,x_c,s_c}(\hat{E}_j) \geq \hat{D}_{\tau,x_c,s_c}(E_j). \quad (\text{C5})$$

Then we bound the difference between $D_\tau(\omega)$ and $\eta g_\tau^2(\omega - E_j)$ using Lemma 2. That is, when we set the imaginary-time as $\tau \geq \frac{2}{\Delta}\sqrt{\ln\frac{2}{\eta\varepsilon_\tau}}$ we have

$$|D_\tau(E_j) - \eta| \leq \eta\varepsilon_\tau, \quad |D_\tau(\hat{E}_0) - \eta g_\tau(\hat{E}_0 - E_0)^2| \leq \eta\varepsilon_\tau. \quad (\text{C6})$$

Here it is worth noting that we do not have to know the value of η .

The maximum real-time is

$$t_c = \tau x_c = \frac{4}{\Delta}\sqrt{\ln(2/\eta\varepsilon_\tau)}\sqrt{\ln(2/\eta\varepsilon_c)}. \quad (\text{C7})$$

According to Proposition 7, when the segment number is set by

$$\nu_c = 4\left(\frac{2(e + c_k)}{\ln 2}\right)^{\frac{1}{4k+1}}(\lambda\tau x_c)^{1+\frac{1}{4k+1}} \quad (\text{C8})$$

$U_{2k}^{(s_c)}(t_i)$ is a $(2, \varepsilon_{s_c})$ -LCU formula of $U(t_i)$ with the approximation error given by $\max_{t_i} \|U_{2k}^{(s_c)}(t_i) - U(t_i)\| \leq \varepsilon_{s_c}$, and we have $|D_{\tau,x_c,s_c}(\omega) - D_\tau(\omega)| \leq \eta\varepsilon_c$ with $\varepsilon_c = 3(\varepsilon_x + \varepsilon_n)$

According to Proposition 9, when the number of measurements $N_s = 32\eta^{-2}\varepsilon_n^{-2}\ln(1/\vartheta)$, we have

$$\begin{aligned} |D_\tau(E_j) - \hat{D}_{\tau,x_c,s_c}(E_j)| &\leq \eta(\varepsilon_c + \varepsilon_n) \\ |D_\tau(\hat{E}_j) - \hat{D}_{\tau,x_c,s_c}(\hat{E}_j)| &\leq \eta(\varepsilon_c + \varepsilon_n) \end{aligned} \quad (\text{C9})$$

with a success probability of $1 - \vartheta$. According to [20], the following inequality holds

$$|\hat{E}_j - E_j| \leq \frac{1}{\tau}g_\tau^{-1}\left(\sqrt{1 - 2(\varepsilon_\tau + \varepsilon_c + \varepsilon_n)}\right). \quad (\text{C10})$$

When we set the precision for each component

$$\varepsilon_\tau = \varepsilon_c = \varepsilon_n \leq \frac{1}{6}(1 - e^{-1}) \leq 0.1 \quad (\text{C11})$$

and $\tau \geq \kappa^{-1}$, we can make sure that the energy estimation precision is no greater than κ . From the precision requirement Eq. (C11) and Eq. (C7), we require

$$t_c \geq \kappa^{-1}\ln(20\eta^{-1}) \quad (\text{C12})$$

when $\kappa \leq \Delta/4$. Using Proposition 7, the segment number is set to be

$$\nu_c = 4\left(\frac{2(e + c_k)}{\ln 2}\right)^{\frac{1}{4k+1}}(\lambda\kappa^{-1}\ln(20\eta^{-1}))^{1+\frac{1}{4k+1}} = \mathcal{O}\left((\lambda\kappa^{-1}\ln(\eta^{-1}))^{1+\frac{1}{4k+1}}\right) \quad (\text{C13})$$

and set s_c by Eq. (B45).

In [24], Wang et al. showed that when using a Gaussian filter, the precision dependence can be improved, where the eigenenergy is also determined by Eq. (C3). Compared to Case I, the key difference is that show that the distance $|D_\tau(\omega) - \eta|$ is modulated by the estimation error $\omega - E_j$. When we set the imaginary time

$$\tau = \frac{1}{0.9\Delta}\sqrt{\ln(20\kappa^{-2}\eta^{-1})} = \mathcal{O}(\Delta^{-1}(\ln(\kappa^{-2}\eta^{-1}))^{-\frac{1}{2}}) \quad (\text{C14})$$

we can distinguish E_j from the others. The cutoff by x_c can be similarly obtained. Using [Proposition 7](#), when the segment number is set to be

$$\mathcal{O}\left((\lambda\Delta^{-1}\ln(\eta^{-1}\kappa^{-1}))^{1+\frac{1}{4k+1}}\right) \quad (\text{C15})$$

the eigenenergy error can be bounded by κ by using the results in [24]. Note that in [24], the error is $\varepsilon_n = \tau\kappa$. Thus the number of samples

$$N_s = \mathcal{O}(\eta^{-2}\tau^{-4}\varepsilon^{-4}\ln(1/\vartheta)) = \mathcal{O}(\eta^{-2}\Delta^4\kappa^{-4}(\ln(\kappa^{-2}\eta^{-1}))^2\ln(1/\vartheta)) \quad (\text{C16})$$

□

When given a Hamiltonian with parameters n , L , $\text{wt}(H)$, and $\text{wt}_m(H)$, the gate complexity of eigenenergy estimation can be similarly obtained by using [Proposition 3](#).

Appendix D: Circuit compilation and gate cost for block-encoding-based methods

1. Stage Setting

In this section, we briefly introduce and estimate the gate cost for block-encoding-based methods. Here we mainly discuss the cost based on the result by Google's team in [56] which is used in our numerical simulation. There are considerable progress in reducing the cost for block encoding. We will not introduce these advanced techniques which are not the main focus of this work.

To estimate the gate cost of each algorithm, we synthesize the circuits to CNOT gates, single-qubit Clifford gates and T -gates. The CNOT gate number is more important for a near-term application on a quantum computer with no or limited fault tolerance, while the T -gate number is more critical for a long-term application on a fully fault-tolerant quantum computer. In some subroutines of the above algorithms, a direct estimation of the T -gate number is hard to obtain. In this case, we first synthesize the circuits to CNOT gates, single-qubit Clifford gates and single-qubit Z -axis rotation gates $R_z(\theta)$. Then we estimate the T -gate number n_T using the $R_z(\theta)$ gate number n_{Rz} . We will consider the optimal ancilla-free gate synthesis algorithm in Ref. [70], which requires $3\log_2(1/\varepsilon) + \mathcal{O}(\log\log(1/\varepsilon))$ T -gates to approximate the $R_z(\theta)$ gate to a precision ε . Here, we set the gate synthesis error of each $R_z(\theta)$ ε_{CS} to be a small value compared to the total error. In practice, we should determine the resource overhead c_T based on the number of R_z gates in the quantum algorithm.

We remark that, if we are allowed to introduce extra ancillary qubits and entangling Clifford gates, one can further reduce the required T gates to

$$1.15\log_2(1/\varepsilon) + 9.2$$

using a repeat-until-success strategy [78]. However, this will introduce extra ancillary qubit requirements and more CNOT gate costs.

In our resource analysis, to streamline the comparison, we exclude the observable estimation error due to a finite sampling cost. We will focus on the circuit depth to achieve a certain level of accuracy of the RCLU formula. Here, we remark that while the RLCU method cannot prepare the state, it can effectively prepare the eigenstate at the level of expectation. To get the resource cost, the key component is to get the segment number ν_c , which is directly related to the maximum real evolution time t_c . The gate count for CNOT gates and single-qubit rotation gates can be obtained by using [Proposition 3](#).

We define

$$\begin{aligned} n_L &:= \lceil \log_2 L \rceil \\ \Lambda &:= \max_l \alpha_l \end{aligned} \quad (\text{D1})$$

In the standard block encoding procedure [79, 80], the n -qubit Hamiltonian H is encoded in a $(n_L + n)$ -qubit unitary, $\text{select}(H)$

$$\text{select}(H) := \sum_{l=1}^{L'} |l\rangle\langle l| \otimes H_l \quad (\text{D2})$$

If we denote,

$$|G\rangle := \text{PREP} |0\rangle^{n_L} = \frac{1}{\sqrt{\lambda}} \sum_{l=1}^L \sqrt{\alpha_l} |l\rangle, \quad (\text{D3})$$

then we have

$$H = \lambda(\langle G| \otimes I) \text{select}(H)(|G\rangle \otimes I) \quad (\text{D4})$$

which indicates that H is block-encoded into $\text{select}(H)$. Here, PREP encodes the amplitude into the state on the ancillary space, and it is also referred to as the amplitude-encoding unitary or PREPARE operation in literature.

Reflection unitary R

$$R := (I - 2|0\rangle\langle 0|) \otimes I \quad (\text{D5})$$

where the operation $(I - 2|0\rangle\langle 0|)$ is defined on the ancillary space with dimension n_L .

2. Gate cost

a. The index enumeration circuit

We follow the circuit construction in Ref. [56] to build the amplitude encoding operation (denoted by PREP or $B(x)$) and controlled select operation C-select(H). A major gadget of both operations is the following operation,

$$\text{C-select } (X) = \sum_{a=0}^1 |a\rangle\langle a| \otimes \sum_{l=1}^L |l\rangle\langle l| \otimes (X_l)^a, \quad (\text{D6})$$

where $X_l \in \{I, X\}$ is a single-qubit Pauli operator. The value of X_l depends on the value of l stored in the classical register. We can regard C-select(X) as a simplified version of C-select(H), where $H = \sum_{l=1}^L X_l$ is a single-qubit Hamiltonian where X_l is either I or X , based on the storage in the classical register.

In Sec. III in Ref. [56], the authors construct a “sawtooth” circuit to realise the C-select(X) gate (which is called the indexed operation in the original paper). In the simplified circuit of C-select(X) in Fig. 7 in Ref. [56], we need $(L - 1)$ computing AND operations, $(L - 1)$ uncomputing AND operations, L control- X_l gates, and $(L - 1)$ extra CNOT gates. If we decompose the computing and uncomputing AND operations based on Fig. 4 in Ref. [56], and synthesize all the gates to Clifford + T gates, we will have the following observation.

Observation 1 (Gate cost in the index enumeration circuit). *If we construct the index enumeration circuit C-select(X) defined in Eq. (D6) following the ‘sawtooth’ way in Ref. [56] and synthesize all the gates to CNOT gates, single-qubit Clifford gates and T gates, then we can realise C-select (X) using*

1. $(6L - 5)$ CNOT gates;
2. $(4L - 4)$ T gates.
3. $(2L - 2)$ Hadamard gates.

3. The amplitude encoding, select gates, and reflection gates

Now, we estimate the gate cost in amplitude encoding, select, and reflection operations. The amplitude-encoding unitary B realises the following transformation,

$$B|0\rangle = \sum_{l=1}^L \sqrt{\omega_l} |l\rangle |\text{temp}_l\rangle$$

where $\omega_l := \alpha_l/\lambda$, is the normalised amplitude of the Hamiltonian. Following Ref. [56], we assume that it is allowed to introduce temporary storage $|\text{temp}_l\rangle$ during the amplitude encoding. This will not cause problems as long as we finally disentangle the system $|\text{temp}_l\rangle$ during the implementation of B^\dagger .

The dominant subroutine of PREPARE circuit is the SUBPREPARE circuit defined in Eq. (48) in Ref. [56], which realise the amplitude encoding to different orbitals, ignoring the spin information first. In our discussion, we first ignore the detailed structure of the Hamiltonian H with respect to different spins. In this case, we can treat SUBPREPARE circuit to be the PREPARE circuit. To realise the SUBPREPARE circuit, we use the method introduced in Sec. IIID in Ref. [56]. The basic idea is to first prepare ancillaries with uniformly distributed coefficients over indecies l and then use a pre-determined binary representation of a probability keep_l , to perform a controlled-swap on the amplitude register l and another predetermined amplitude location alt_l . With well-designed values of swap probability keep send swap location alt_l , we can use the circuit in Fig. 11 in Ref. [56] to realise the SUBPREPARE circuit.

Suppose we want to realise the amplitude encoding with an accuracy of ε_{AE} , that is, to realise the following transformation,

$$B^{\varepsilon_{AE}} |0\rangle = \sum_{l=1}^L \sqrt{\tilde{\omega}_l} |l\rangle |\text{temp}_l\rangle \quad (\text{D7})$$

where $\tilde{\omega}_l$ is a n_{AE} bit approximation to the true value ω_l

$$|\tilde{\omega}_l - \omega_l| \leq \varepsilon_{AE}, \quad l = 1, \dots, L.$$

and we require the number of ancillary qubits to be

$$n_{AE} = \lceil -\log_2 \varepsilon_{AE} \rceil.$$

Due to the relation of the rescaled spectrum by block encoding, we have the relation

$$\varepsilon_{\text{PREP}} = \frac{\varepsilon}{\lambda}. \quad (\text{D8})$$

The relation of the amplitude encoding error and PREP error could be derived by considering the norm of the Hamiltonian, and a simple relation is given by

$$\varepsilon_{AE} \sim \frac{\varepsilon_{\text{PREP}}}{L}. \quad (\text{D9})$$

Following Ref. [56] (see Fig. 11), we need to introduce at least $2n_{AE} + 2n_L + 1$ extra ancillary qubits, and $n_L := \lceil \log_2 L \rceil$. To simplify the gate cost, we assume L is a power of 2. In this case, the first layer of the circuit in Fig. 11 in Ref. [56] can be realised using Hadamard gates. If L is not a power of 2, additional quantum resources are needed.

The second and the third layer of the circuit requires the QROM circuit in Fig. 10 in Ref. [56], which is a modified version of the index enumeration circuit C-select(X) defined in Eq. (D6).

Based on **Observation 1**, the second layer of date loading requires $5(L-1) + L(n_L + n_{AE})$ CNOT gates, $4(L-1)$ T gates. The third layer is a coherent inequality test, which requires $(n_{AE}-1)$ AND and uncomputing AND operations, and additional $6(n_{AE}-1)$ CNOT gates plus 1 Toffoli gate. Thus, it requires $11n_{AE} - 5$ CNOT gates and $4n_{AE} + 3$ T gates.

The fourth layer is a Fredkin gate, which is controlled swap gate. Following Fig. 5 in [81], this gate can be synthesised into Clifford + T gates using $8n_L$ CNOT gates and $7n_L T$ gates.

Observation 2 (Ancillary qubit and gate costs in the second-type amplitude encoding operation). *If we synthesize the $B^{\varepsilon_{AE}}$ unitary defined in Eq. (D7) to CNOT gates, single-qubit Clifford gates and T gates, then the approximate ancillary and gate cost of $B^{\varepsilon_{AE}}$ are listed as follows,*

1. $2n_{AE} + 2n_L + 1$ extra ancillary qubits;
2. $n_L(L+8) + n_{AE}(L+11) + 5L - 10$ CNOT gates;
3. $4(L+n_{AE}) + 7n_L + 3$ T gates;

Here, $n_{AE} := \lceil -\log_2 \varepsilon_{AE} \rceil$ and $n_L := \lceil \log_2 L \rceil$.

With the above result, it is easy to analyse the gate cost of the C-select(H) gate. A straightforward implementation of the C-select(H) gate is to replace of X_l gate in C-select(X) defined in Eq. (D6) to multi-qubit Pauli gates P_l . For instance, consider the transverse field Ising model

$$H = J \sum_i \sigma_i^z \sigma_{i+1}^z + h \sum_i \sigma_{i+1}^x \quad (\text{D10})$$

with the periodic boundary condition. The gate cost for the lattice Hamiltonian is shown in [Corollary 2](#).

Corollary 2 (Gate cost in the C-select(H) operation of the lattice model). *If we construct the controlled-select circuit C-select(H) of the lattice model following the ‘sawtooth’ way in Ref. [56] and synthesize all the gates to CNOT gates, single-qubit Clifford gates and T gates, then the approximate gate cost of C-select(H) is listed as follows,*

1. $5(L - 1) + \text{wt}(H)$ CNOT gates;
2. $(4L - 4)$ T gates.

Next, we consider the gate cost for fermionic Hamiltonian in Eq. (49).

The fermionic Hamiltonian can be mapped to a qubit form by JW transformation. We suppose there are L terms with distinctive coefficients in total. To further improve the gate cost in a fermionic Hamiltonian, Ref. [56] introduces an accumulator during the Pauli gate query process (Sec. IIIB and Fig. 8 in Ref. [56]). The accumulator will ‘accumulate’ the effect of the Pauli operators accessed in the previous data queries and save the CNOT gate cost. Using this improved select operation, we can reduce the CNOT cost for each Pauli operator P_l to a constant independent of the weight of P_l . We will use an optimistic estimate of the CNOT gate cost for controlled- P_l operations, which is $5(L - 1) + 3L = 8L - 5$ for QSP in the numerical simulation. The actual cost should be greater than this value.

Observation 3 (Ancillary qubit and gate costs in the reflection operation [82]). *If we construct reflection operation $I - 2|0\rangle\langle 0|$ on n qubits following methods in Proposition 4 in [82] and synthesize all the gates to CNOT gates, single-qubit Clifford gates and T gates, then the approximate ancillary qubit and gate costs are listed as follows,*

1. $\lceil \frac{n-3}{2} \rceil$ ancillary qubits
2. $(6n - 12)$ CNOT gates;
3. $(8n - 17)$ T gates.

4. Gate cost for Trotter methods

In the Trotter methods, we first divide the real-time evolution into ν segments,

$$e^{-iHt} = (e^{-iHx})^\nu. \quad (\text{D11})$$

where $x := t/\nu$. The first-order Trotter formula is

$$S_1(x) = \prod_{l=1}^L e^{-ixH_l}. \quad (\text{D12})$$

and the second-order Trotter formula is

$$S_2(x) = \prod_{l=L}^1 e^{-i(x/2)H_l} \prod_{l=1}^L e^{-i(x/2)H_l}. \quad (\text{D13})$$

The $(2k)$ th-order Trotter formula is

$$S_{2k}(x) = [S_{2k-2}(p_k x)]^2 S_{2k-2}((1 - 4p_k)x) [S_{2k-2}(p_k x)]^2 \quad (\text{D14})$$

with $p_k := 1/(4 - 4^{1/(2k-1)})$ for $k \geq 1$

We use the results for $2k$ th-order Trotter formula from [61, 83] to analyse the Trotter Cost. We put their results below for the ease of readers.

Lemma 3 (Simple Trotter error bound for the $2k$ th-order Trotter formula ([61, 83])). *Let $H = \sum_{l=1}^L H_l$ be a Hamiltonian consisting of L summands and $t \geq 0$. We denote*

$$a_{2k}(\nu) := 2 \frac{(2 \cdot 5^{k-1} L \Lambda t)^{2k+1}}{(2k+1)! \nu^{2k+1}} e^{2 \cdot 5^{k-1} L \Lambda t / \nu}, b_{2k}(\nu) := \frac{L^{2k} (2 \cdot 5^{k-1} \Lambda t)^{2k+1}}{(2k-1)! \nu^{2k+1}} e^{2 \cdot 5^{k-1} L \Lambda t / \nu}, \quad (\text{D15})$$

where $k \geq 1, \nu$ is the time segment number, Λ is defined in Eq. (2). If we set the segment number ν to be

$$\nu_{2k}^{\det} = \min \left\{ \nu \in \mathbb{N} : \frac{\nu}{2} a_{2k}(\nu) \leq \varepsilon \right\} \quad (\text{D16})$$

for the deterministic first-order Trotter formula, or set ν to be

$$\nu_{2k}^{random} = \min \left\{ \nu \in \mathbb{N} : \frac{\nu}{2} (a_{2k}(\nu)^2 + 2b_{2k}(\nu)) \leq \varepsilon \right\}, \quad (\text{D17})$$

for the randomized first-order Trotter formula, then the spectral norm distance of the resulting simulation channel to the unitary channel of e^{-iHt} is at most ε .

From Eq. (D16), the time segment can be roughly approximated by

$$\nu_{2k} \leq \frac{(2 \cdot 5^{k-1} L \Lambda t)^{1+\frac{1}{2k}}}{((2k+1)!)^{\frac{1}{2k}} \varepsilon^{\frac{1}{2k}}}. \quad (\text{D18})$$

In our numerical simulation, we search the required segment number by Eq. (D16).

Appendix E: Ground state property estimation by quantum signal processing proposed by Lin and Tong

1. Overview

In this section, we first review the key ingredient of the seminal algorithm proposed by Lin and Tong [29]. Their method relies on the block encoding of a non-unitary matrix in the quantum circuit. To build up a tight connection to the [29] and ease the readers, we will follow the notation and convention used in [29].

To simplify the notations, we denote the CNOT gate and T gate required for select(H) operation as S_{CNOT} and S_T , and the CNOT gate and T gate required for PREP operation as P_{CNOT} and P_T , respectively.

A matrix $A \in \mathbb{C}^{N \times N}$ where $N = 2^n$ can be encoded in the upper-left corner of an $(n_L + n)$ -qubit unitary matrix if

$$\|A - \alpha(\langle 0^{n_L} | \otimes I)U(|0^{n_L}\rangle \otimes I)\|_2 \leq \varepsilon. \quad (\text{E1})$$

and we refer to U as an $(\alpha, n_L, \varepsilon)$ -block-encoding of A . In this work, we consider the Hamiltonian written in a linear combination of unitaries in Problem 1. In the standard block encoding procedure, the n -qubit Hamiltonian H can be explicitly block-encoded into $U_H := \text{PREP}^\dagger \cdot \text{select}(H) \cdot \text{PREP}$, as shown in Eq. (D4).

The state preparation algorithm based on QSP is summarised below.

1. Obtain the $(\lambda, n_L, 0)$ -block-encoding of a Hermitian matrix $H = \sum_k E_k |\psi_k\rangle \langle \psi_k| \in \mathbb{C}^{N \times N}$, $N = 2^n$, $\mathbb{E}_k \leq \mathbb{E}_{k+1}$. This block encoding is constructed by U_H .
2. Construct a $(\lambda + |\mu|, n_L + 1, 0)$ -block-encoding of matrix $H - \mu I$ using of [31, Lemma 29] for any $\mu \in \mathbb{R}$.
3. Construct an $(1, n_L + 2, \varepsilon)$ -block-encoding of

$$R_{<\mu} = \sum_{k:\mathbb{E}_k < \mu} |\psi_k\rangle \langle \psi_k| - \sum_{k:E_k > \mu} |\psi_k\rangle \langle \psi_k|.$$

This is realised by constructing a block encoding of the sign function $-S(\frac{H-\mu I}{\alpha+|\mu|}; \delta, \varepsilon)$ for any δ and ε where $S(\cdot, \delta, \varepsilon)$ is the sign function of degree $d = \frac{\varepsilon}{2\delta} \ln(32\pi^{-1/2}\varepsilon^{-1})$. Note that if we assume further that $\Delta/2 \leq \min_k |\mu - \mathbb{E}_k|$, then we let $\delta = \frac{\Delta}{4\lambda}$, all the eigenvalues of $-S(\frac{H-\mu I}{\lambda+|\mu|}; \delta, \varepsilon)$ are ε -close to either -1 or 1, and thus $-S(\frac{H-\mu I}{\lambda+|\mu|}; \delta, \varepsilon)$ is ε -close, in operator norm, to the reflector about the direct sum of eigen-subspaces corresponding to eigenvalues smaller than μ :

4. Using the block encoding of $R_{<\mu}$, we can construct an $(1, n_L + 3, \varepsilon/2)$ block encoding of the projection operator $P_{<\mu} := \frac{1}{2}(R_{<\mu} + I)$.
5. Obtain the ground state with a success probability close to 1 by amplitude amplification.
6. Observable estimation.

Next, we show the resource analysis of each step at a gate level. we denote the resource as $(\cdot, \cdot, \cdot, \cdot)$ with the four elements (\cdot) representing the ancillary qubits, the number of CNOT gates, the number of T gates, and single-qubit R_z rotations.

1. Block encoding: $(n_L, S_{\text{CNOT}} + 2P_{\text{CNOT}}, S_{\text{T}} + 2P_{\text{T}}, 0)$
2. Controlled select(H) and two PREP operations: $(n_L + 1, S_{\text{CNOT}} + 2P_{\text{CNOT}}, S_{\text{T}} + 2P_{\text{T}}, 2)$
3. QSP of the sign function and hence the R operator: $(n_L + 2, d(S_{\text{CNOT}} + 2P_{\text{CNOT}}) + 2d, d(S_{\text{T}} + 2P_{\text{T}}), 3d)$ with $d = [\frac{2e\lambda}{\Delta} \ln(32\pi^{-1/2}\varepsilon^{-1})]$ obtained from [Lemma 4](#)
4. Projector, which is a controlled version of R : $(n_L + 3, d(4 + 6S_{\text{CNOT}} + 2P_{\text{CNOT}} + 2S_{\text{T}} + 2L), d(7S_{\text{CNOT}} + 5S_{\text{T}} + 2P_{\text{T}} + 4L), 4d)$.
5. Amplitude amplification. $(n_L + 3 + \lceil \frac{n-3}{2} \rceil, d\gamma^{-1}(S_{\text{CNOT}} + 2P_{\text{CNOT}} + 6n - 10), d\gamma^{-1}(S_{\text{T}} + 2P_{\text{T}} + 8n - 17), 3d\gamma^{-1})$ with $d = [\frac{2e\lambda}{\Delta} \ln(32\pi^{-1/2}\gamma^{-1}\varepsilon^{-1})]$.

In the 4th step. In each block, the controlled gates:

1. Controlled Phase iterate: 2 CNOT + 2 single-qubit rotation. Thus, the total single-qubit Pauli rotation gate is $4d$.
2. Controlled select(H) and 2 PREP. CNOT: $6S_{\text{CNOT}} + 2P_{\text{CNOT}} + 2S_{\text{T}}$. The third $2S_{\text{T}}$ is from that one controlled T gate can be synthesised by 2 CNOT and $2\sqrt{\text{T}}$ gates.
T gate: $7S_{\text{CNOT}} + 5S_{\text{T}} + 2P_{\text{T}}$, where the first 7 comes from Toffolis gates, the second 5 is from that one controlled T gate can be synthesised by 2 CNOT and $2\sqrt{\text{T}}$ gates, and we simply assume that $2\sqrt{\text{T}}$ may be catalysed by 5 T gates using Hamming weight by [58].
Note that the select(H) has the Hadamard gates: each controlled Hadamard gives 2 T gates and 1 CNOT gate.
At least, we have $2L + n_L$ Hadamard gates in select(H).
3. The other operations are symmetric.

In total, QSP requires the number of CNOT gates

$$d(2 + 2 + 6S_{\text{CNOT}} + 2P_{\text{CNOT}} + 2S_{\text{T}} + 2L)$$

T gates

$$d(7S_{\text{CNOT}} + 5S_{\text{T}} + 2P_{\text{T}} + 4L)$$

In the 5th step, the additional cost is from the reflection from [Observation 3](#).

The ground state preparation error is composed of two parts: the error from the approximation of the sign function, and the block-encoding error of the PREP operation

$$\varepsilon = \varepsilon_{sgn} + \varepsilon_{tot,\text{PREP}}. \quad (\text{E2})$$

Considering the $2d$ repetition of the PREP operation and the relation indicated by, we have

$$\varepsilon_{\text{PREP}} = \frac{\varepsilon}{4d\lambda} \quad (\text{E3})$$

we choose to set the amplitude encoding error as

$$\varepsilon_{AE} \sim \frac{\lambda}{L} \varepsilon_{\text{PREP}} = \frac{\varepsilon}{4Ld} \quad (\text{E4})$$

and $n_{AE} = \lceil -\log_2 n_{AE} \rceil$.

A key component in [29] is a polynomial approximation of the sign function in the domain $[-1, -\delta] \cup [\delta, 1]$. To derive the actual degree, we use an explicit construction of a polynomial with the same error scaling provided in [64] based on the approximation of the erf function.

Lemma 4 (Polynomial approximation to the sign function $\text{sgn}(x)$ (QETU overhead) [64]). *For any $\delta < 1$, $\varepsilon \leq \sqrt{2/\pi e}$, the polynomial $S(x, \delta, \varepsilon) = p_{sgn, \delta, n}(x) = p_{erf, k, n}(x)$ of odd degree $d = [\frac{e}{2\delta} \ln(32\pi^{-1/2}\varepsilon^{-1})] = \mathcal{O}(\delta^{-1} \log(\varepsilon^{-1}))$ satisfies*

$$\varepsilon_{sgn, \delta, n} = \max_{x \in [-1, -\delta] \cup [\delta, 1]} |p_{sgn, \delta, n}(x) - \text{sgn}(x)| \leq \varepsilon. \quad (\text{E5})$$

The actual gate cost for QETU method is analysed by [Lemma 4](#)

Appendix F: Ground state property estimation with phase estimation

For the canonical QPE algorithm [84], we apply a series controlled U, U^2, \dots, U^{2^k-1} and an inverse quantum Fourier transform on the ancillary k qubits, such that the state becomes

$$\sum_i c_i |0^{\otimes k}\rangle |E_i\rangle \rightarrow \sum_i p_i |\text{bin}(E_i)\rangle |E_i\rangle \quad (\text{F1})$$

1. Complexity of phase estimation

To obtain a binary estimate of the energy precise to $n = \lceil \log_2 \varepsilon^{-1} \rceil$ bits, we require $k = \mathcal{O}(\log_2 \varepsilon^{-1} + \log_2 \eta^{-1/2})$ ancillary qubits [14]. The coherent runtime for each phase estimation is $2^{k+1}\pi = \mathcal{O}(\varepsilon^{-1}\eta^{-1/2})$, and the number of calls to phase estimation is $\mathcal{O}(\eta^{-1/2})$. The total gate complexity is

$$\mathcal{O}(C_{\text{gate}}\eta^{-1}\varepsilon^{-1}) \quad (\text{F2})$$

where C_{gate} is the gate cost within each segment.

To obtain a binary estimate of the energy precise to $n = \lceil \log_2 \varepsilon^{-1} \rceil$ bits, we require $k = \mathcal{O}(\log_2 \varepsilon^{-1} + \log_2 \eta^{-1/2})$ ancillary qubits. The total error is composed of following parts: the error of phase estimation, Hamiltonian simulation, and circuit synthesis.

$$\varepsilon_{\text{tot}} = \varepsilon_{PE} + \varepsilon_{HS} + \varepsilon_{CS}$$

The coherent runtime for each phase estimation is lower bounded by

$$t_{PE}^{En} = \frac{\pi}{2\eta\varepsilon_{PE}} \quad (\text{F3})$$

In the following, we will discuss the Hamiltonian simulation

Lemma 5 (Ground state preparation with phase estimation for known ground energy). *Using the canonical phase estimation, the state can be prepared ε close to ground state using $k = \mathcal{O}(\log_2 \varepsilon^{-1} + \log_2 \Delta^{-1} + \log_2 \eta^{-1/2})$. The runtime for each phase estimation is $2^{k+1}\pi = \mathcal{O}(\varepsilon^{-1}\Delta^{-1}\eta^{-1/2})$, and the number of calls to phase estimation is $\mathcal{O}(\eta^{-1/2})$ using fixed point search. The total gate complexity is $\mathcal{O}(\frac{C_{\text{gate}}}{\eta^2\Delta\varepsilon})$.*

The coherent runtime for each phase estimation is lower bounded by

$$t_{PE}^{\text{prep}} = \frac{\pi}{2\Delta\varepsilon_{PE}} \quad (\text{F4})$$

The error of estimation of an observable O consists of the following components:

$$\varepsilon = \varepsilon_{PE} + \varepsilon_{HS} + \varepsilon_{CS} + \varepsilon_{\text{observ}}.$$

The error of estimating observables using N_s samples is given by

$$\varepsilon_{\text{observ}} = \frac{C_{\text{observ}}}{\sqrt{N_s}} \quad (\text{F5})$$

Suppose we use the importance sampling to estimate the observable $O = \sum_l o_l P_l$, the measurement overhead is $C_{\text{observ}} = \|O\|_1$, and we may use other methods to reduce C_{observ} , such as Pauli grouping or classical shadow methods to reduce the cost. In our numerical simulation, we use an optimistic estimation by only considering the dominant cost from the last operations $C - U^{2^{k-1}}$ only, and neglect the cost by controlled operations. The gate cost for QFT is neglected as well, which scales as $\mathcal{O}(k)$.

2. Hamiltonian simulation by Trotterisation

The overall circuit complexity for $2k$ order achieves minima when $\varepsilon_{PE} = \varepsilon_{HS} = \varepsilon/2$

$$\frac{(\pi \cdot 5^{k-1} L \Lambda \eta^{-1})^{1+\frac{1}{2k}}}{((2k+1)!)^{\frac{1}{2k}} \varepsilon_{PE}^{1+\frac{1}{2k}} \varepsilon_{HS}^{\frac{1}{2k}}} \quad (\text{F6})$$

Its minimum is obtained at

$$\varepsilon_{PE} = \frac{2k+1}{2(k+1)}\varepsilon, \quad \varepsilon_{HS} = \frac{1}{2(k+1)}\varepsilon$$

Ground state energy estimation with phase estimation + higher-order Trotter:

Gate count for eigenenergy estimation.

1. Get the runtime $t_{PE}/2$ with $\varepsilon_{PE} = \varepsilon/2$ in [Eq. \(F3\)](#).
2. Determine the number of segment ν using [Lemma 3](#).
3. CNOT gates: $2 \cdot 5^{k-1} \nu \eta^{-1/2} (2 \text{wt}(H) - L + 2)$.
4. Single-qubit z-axis Pauli rotation gate: $4 \cdot 5^{k-1} \nu \eta^{-1/2} L$.

Gate count for eigenstate property estimation.

1. Get the measurement overhead C_{observ} , runtime $t_{PE}/2$ as a function of ε_{observ} and ε_{PE} , respectively.
2. Determine the number of segment ν using [Lemma 3](#) as a function of ε_{HS} . An approximation of ν is given by [Eq. \(D18\)](#).
3. CNOT gates: $2 \cdot 5^{k-1} \nu \eta^{-1/2} C_{observ} \varepsilon_{observ}^{-2} (2 \text{wt}(H) - L + 2)$.
4. Single-qubit z-axis Pauli rotation gate: $4 \cdot 5^{k-1} \nu C_{observ} \varepsilon_{observ}^{-2} \eta^{-1/2} L$.
5. Get the gate count by optimising over the distribution of ε

3. Hamiltonian simulation by qubitised quantum walk

The phase estimation combining the qubitisation methods have been discussed in [\[56\]](#) which are compared to other algorithms. We review the method below. The key idea is that the spectrum of H can be obtained by performing phase estimation on the Szegedy quantum walk operator, defined as

$$\mathcal{W} := (2|G\rangle\langle G| \otimes I - I) \cdot \text{select}(H) \tag{F7}$$

with $|G\rangle = \text{PREP}|\bar{0}\rangle$. The spectrum has the relation

$$\text{spectrum}(H) = \lambda \cos(\arg[\text{spectrum}(\mathcal{W})]) \tag{F8}$$

with $\arg(e^{i\phi}) = \phi$. Their results suggest that we can estimate the phase to a number of bits given by

$$k = \left\lceil \log \left(\frac{\sqrt{2}\pi\lambda}{2\varepsilon_{PE}} \right) \right\rceil \tag{F9}$$

with k extra ancillary qubits. Here, we further assume a small error of gate synthesis in PREP and QFT. Using phase estimation, the query number is

$$d := 2^k \leq \frac{\sqrt{2}\pi\lambda}{2\varepsilon_{PE}} + 1. \tag{F10}$$

The state preparation error $\varepsilon_{\text{PREP}}$ for a single application of \mathcal{W} is

$$\varepsilon_{tot,\text{PREP}} \leq \|e^{i\arccos(H/\lambda)} - e^{i\arccos(\tilde{H}/\lambda)}\| \tag{F11}$$

It is related to the amplitude encoding error ε_{AE} by

$$\varepsilon_{\text{PREP}} \leq \frac{L\varepsilon_{AE}}{\lambda} \left(1 - \left(\frac{\|H\| + L\varepsilon_{AE}}{\lambda} \right)^2 \right)^{-1/2} \tag{F12}$$

Suppose that we require the preparation error to be $\varepsilon_{\text{PREP}}$. One can choose to set

$$\varepsilon_{AE} = \frac{\varepsilon_{\text{PREP}}}{(1 + \varepsilon_{\text{PREP}}^2)L} \quad (\text{F13})$$

assuming that $\Omega(\frac{\|H\|}{\lambda}) = 0$. The preparation error is set to be

$$\varepsilon_{\text{PREP}} \leq \frac{\sqrt{2}}{2\lambda} \frac{\varepsilon_{PE}}{2^k} = \frac{\sqrt{2}\varepsilon_{PE}}{\lambda 2^{k+1}} \quad (\text{F14})$$

and hence for a single block

$$\varepsilon_{AE} = \frac{\sqrt{2}\varepsilon}{4L\lambda d} \quad (\text{F15})$$

and we have 2 preparation in one block. By Eq. (F13), we can determine the amplitude encoding error ε_{AE} as

$$\varepsilon_{AE} = \frac{\varepsilon_{PE}^2}{\pi L \lambda} \quad (\text{F16})$$

Again, the cost from the QFT is ignored, which scales as $\mathcal{O}(k \log k)$.

The overall gate complexity of the eigenenergy estimation is

$$\mathcal{O}\left(\frac{\lambda L}{\varepsilon}\right) \quad (\text{F17})$$

The total gate count can be estimated by using Observation 2, Observation 3, and the Hamiltonian dependent select(H), given by Corollary 2.

Each block requires: 1 controlled select(H), 2 PREP and 1 Reflection on n_L qubits, which has the gate count

$$(n_L + \max(k, n_L + 2n_{AE} + 1), S_{\text{CNOT}} + 2P_{\text{CNOT}} + 6(n_L - 2), S_{\text{T}} + 2P_{\text{T}} + (8n_L - 17), 0). \quad (\text{F18})$$

and additional k repetition of controlled reflection, each block (2 preparation) has the cost:

$$(0, 2P_{\text{CNOT}} + 6(n_L - 1), 2P_{\text{T}} + (8n_L - 9), 0) \quad (\text{F19})$$

We require d queries and $\eta^{-1}\Delta^{-1}$ repetitions

$$(n_L + \max(k, (n_L + 2n_{AE} + 1), \eta^{-1}\Delta^{-1} (d(S_{\text{CNOT}} + 2P_{\text{CNOT}} + 6(n_L - 2)) + k(2P_{\text{CNOT}} + 6(n_L - 1)))), \eta^{-1}\Delta^{-1} (d(S_{\text{T}} + 2P_{\text{T}} + (8n_L - 17)) + k(2P_{\text{T}} + (8n_L - 9))), 0). \quad (\text{F20})$$